Evaluation of aDcps for Suspended Sediment Transport Monitoring, Fraser River, British Columbia

by

Maureen E. Attard
B.Sc. (Mathematics), Queen's University, 2009

THESIS SUBMITTED IN PARTIAL FULFILLMENT OF THE REQUIREMENTS FOR THE DEGREE OF

MASTER OF SCIENCE

in the
Department of Geography
Faculty of Environment

SIMON FRASER UNIVERSITY

Summer 2012

Approval

Name: Maureen E. Attard

Degree: Master of Science (Geography)

Title of Thesis: *Evaluation of aDcps for Suspended Sediment Transport Monitoring, Fraser River, British Columbia*

Examining Committee:

Chair: **Dr. Eugene McCann**
Associate Professor, Department of Geography
Simon Fraser University

Dr. Jeremy G. Venditti
Senior Supervisor
Assistant Professor, Department of Geography
Simon Fraser University

Dr. Michael Church
Committee Member
Professor Emeritus, Department of Geography
University of British Columbia

Dr. Ilja van Meerveld
Committee Member
Assistant Professor, Department of Geography
Simon Fraser University

Dr. David McLean
External Examiner
Senior Partner
Northwest Hydraulic Consultants Ltd.

Date Defended/Approved: August 13th , 2012.

Abstract

Our ability to predict the timing and quantity of suspended sediment transport is limited because fine sand, silt and clay delivery are supply-limited, requiring empirical modelling approaches of limited temporal stability. Here, I evaluate a 300 kHz side-looking acoustic Doppler current profiler (aDcp), mounted in the Fraser River, BC, for continuous measurement of suspended sediment flux. I also evaluate a downward-looking 600 kHz aDcp at the same site. Both aDcps are calibrated against conventional bottle samples obtained with a USGS P63 sediment sampler. The results suggest that it is possible to estimate total suspended sediment flux using a 300 kHz side-looking aDcp in the Fraser River, but that it underestimates observed flux. The calibration of the 600 kHz aDcp is strong (R^2=0.72), but it underestimates total sediment flux at low-moderate flows and overestimates flux at high flows.

Keywords: Fraser River; suspended sediment transport; aDcp; suspended sediment sampling

Acknowledgements

I would like to thank my co-supervisors, Dr. Jeremy Venditti and Dr. Michael Church, for their guidance and feedback. I would also like to express my gratitude to the examining committee Dr. Ilja van Meerveld and Dr. David McLean for offering insightful comments to improve my thesis.

I would like to acknowledge those who worked in the field: Dr. Ray Kostaschuk, Megan Hendershot, Jordan MacDonald, Sally Haggerstone, Dr. Colin Rennie, and WSC staff, especially Emily Huxter. I would also like to acknowledge the following funding sources: Water Survey of Canada (Russel White, Bruno Tassone & Curt Naumann) and NSERC Discovery grants (Jeremy Venditti, Michael Church & Ray Kostaschuk).

Special thanks to Ryan Bradley and Sheena Spencer for being my sounding boards when I was trying to solve problems and providing valuable emotional support. Finally, I would like to thank my family and friends, both in Vancouver and in Ontario, for their understanding and encouragement over the past couple of years.

Table of Contents

List of Figures

List of Tables

1: Introduction

1.1 A problem of sediment transport measurement

Large rivers like the Fraser River in British Columbia transport significant amounts of sediment. In the distal sand-bedded portion, these sediments range in size from clay and silt to fine and coarse sands. This sand load is important because it sets the downstream sediment budget that is related to channel stability, while the silt-clay load contributes to the physical and ecological development of the Fraser delta. The budget has been perturbed in the delta by dredging for navigation purposes. Deepening the shipping channel has led to an upstream migrating knickpoint in the river bed that is causing channel bed degradation and lower water levels that are progressing upstream from New Westminster toward Mission. Aggradation occurs in the shipping channel that requires continued dredging as the step changes caused by sediment removal are being filled. Another consequence is a reduction in sediment delivery to the delta and the associated ecological changes, such as a declining rate of delta front advancement, limiting wildlife habitat (Church, 2007).

The sediment budget of the Fraser River at Mission, British Columbia determines the sediment influx to the downstream reaches. Current estimates of sediment influx to the delta are based on historical sediment rating curves built on the Water Survey of Canada's (WSC) 1965-1986 measurements. According to the WSC's sediment transport records, the Fraser River at Mission (station no. 08MH024) has an annual total suspended load, on average, of 17×10^6 tonnes per year (t/a). The total sediment load is broken down by particle size in Table 1. About one third, or 5.5×10^6 t/a, is suspended

sand and more than half of that, or $3.1x10^6$ t/a, is sand finer than 0.177 mm (McLean et al., 1999). This fine sediment is generally absent from the river bed indicating that a portion of the sand load is wash load (McLean et al., 1999). Another way to consider the load is as total bed material load – bed load and suspended sand coarser than 0.177 mm that is carried in intermittent suspension. This bed material load is $3.0x10^6$ t/a, accounting for 18% of the total. All but 5% is transported in intermittent suspension near the bed (McLean et al., 1999).

Table 1: Mission sediment load grain-size distribution (McLean et al., 1999).

Grain-size	**Sediment Load (t/a)**
Clay	$2.7x10^6$
Silt	$8.3x10^6$
Sand (<0.177mm)	$3.1x10^6$
Sand (>0.177mm)	$3.0x10^6$
Total	$17x10^6$

The estimates of sediment influx to the delta may no longer be accurate. A new sediment budget assessment was set up by Fraser River Estuary Management Program (FREMP) to examine the effects of dredging on sediment inputs to the furthest downstream reaches of the Fraser River (Church, 2007). FREMP uses the sediment budget of the Lower Fraser River to provide a long-term perspective of the net changes in channels and in sediment delivery to Fraser Delta (nhc, 1999; 2002). For the purposes of analysis, the sediment budget of the lower river is defined as

$$\Delta S_{chan} = -S_{dredge} + S_{spoil} + (S_{in} - S_{out})$$

where S_{in} is the sediment inflow to the reach during the designated time period, S_{out} is the sediment outflow from the reach during the period, S_{dredge} is the quantity of sediment dredged from the reach during the time period, S_{spoil} is the quantity of dredge spoil

disposed of in the reach (i.e., dredged material that was not actually removed from the river), ΔS_{chan} is the net change in sediment stored within the reach.

Unknown sediment inputs and outputs mean that measurements of the net change in sediment stored, ΔS_{chan}, are insufficient to determine the total sediment budget. Therefore, the budget cannot be fully implemented unless additional measurements are obtained so that the sediment budget may be closed (Church and Venditti, 2008). Furthermore, our ability to predict the timing and quantity of suspended sediment transport is poor because the delivery of fine sand, silt and clay is supply-limited, requiring empirical modelling approaches of limited temporal stability. Consequently, reestablishment of suspended sediment transport measurements at Mission gauge is advised so that the sediment budget no longer needs to rely on historical rating curves (Church and Venditti, 2008).

Conventional methods of measuring sediment transport are labour-intensive and do not provide the desired continuous monitoring. Semi- or fully automated methods are needed to measure medium to fine sand, which does not consistently relate to measured hydraulic variables and thus cannot be predicted with acceptable precision (Church and Venditti, 2008). Options for continuous monitoring include optical sensors, but these are susceptible to biofouling and typically only provide a point measurement. Acoustic sensors, such as those employed in an acoustic Doppler current profiler (aDcp), are an attractive option because they do not biofoul, they measure profiles of backscatter, which has been shown to relate to sediment concentration (Topping et al., 2007; Wright & Topping, 2009) and provide a velocity necessary to calculate sediment flux. However, using aDcps to estimate sediment concentrations has not been tested extensively. Here, I examine whether an aDcp can be used to monitor suspended sediment transport in the Fraser River at Mission, British Columbia.

1.2 Context

1.2.1 Suspended Sediment Transport Theory

Measurements can be made most efficient by taking advantage of what is known in theory about sediment movement. Based on measurement principles, the sediment load of a river can be divided into bedload (rolling and sliding particles, and saltation) and suspended load (including wash load). When sediment is entrained and becomes suspended in the flow, it is classified as suspended load (Church, 2006). Suspended sediment is usually described as a concentration, measured as solid volume (m^3) per unit fluid volume (m^3) or as solid mass (kg) per unit fluid volume (m^3 or L) (van Rijn, 1993). It is important to note that the formulas described apply only to clastic particles of the load and do not take into account organic components. Depth-integrated suspended sediment load is given by

$$q_s = \int_{z_1}^{z_2} cu \, dz \qquad (1)$$

where u is velocity at height z above the bed, and c is the concentration from the top of the bedload layer (z_1) to the water surface ($z_2=h$, the flow depth) (van Rijn, 1993).

Wash load is part of suspended load but is distinct in that it is so fine that, once entrained, it is apt to travel out of a given river reach (Church, 2006). The volume concentration of wash load does not vary greatly with distance from the bed (Bridge, 2003) and wash material is not found in large quantities in the bed (Church, 2006). However, wash material in one reach of a river may become bed material in another reach with lower sediment transporting capacity (Church, 2006). In practice, it is difficult to divide wash load and bed material load.

It is commonly asserted that a sediment particle remains in suspension if the upward-directed turbulent forces balance the immersed weight of the sediment grain

(Bridge, 2003). There are, however, various opinions on the value of this ratio. Due to the effect of the fluctuating vertical velocity component of turbulent eddies, values between 0.8 and 1.2 are employed in literature (Komar, 1988). Diffusion models for suspended sediment assume that sediment particles in a river will passively follow the momentum flux of the river (Venditti, 2010). Diffusivity, ε, represents the vertical transport of momentum and is assumed to be governed by the velocity gradient. Suspended sediment diffusivity is described in the convection-diffusion equation

$$\omega_s c + \varepsilon_s \frac{\partial c}{\partial z} = 0 \tag{2}$$

where the particle fall velocity is ω_s, concentration is c, and sediment diffusivity is ε_s and is assumed equal to the diffusivity of momentum in the fluid. Four methods have been proposed to define the variation in fluid diffusivity with depth:

1) Constant $$\varepsilon = \frac{1}{\alpha_1} \kappa u_* h \tag{3}$$

2) Linear $$\varepsilon = \frac{1}{\alpha_2} \kappa u_* h \frac{z}{h} \tag{4}$$

3) Parabolic $$\varepsilon = \kappa u_* h \frac{z}{h}(1 - \frac{z}{h}) \tag{5}$$

4) Parabolic-constant $$\varepsilon = \kappa u_* h \frac{z}{h}(1 - \frac{z}{h}) \text{ for } z/h < 0.5$$
$$\varepsilon = 0.25 \kappa u_* h \text{ for } z/h \geq 0.5 \tag{6}$$

where κ is the von Kármán universal constant, 0.41, z is height above the bed, h is flow depth, and u_* is the shear velocity.

By integrating the convection-diffusion equation from the bed to the water surface, the concentration profiles of suspended sediment are obtained. The parabolic distribution is based on the log-linear velocity profile and is often assumed the most appropriate representation of fluid diffusivity. Integration using the parabolic representation of diffusivity (ε) yields the Rouse equation for sediment transport:

$$\frac{C}{C_a} = \left(\frac{h-z}{z}\,\frac{a}{h-a}\right)^{R_o},\ R_o = \frac{\omega_s}{\beta\kappa u_*} \tag{7}$$

where c_a is the concentration at $z=a$, a is reference height with respect to the bed, and β =1, assuming the suspended sediment is a passive tracer (Bridge, 2003). Rousian theory describes suspended sediment concentration as decreasing continuously and smoothly with distance from the bed. The value of R_o is responsible for the change in curve slope; a smaller R_o gives a steeper slope (Figure 1). The distribution of suspended sediment becomes more uniform throughout the flow depth as exponent R_o decreases, that is, particle fall velocity (grain-size) decreases (Bridge, 2003).

It is relevant to note three other equations for modelling the concentration profiles, each derived from one of the assumptions about the variation of fluid diffusivity:

1) Constant ε: $\frac{C}{Ca} = exp\left(-\alpha_1\,\frac{\omega_s}{\beta\kappa u_*}\frac{z-a}{h}\right)$ (8)

2) Linear ε: $\frac{C}{C_a} = \left(\frac{a}{z}\right)^{\left(\frac{\alpha_2\omega_s}{\beta\kappa u_*}\right)}$ (9)

3) Parabolic-constant ε: $\frac{C}{C_a} = \begin{cases} \left(\frac{h-z}{z}\,\frac{a}{h-a}\right)^{\frac{\omega_s}{\beta\kappa u_*}} & ,\ {}^{z}/_{h} < 0.5 \\ \left(\frac{a}{h-a}\right)^{\frac{\omega_s}{\beta\kappa u_*}} exp\left(-4\,\frac{\omega_s}{\beta\kappa u_*}\left[\frac{z}{h} - 0.5\right]\right), & {}^{z}/_{h} \geq 0.5 \end{cases}$ (10)

(Venditti, 2010). The concentration profiles can then be converted to a unit flux by convolution with the velocity profile. To adapt the theory to the supply-limited character of fine sediment supply, a value of c_a is required to employ a model for calculation of total sediment transport of the channel (Vanoni, 1946).

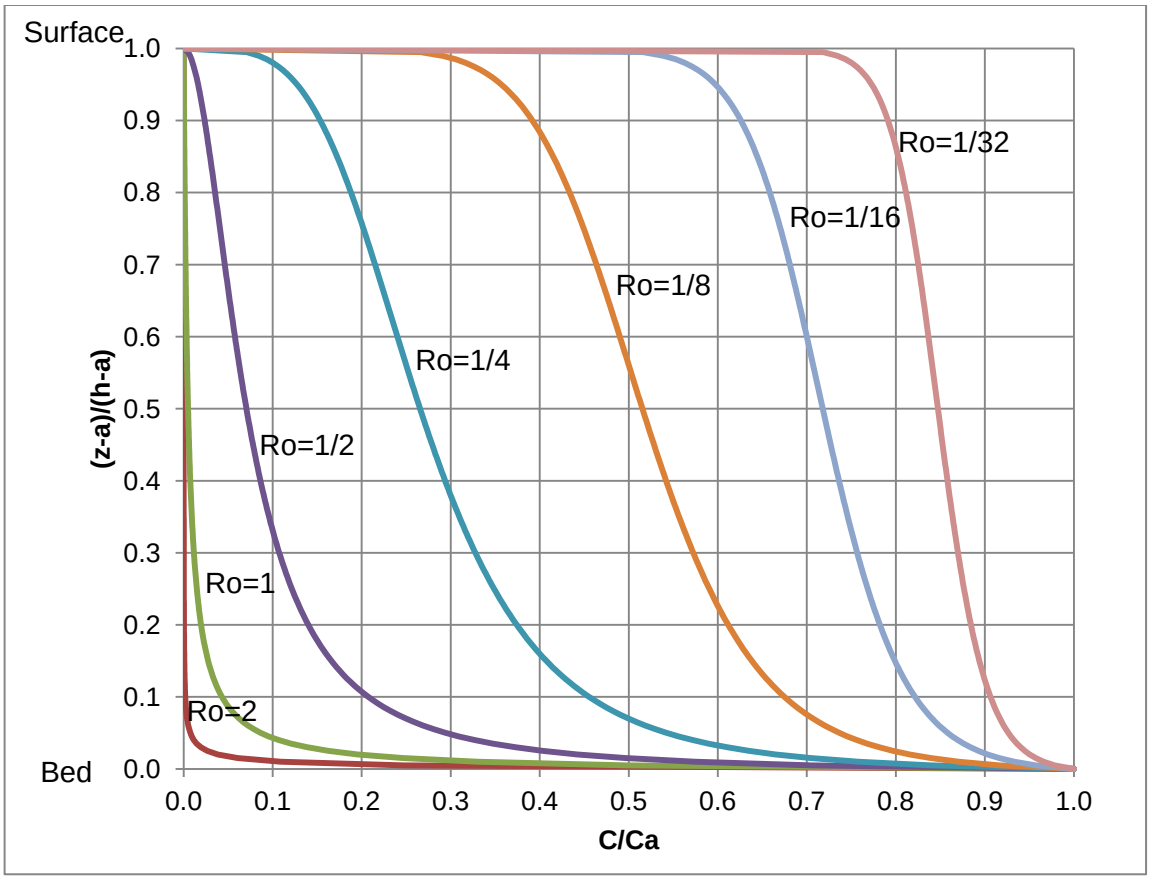

Figure 1: Parabolic concentration profiles for different values of the Rouse number, Ro, shear velocity held constant.

There are various approaches to finding the reference concentration near the bed. One may adopt estimates of the bedload from a theoretical function, incorporating an entrainment function, or an empirical bedload function. Directly measuring the concentration is also an option. Regardless of the approach one uses, the Rousian profile is often employed to estimate the suspended sediment concentration throughout the water column using the concentration near the bed as a reference concentration.

1.2.2 Theoretical and empirical estimations of near-bed concentrations

The theoretical approach calculates the suspended sediment concentration near the bed by employing an entrainment function. The coarser part of the transported sediment load may move as either bedload or as intermittently suspended load (Church,

2006). Bedload is material that moves through the channel via traction (rolling, sliding, or bouncing along the bottom) supported by the bed itself. When sediments roll and slide along the bed they are kept in motion by low shear stress acting at the boundary, relative to the critical shear stress required to move a particle. Shear stress near the critical value to move sediment and traction transport are usually considered in relation to gravel. In contrast, saltation, which occurs at larger excess shear stress, is the process by which particles leave the bed in short jumps (Church, 2006). Saltation is widely accepted as the most typical type of particle motion for sand-sized particles (Venditti, 2010), and so this process is assumed for the remainder of the theory- based sand transport discussion.

Bedload flux for sand-bedded rivers, as the Fraser at Mission, is described by

$$q_b = c_b u_b \delta_b, \tag{11}$$

the product of particle concentration (c_b), velocity (u_b), and bed load layer thickness (δ_b) (van Rijn, 1993). The saltation model defines bedload transport based on estimating saltation characteristics (Venditti, 2010). Particle velocity is described as the ratio between the saltation length and the saltation period ($u_b = \lambda / T$) and so:

$$q_b = \frac{c_b \delta_b \lambda}{T} = E\lambda \tag{12}$$

where $E = c_b \delta_b / T$ is the eroded volume of particles per unit area and time (van Rijn, 1993). It is important to also consider particle motion and the rate at which they become entrained in the flow.

The initiation of particle motion occurs when the shear stress exceeds the critical shear stress applied to the bed, which is represented by the non-dimensional Shields Number,

$$\tau_s^* = \frac{\tau_{bs}}{(\rho_s - \rho) g h} \tag{13}$$

where ρ_s is the density of the sediment, ρ is the density of water, g is acceleration due to gravity, and τ_{bs} is the boundary skin shear stress (van Rijn, 1993). Total shear stress consists of both skin and form stresses, where the skin stresses are those acting directly on the particle surface from above and form stresses are those exerted against the boundary geometry.

According to the particle suspension criterion, when the bed shear velocity exceeds the particle fall velocity, particles can be entrained, or lifted to a level where the upward turbulent fluctuations exceed the submerged particle weight (van Rijn, 1993). There are several proposed particle entrainment equations. McLean and Smith (1977) describe the particle pick-up rate, E, for large rivers, like the Fraser, as

$$E = 0.65\gamma_o \left(\frac{\tau_{bs}}{\tau_s^*} - 1\right) \Big/ \left[1 + \left(\frac{\tau_{bs}}{\tau_s^*} - 1\right)\right], \gamma_o = 0.0024 \quad (14)$$

(Venditti, 2010). Wright and Parker (2004) define pick-up rate for large low gradient streams as

$$E = \frac{AZ_u^5}{1+\frac{A}{0.3}Z_u^5}, Z_u = \frac{u_{*s}}{\omega_s} Re_p^{0.6} S^{0.07}, A = 5.7x10^{-7} \quad (15)$$

where A is a constant, u_{*s} is skin shear velocity, S is slope, and Re_p is the Grain Reynolds Number (Venditti, 2010). If the appropriate pick-up rate, E, and the saltation length, λ, are substituted into the bedload equation (12), then the bedload transport rate can be calculated (Venditti, 2010). The entrainment rate is the near bed concentration for the Rouse profile (Parker, 2004).

1.2.3 Direct measurement of suspended sediment concentration

Approaches that have a basis in estimation of bedload, do not take into account the fine sediment of the wash load component. Another method is to measure the

reference concentration, somewhat in accordance with the concept of deriving the reference quantity from a bedload function.

Traditional approaches to measuring c_a include bottle or pump sampling, where water-sediment samples are obtained isokinetically (Wren et al., 2000). Among the modern methods are optical and acoustic sensors. Church and Venditti (2008) conclude that acoustic methods are the optimal choice in large rivers like the Fraser because they provide a continuous signal of sediment concentration with minimal labour after initial calibration. They do not easily biofoul like optical and laser-based methods and velocity measurements are also recorded to allow for sediment flux calculations.

Acoustic methods utilize an instrument called an acoustic Doppler current profiler (aDcp), which uses the Doppler shift to convert backscattered sound into the three principal water velocity components. The instrument transmits an acoustic pulse at a fixed, known frequency and captures the portion scattered and reflected back to the aDcp by particles in the water. The sound scatterers are assumed to move at the same horizontal velocity as the water. As the scatterers move away from the aDcp, the sound they perceive is Doppler-shifted to a lower frequency proportional to the relative velocity between the aDcp and the scatterer. When the sound is scattered back, the instrument 'sees' the backscattered sound as if it is coming from the sound source and so the Doppler shift is doubled and can be determined via (Teledyne RD Instruments, 2006):

$$F_d = 2F_s(\frac{V}{C}) \tag{16}$$

where F_d is the change in the received frequency at the receiver, F_s is the frequency of the transmitted sound, V is the relative velocity between the source and receiver and C is the speed of sound in the water.

An aDcp uses 2-4 transducers to measure velocity components and assumes that currents are homogeneous across layers of constant depth. The Doppler shift

measured by a single transducer reflects the velocity of water along the axis of the acoustic beam. A transducer aimed at the measurement volume emits short pulses of high frequency sound with the majority of energy concentrated in a cone a few degrees wide. The transducers are oriented in different directions to sense the different velocity components (Figure 2 a).

The profile of water velocity is divided into range cells, where each cell represents the average of the return signal for a given period. Averaging reduces the effect of the process of frequency aliasing. The averaging is not uniform over the depth range of a cell; the depth cells are more sensitive to velocities at the centre and least sensitive at the extremities (Figure 2 b). Adjacent bins obtain overlapping measurement volumes because of a triangularly weighted window, resulting in a correlation between neighbouring bins. The consistent spacing of the data cells over the profile allows for easier processing and interpretation of the measured data (Teledyne RD Instruments, 2006).

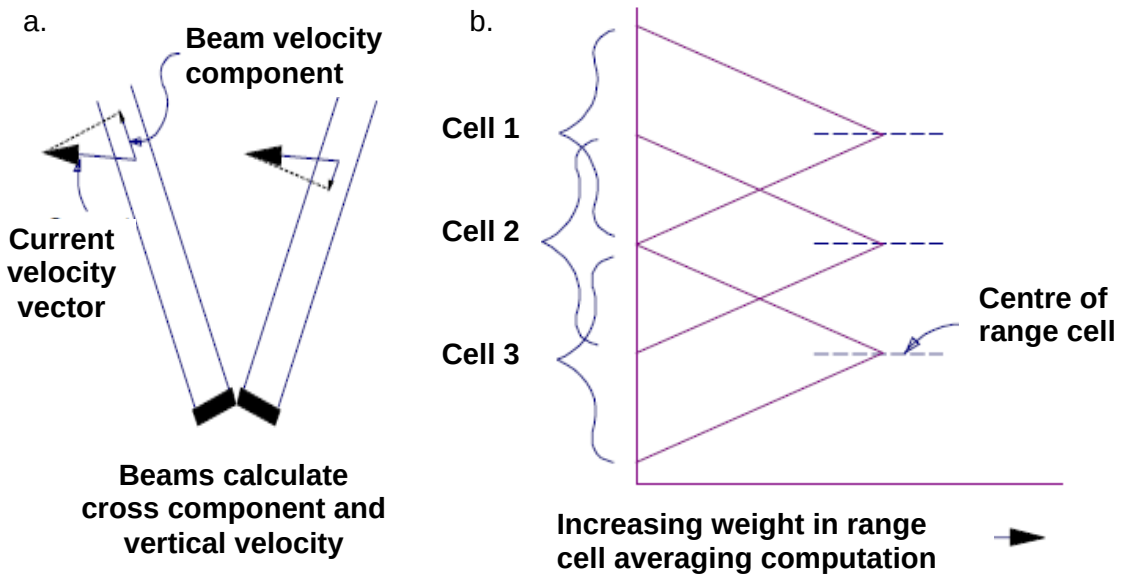

Figure 2: a. aDcp computation of velocity components using beams; shows the relation between beam and velocity components. The orientation is arbitrary (modified from Teledyne RD Instruments, 2006). b. Range cell weight function: range cells are more sensitive to currents at the centre of the cell than at the edges (modified from Teledyne RD Instruments, 2006).

When working with natural sediments, as in the Fraser River, an empirical relation between backscatter and sediment concentration allows for the calculation of sediment concentration. This empirical relation accounts for the variability of sediment characteristics from river to river, which influences the backscatter signal.

The United States Geological Survey (USGS) has taken advantage of commercially available acoustic profilers by developing techniques for converting the backscatter data into sediment concentration. Topping et al. (2007) used a side-looking acoustic-Doppler profiler to measure the concentration of suspended silt and clay and the concentration of suspended sand in the Colorado River in Grand Canyon. Underwater acoustics theory and measurements indicate that suspended sediment can be separated into two size classes at a given sound frequency. In the finer acoustic size class of particles less than 62.5 microns, attenuation of sound is increased due to viscous loss from increasing concentration or decreasing grain-size when concentration

is constant. In the coarser acoustic size class of sand-sized particles greater than 62.5 microns, an increase in the acoustic backscatter occurs because of increasing concentration or increasing grain-size when concentration is constant (Topping et al., 2007). At each frequency of sound, the maximum grain-size of the coarser acoustic size class is about 40% of the πD wavelength limit, where D is grain-size (Topping et al., 2007). This implies that most of the scattering from particles in the coarser acoustic class is backscattering.

The relation between suspended sediment concentration and acoustic backscatter is based on a formula, which was derived from the sonar equation for sound scattering from small particles (Gartner, 2004). The equation in exponential form is:

$$SSC_{est} = 10^{(A+B*ABS)} \quad (17)$$

The exponent contains a term for the acoustic backscatter, ABS, and terms for an intercept, A, and slope, B, determined by regression of simultaneous measurements of ABS and mass concentration (SSC_{meas}) on a semi-log plot in the form of $log_{10}(SSC_{meas}) = A + B * ABS$ (Gartner, 2004).

For a wide range of conditions, increases in acoustic attenuation due to sediment are related linearly to the concentration of finer acoustic size classes and increases in backscatter are related nonlinearly to increases in concentration of the coarser acoustic size class (Topping et al., 2007). The USGS group developed a multi-step approach to using acoustics to measure suspended-silt and clay concentration, and suspended sand concentration (Topping et al., 2007):

1) Two-way transmission losses associated with beam spreading and water absorption are removed

2) Calculate sediment attenuation from the finest particles using linear regression

3) Compute relations between backscatter in each cell and the measured

concentration of sand in a discrete size range (coarser acoustic class)

4) Compute relations between sediment attenuation and measured silt and clay concentrations.

The results reported in Topping et al. (2007) show a strong positive correlation between the sediment concentration of coarse particles (sand) and the sediment-corrected backscatter, and concentration of fines (silt and clay) and sediment attenuation. Positive correlation between total sediment concentration and water-corrected backscatter is also found. This approach yielded silt/clay and sand concentrations within 5-10 % of the values computed using conventional bottle sampling data for the Grand Canyon site where concentrations ranged from 10 to 20000 mg/L of silt-clay and 3000 mg/L of sand.

1.2.4 Synthesis

In order to model suspended sediment transport in river channels one must incorporate bed and wash material. To capture the wash load portion of suspended load, direct measurement of sediment concentration may work better than estimating bedload from theoretical, empirical, or entrainment functions. The Rouse equation models the suspended sediment concentration for clastic particles of reasonably uniform density as distance from the bed increases based on the near-bed reference concentration. There are acoustic technology methodologies that use the backscatter of sound reflected by particles in the water and the velocity profile to measure suspended sediment concentration within the instrument range across the channel.

Recent tests of the technology suggest that acoustic backscatter and attenuation can be used to calculate sediment loads in rivers with a wide range of concentrations and grain-sizes. The acoustics method remains experimental and needs to be tested in

a variety of rivers systems before it is universally adopted as a suitable sediment concentration surrogate. This approach may contribute to a more complete record of grain-size discriminated suspended sediment transport in lower sediment concentration conditions of the Fraser River at the Mission gauge.

Given that, of the $5.5x10^6$ t/a suspended sand load, 50% are sands finer than 177 microns wash load (McLean et al., 1999), capturing suspended load including wash load is vital in the monitoring of suspended sediment transport in the Fraser River. Seasonal variations in the proportion of suspended sand load are also important as well as further testing of the 177 micron division point.

1.3 Research Objectives

In this research, I seek to understand whether an acoustic Doppler current profiler is an appropriate instrument to monitor suspended sediment transport in the Fraser River at Mission, British Columbia. The specific research questions are:

(1) How does suspended sediment move in the Fraser River at Mission and what is an accurate way to compute suspended sediment transport in the reach?

(2) Can available theory be applied to model suspended sediment distributions in the reach?

(3) How do the recent measures of suspended sediment transport compare to historical records?

(4) Are acoustic signals sensitive to variation in suspended sediment concentration in Fraser River at Mission, BC?

(5) What is an appropriate methodology for the calibration of acoustic data with Fraser River sediment data?

(6) How do measurements from different frequency acoustic data compare to observational data?

1.4 Field Study Site: Fraser River near Mission City, BC

The Fraser River drains part of the humid Coast Range, the subhumid Interior Plateaux, and the Columbia and Rocky Mountains of BC for a total basin area at Mission of 228,000 km^2. The runoff pattern is dominated annually by the spring snowmelt in May-June. High flows occur throughout late May, June and early July and recede in August and September (Figure 3). The mean annual flow at Mission is 3410 m^3/s, the mean annual flood is 9790 m^3/s, and the 1894 flood, in which flows are estimated to have reached 17,200 m^3/s, is the historic flood of record. The largest flood during the period of sediment transport measurements occurred in 1972 and had a peak flow of 14,400 m^3/s (McLean et al., 1999).

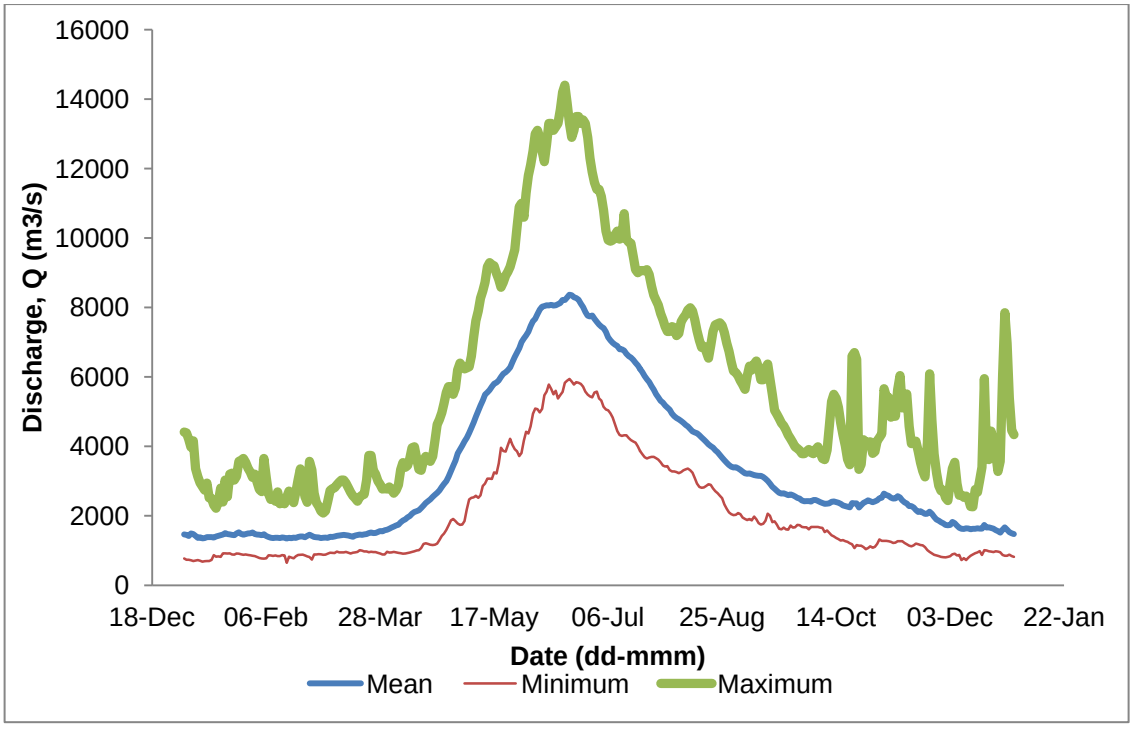

Figure 3: 30-year long-term hydrograph for Fraser River at Mission (data source: http://www.wateroffice.ec.gc.ca/index_e.html, accessed March, 2010).

The sediment load is mainly fine Quaternary glacial deposits eroded directly from the river banks and terraces. The total sediment yield of the Fraser is not considered large compared to other major river systems (McLean et al., 1999).

At Sumas Mountain near Mission, British Columbia, the Fraser River changes from a wandering gravel-bedded river to a single-thread, sand-bedded channel. A reduction in gradient to 6×10^{-5} follows the gravel-sand transition. The gravel-sand transition also marks the upstream extent of tidal influence. At Mission, just below Sumas Mountain, the tidal range varies from a few centimetres during the freshet to over one metre during the highest winter tides (see Figure 4) (McLean et al., 1999). Though the river here is tidally influenced, salt water reaches only as far upstream as the head of the delta at the city of New Westminster.

This study focuses on Fraser River at Mission, just upstream of the Mission Railway Bridge (Figure 5). Here, the river has a mean annual flood width of approximately 540 m (McLean and Church, 1986).

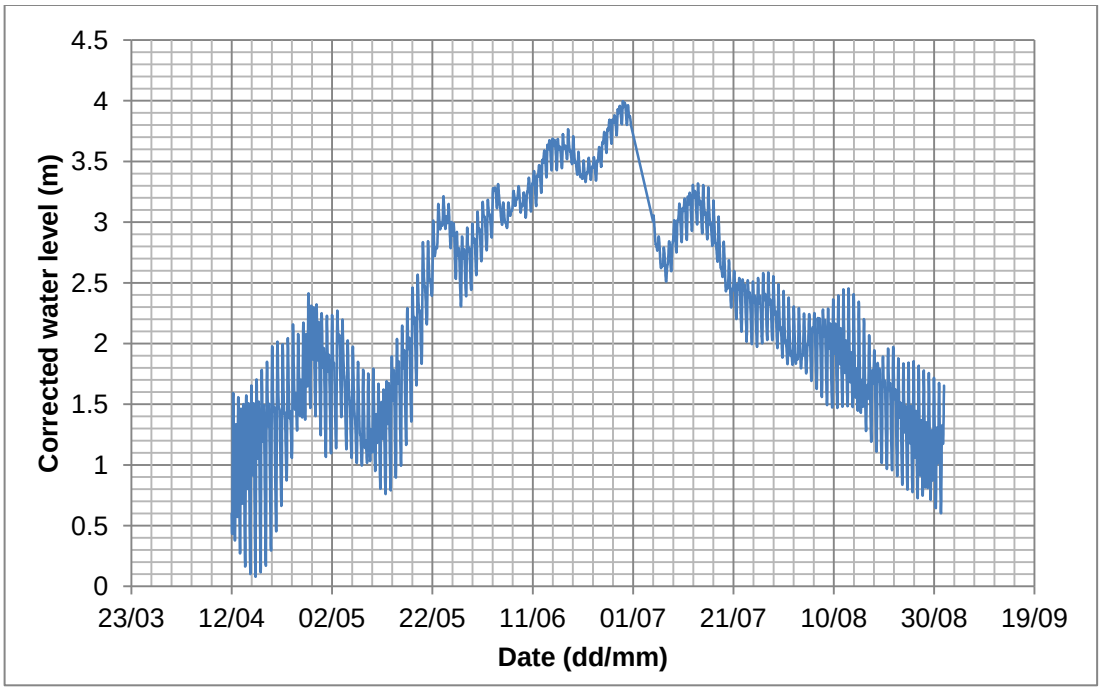

Figure 4: Hourly water level for the period 12/04-31/08 2010 for Fraser River at Mission (data source: WSC, http://www.wateroffice.ec.gc.ca/index_e.html, accessed Mar., 2011).

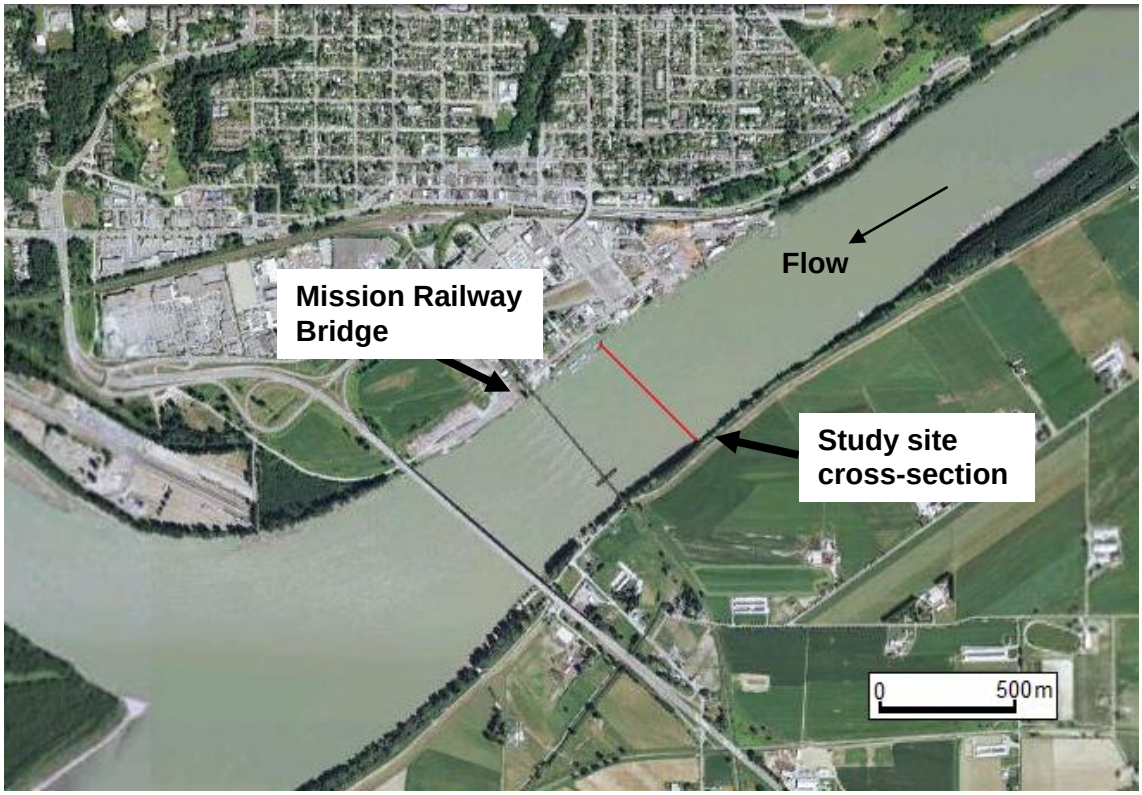

Figure 5: Study site location just upstream of the Mission Railway Bridge, Mission, BC (data source: Google Earth, accessed Oct 12, 2011).

2: Sediment Sampling Program

2.1 Introduction

The sediment budget at Mission determines the sediment influx to the downstream reaches of Fraser River and sediment delivery to the delta. Current estimates of sediment influx to the delta are based on historical sediment rating curves built on the Water Survey of Canada's (WSC) 1965-1986 measurements at Mission. These rating curves, and hence the estimates of sediment influx to the delta, may no longer be accurate because of ongoing anthropogenic changes to the river. Consequently, reestablishment of suspended sediment transport measurements at the Mission gauge is advised so that the sediment budget no longer needs to rely on historical rating curves (Church and Venditti, 2008).

A sediment-sampling program using traditional bottle-sampling methods was carried out on the Fraser River at Mission gauge during the 2010 freshet to examine suspended sediment transport. Observations of suspended sediment concentrations, velocity, depth, discharge, and bed material were obtained at five positions along the test cross-section (Figure 5; Figure 6). Data were collected over the rise and fall of the annual freshet hydrograph (Figure 7) to compute current suspended sediment transport rates. These estimates of total and sand sediment concentration and flux were compared with historical records.

2.2 Measurements

The sampling program consisted of six campaigns to catch the rise, peak and fall of the 2010 hydrograph (Figure 7). The campaigns took place on the following dates: 1) April 15-16, 2) May 18-19, 3) May 27-28, 4) June 7-8, 5) June 27-28, and 6) August 3-4

(Figure 7). Observations of suspended sediment concentrations, velocity, depth and discharge, and bed material sampling were obtained along a cross-section of the river (Figure 5; Figure 6).

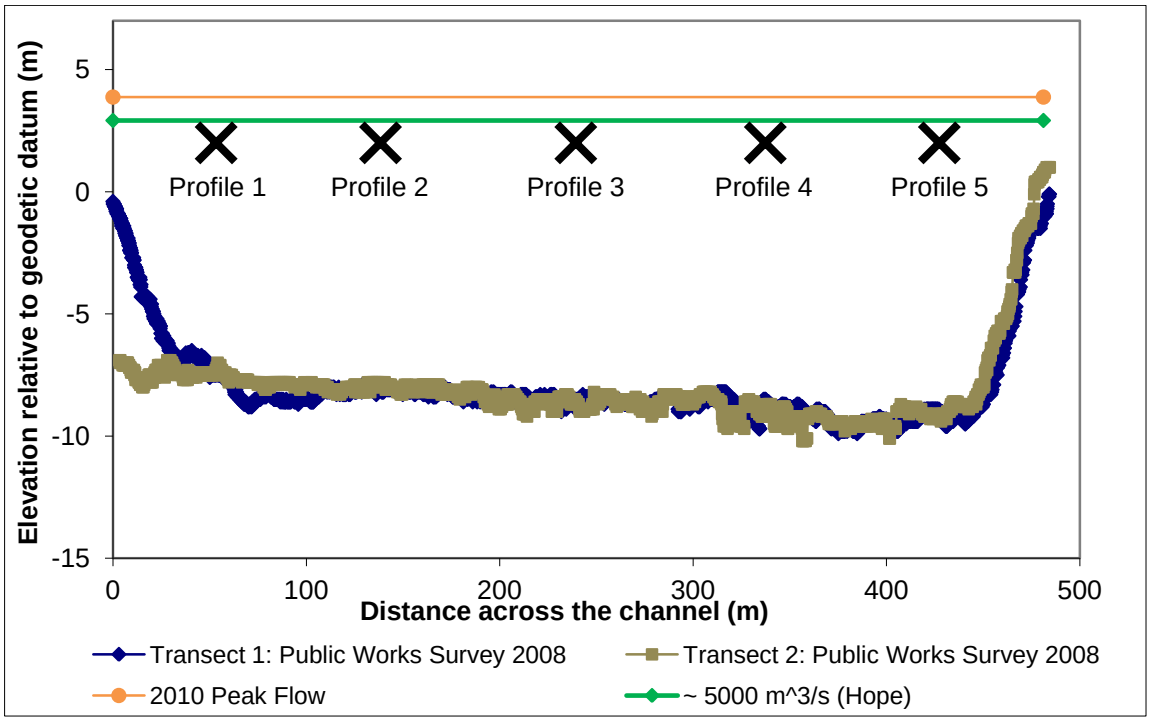

Figure 6: Fraser River at Mission cross-section indicating sampling locations relative to 2010 Mission water levels (peak flow and when flow at Hope was ~5000 m^3/s) (data source: WSC, http://www.wateroffice.ec.gc.ca/index_e.html, accessed June 6, 2012) , and bed elevation. When flow at Hope reaches approximately 5000 m^3/s, significant bed material suspension occurs (McLean et al., 1999). Bed elevation transects are from 2 transects surveyed in 2008.

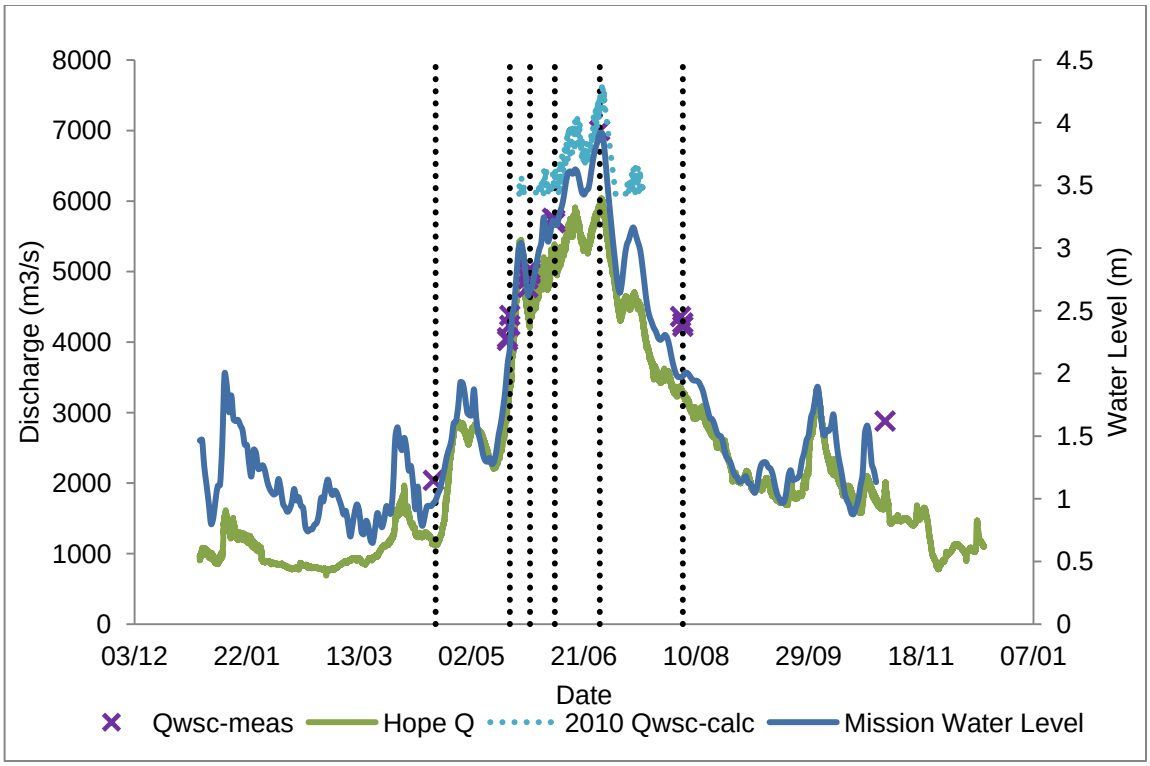

Figure 7: Fraser at Mission discharge measurements, Hope flow record and Mission water level. Note: scales for discharge and water level are independent. Discharge at Mission is calculated only when flow at Hope exceeds 5000 m^3/s. The dotted vertical lines highlight dates of the sampling campaigns. (data source: http://www.wateroffice.ec.gc.ca/index_e.html, accessed Mar 2011).

Table 2: Channel location of vertical profiles

Profile	Distance across channel from aDcp/Right bank	UTM Coordinates (Eastings; Northings)
1	50 m	551,138.74; 5,441,795.36
2	135 m	551,190.91; 5,441,734.81
3	236 m	551,254.69; 5,441,656.74
4	334 m	551,307.86; 5,441,581.06
5	424 m	551,378.54; 5,441,510.75

2.2.1 Bottle-Sampling Program

Suspended sediment measurements were made via conventional bottle-sampling methods. Sampling was conducted when water levels were approaching low tide to capture the maximum current when flow was least affected by tides. A P63 sampler was used to collect point and depth- integrated suspended sediment samples at five vertical profiles (Figure 6; see Table 2 for locations). This streamlined instrument was deployed from a 19-ft launch fitted with a davit, a motorized winch and a manual USGS B-reel that was used measure depths and trigger the P63 sampler (Figure 8 and Figure 9). The P63 is an isokinetic sampler with a valve that opens and closes when triggered by a 48-volt battery connected to the B-reel. The sample was collected for approximately 30 to 120 seconds depending on the flow in a quart-sized bottle (0.95L). At each of the verticals, point samples were collected at five depths corresponding to the following relative depths: 0.1h, 0.2h, 0.4h, 0.6h and 0.8h, where h is flow depth. A depth-integrated sample was also obtained at each vertical, with two samples collected at the centre of the channel (profile 3). This was less strictly followed during low stage and flow conditions in April, when sometimes only 4 points in the water column were sampled and so sampling depths were different from the aforementioned procedure.

During the June 27-28 campaign, only four vertical profiles (profiles 1, 2, 3, 4) were collected because the winch for the electric motor broke; no data were collected at profile 5.

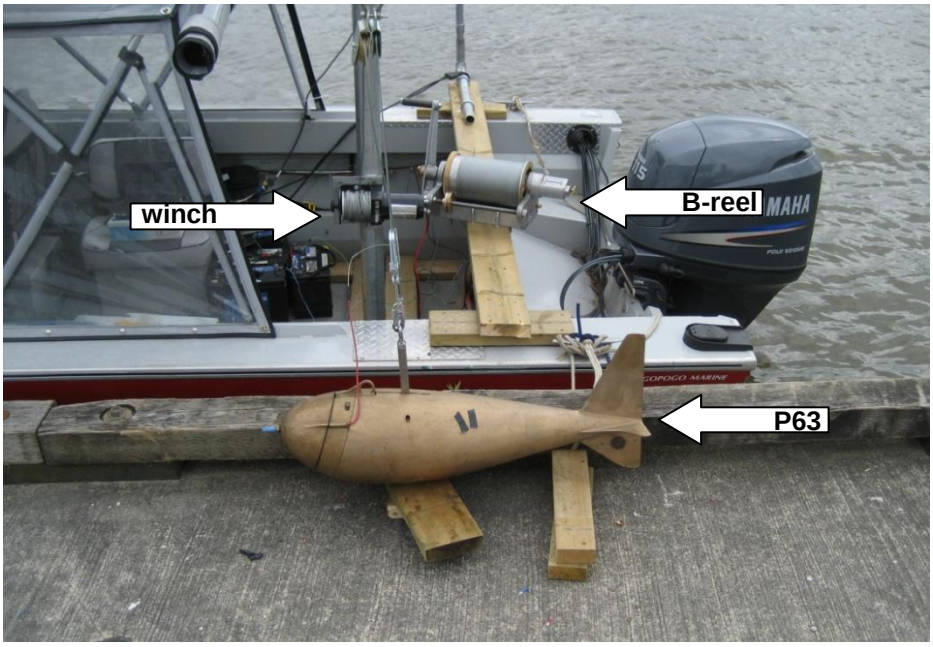

Figure 8: P63 sampler with B-reel and motorized winch (arrow).

2.2.2 Complementary Observations

During each sampling campaign, the Water Survey of Canada obtained several discharge measurements. A final supplementary measurement was also taken on November 2, 2010. Data were collected with a Teledyne RD Instruments downward-looking 1200 kHz aDcp, except for June 28 when peak flows had depths beyond the range of the 1200 kHz instrument and so a 600 kHz instrument was used. For each measurement, four cross-stream transects were obtained as the tide was approaching low tide.

Velocity profiles and depth measurements were obtained using a 600 kHz Workhorse Rio Grande aDcp by Teledyne RD Instruments at each profile location during each sampling campaign. The aDcp was also deployed from a 19-ft launch,

approximately two metres away from the suspended sediment sampler (P63) on the opposite side of the vessel (Figure 9). Positioning of the aDcp was accomplished using real time kinematic (RTK) GPS. Both the aDcp and RTK-GPS were connected to a laptop and data were streamed and logged through WinRiver software. Velocity data were captured simultaneously with all the suspended sediment samples, except profile 3 in April and for samples 2-5 for profile 3 on June 7th when the aDcp was inoperable. The downward orientation of the aDcp allowed velocity profiles to be obtained for the purpose of suspended sediment flux calculations.

Bed material samples were collected with a pipe dredge at the approximate location of each vertical profile and for all sampling periods, except for the April 15-16 campaign.

Figure 9: The 19-ft aluminium launch from which the P63 sampler and downward facing aDcp were deployed.

2.3 Data and Sample Processing

2.3.1 Suspended sediment

After data collection in the field, samples that could not be processed promptly were treated with 1 mL of 0.4 g/L copper sulphate solution to slow the growth of organic material. Each of the P63 suspended sediment samples was processed using a Sequoia Scientific LISST-Portable (laser in-situ scattering transmissiometry) instrument (Figure 10) that uses laser diffraction to calculate the grain-size distribution, and other grain-size statistics, such as mean, D_{10}, D_{16}, D_{50}, D_{60}, D_{84}, and D_{90} through Version 3 of the LISST-Portable Excel Report Template Software provided by the manufacturer (Sequoia Scientific, 2007).

Water-sediment samples were transferred to the instrument's measurement chamber and agitated during the measurement process. When the laser beam enters water, light is scattered by particles and sensed by a multi-ring detector behind a receiving lens. The LISST-Portable calculated the grain-size distribution in 32 logarithmically-spaced angle ranges: from a lower limit of 1.9 µm to the upper limit of 381 µm. The data is presented as a volumetric concentration (µL/L) for each of the 32 logarithmically-spaced bins. The instrument also gives a measure of total sediment concentration, which is the sum of the 32 bins.

Due to the instrument's chamber capacity of 180 mL, the samples were allowed to settle for several days (minimum 5 days) and the clear water on the top was siphoned off to the volume required for the LISST. This concentrated the sample. The volume of water removed was recorded and used in calculation of the sample total volume. The smallest particle size sensed by the LISST (1.9 µm) has a settling velocity, assuming spherical particles, of 1.24x10-6 m/s (Dietrich, 1982). A 5-day settling period allows

these fines to travel a distance of 54 cm, which is greater than the depth of the water within the sample bottle (maximum 16 cm), assuring the settling time was sufficient.

Figure 10: LISST-Portable (Sequoia Scientific Inc., sequoiasci.com, accessed Mar, 2010).

Sediment concentration was also obtained using the traditional filter method. The samples were filtered using 47 mm Whatman® glass microfibre filters with a pore size of 1.6 µm to obtain a second measure of total sediment concentration. The entire sample, including the portion siphoned off for the LISST analysis, was filtered and mass obtained for concentration in mg/L.

To convert the LISST-Portable measures of volumetric concentration in µL/L to mass concentration the instrument manufacturer recommends a conversion factor of 2.65, based on the density of clastic sediment (Sequoia Scientific, 2010). I explored the conversion factor by plotting the LISST concentrations against those from the filter method. The grain-size distribution provided by the LISST was used to separate the total concentration from the lab filter method into two size classes: sand and silt-clay concentrations.

In order to examine the organic content of the samples, select vertical concentration profile samples were combusted. The vertical profiles were chosen to represent low, increasing, and peak flows and capture variation through the water column. Samples were baked at 375 degrees Celsius for a minimum of 16 hrs and reweighed to obtain the difference between pre and post combustion.

The Rouse profiles for each of the 32 logarithmically spaced grain-sizes from the LISST-Portable were calculated. Rouse profiles were fit to the sediment concentration profiles based on the Rouse Number, $R_o = \omega_s/\beta\kappa u_*$ (ω_s is the particle settling velocity from Dietrich (1982), u_* is the shear velocity calculated based on the logarithmic velocity profile (equation 18), β is assumed to be equal to one and κ=0.41). The profiles were then summed and divided by 32 to give a concentration that ranged from 0 at the water surface to 1 at the height of the reference concentration.

Velocity profiles obtained from the downward-looking aDcp were averaged over the sampling time of each P63 bottle sample. Sample means were then averaged over all five (four in April) samples to obtain an average velocity profile for each profile location. The plots were compared against the logarithmic velocity profile for hydraulically rough flow,

$$u(z) = \frac{u_*}{\kappa} \ln\left(\frac{z}{z_0}\right) \quad (18)$$

where κ=0.41 is the von Kármán constant, z is the height above the bed, and $z_o = k_s/30$ is the bottom roughness parameter. The zero level of the bed is the mean level of the centre of the particles of the bed surface (Wiberg and Smith, 1987). Shear velocity was estimated from the slope of the logarithmic fit to the velocity profile, m, where $u_* = m\kappa$. The bed roughness, k_s, was back calculated using a known velocity, $u(z)$, at a known height above the bed, z.

Historical SSC profiles during similar daily discharge conditions were plotted with profiles obtained in this study and the Rouse profiles for comparison. Concentration profiles from 1986 were selected because the daily discharge during the point-integrated sampling (7150 m^3/s) was similar to the 2010 peak discharge (7002 m^3/s).

Total unit suspended sediment flux was obtained for total suspended sediment, suspended sand, and suspended silt/clay. First, suspended sediment flux for a vertical water column was calculated from the bin velocities and the sediment concentration at the bin height above the bed and summed over the entire water column using:

$$q_{s-vert} = \sum_{z=a}^{z=h} c(z)u(z)dz \quad (19)$$

where $c(z)$ and $u(z)$ are the sediment concentration and velocity, respectively, at height z above the bed, h is flow depth, and dz is the portion of the water column each point represents (Venditti, 2010). To obtain a measure of cross-channel suspended sediment flux, the flux for each vertical, $q_{s\text{-}vert}$, was multiplied by dy, the width of the panels 1 through 5 which is the portion across the channel flow each vertical represents (Venditti, 2010) using:

$$Q_s = \sum_{z=a}^{z=h} \sum_{y=1}^{y=5} c(z)u(z)dzdy \quad (20)$$

Often, only a single vertical is measured and while the Rouse model gives the vertical distribution of sediment in a water column, there is also cross-stream variation. Previous investigations of the cross-stream variation in sediment flux in the cross-section have established a method to convert the measured single-vertical depth-integrated samples to cross-section averages using a K-factor defined as:

$$K = \frac{c_R}{c_K} \quad (21)$$

the ratio of the cross-sectional average concentration c_R and the single-vertical depth-integrated samples c_K (as reported by McLean & Church (1986), but developed prior to that by WSC). The K-factor for the recent data was calculated using c_R equal to the mean of the depth-integrated samples taken at each of the 5 profile locations and c_K equal to the second depth-integrated sample obtained at the centre of the channel at profile 3. Daily average suspended sediment concentration was plotted against daily average discharge to display the seasonal hysteresis and to examine whether the recent data fit within the data from historical records.

2.3.2 Complementary Observations

The discharge data were analyzed by the WSC via standard WSC procedures using Teledyne RD Instruments WinRiver II software. The discharge reported is an average from four cross-stream transects. The transect data were also processed in software developed by the USGS (VMT Version 2.3, ftp://ftpext.usgs.gov/pub/er/il/urbana/pjackson/Software/ADCPSoftware/, accessed May 1, 2012) that provides cross-sectional maps of primary and secondary flows, averaged from the 4 transects obtained and projected onto a single line across the channel.

Bed material samples were analyzed for grain-size distribution in order to establish the size classes present on the bed at each vertical profile. The samples were also used to distinguish between the coarser bed material and finer wash material. Samples were dried, weighed and sieved at ½ phi increments. Particle-size distribution statistics were calculated using GRADISTAT Version 4.0 (Blott & Pye, 2001; software downloaded from www.kpal.co.uk/gradistat.html, accessed September 19, 2011).

2.4 Results

2.4.1 Flow in the cross-section

All discharge measurements collected during the sampling campaigns are displayed Table 3. Figure 7 shows the 2010 measured discharge at Mission and Hope as well as water levels at Mission. Discharge follows the commonly observed hydrograph shape for Mission with low-increasing flows in April to mid-May, rising flows in late May and early June, peak discharge during the June 27/28 sampling campaign and decreasing flows during the falling limb through July and August. The 2010 freshet peaked at approximately 7000 m^3/s. This is less than the mean annual flood of 9790 m^3/s.

Select cross-sections of velocity are displayed to represent low, rising and peak flow conditions for primary velocity on April 15, 2010, May 19, 2010 and June 28, 2010, respectively (Figure 11) and secondary velocity for peak flows on June 28, 2010 (Figure 12). The difference in daily discharge between the selected April and May flows is 2200 m^3/s and between May and June is about 2700 m^3/s. An increase in primary velocity is evident as flows increase. The thalweg is on river right (looking downstream) at y=300-350 m and the location does not vary greatly with flow. Mean velocities in the thalweg vary from 0.7-0.8 m/s at low flow to greater than 1.5 m/s at high flows (Figure 11). Profile 1 consistently displays the lowest velocities while profiles 2 and 4 have the greatest; profiles 3 and 5 have relatively moderate velocities (Figure 13). There is no persistent secondary circulation in the cross-section and some patterns may be due to vertical boat motion (Figure 12).

Vertical velocity variation is also evident. During low flows in April, average velocities ranged from 0.25 m/s to 0.6 m/s and displayed little variation throughout the

water column, evident by the approximate vertical line (Figure 13). In May, while flows were increasing, the velocity range increased to 0.5 m/s - 1.25 m/s (Figure 13). Velocities were lower near the bed and increased towards the surface. At peak flows in late June, velocities ranged from 0.75 m/s near the bed to 1.75 m/s near the surface, showing the greatest variation throughout the vertical water column evident by the lower slope of profile lines (Figure 13). Generally, velocity was lower near the bed, as expected, and increased toward the surface with greater difference between near bed and near surface occurring during peak flows. The velocity profiles obtained from the downward-looking aDcp were log-linear and fit the Law of the Wall well (equation 18) (Figure 13).

Table 3: 2010 Fraser River discharge measurements at Mission provided by WSC.

Sampling Campaign	Date Collected (dd-mmm-yy)	WSC Total Q (m^3/s)
Apr 15-16, 2010	15-Apr-10	2040
May 18-19, 2010	18-May-10	4062
May 18-19, 2010	18-May-10	4024
May 18-19, 2010	19-May-10	4378
May 18-19, 2010	19-May-10	4237
May 27-28, 2010	27-May-10	4898
May 27-28, 2010	27-May-10	4775
May 27-28, 2010	28-May-10	4991
May 27-28, 2010	28-May-10	5037
May 27-28, 2010	28-May-10	4967
June 7-8, 2010	07-Jun-10	5755
June 7-8, 2010	08-Jun-10	5736
June 7-8, 2010	08-Jun-10	5693
June 27-28, 2010	28-Jun-10	7002
Aug 3-4, 2010	03-Aug-10	4363
Aug 3-4, 2010	04-Aug-10	4272
Aug 3-4, 2010	04-Aug-10	4224
Supplementary measurement	02-Nov-10	2880

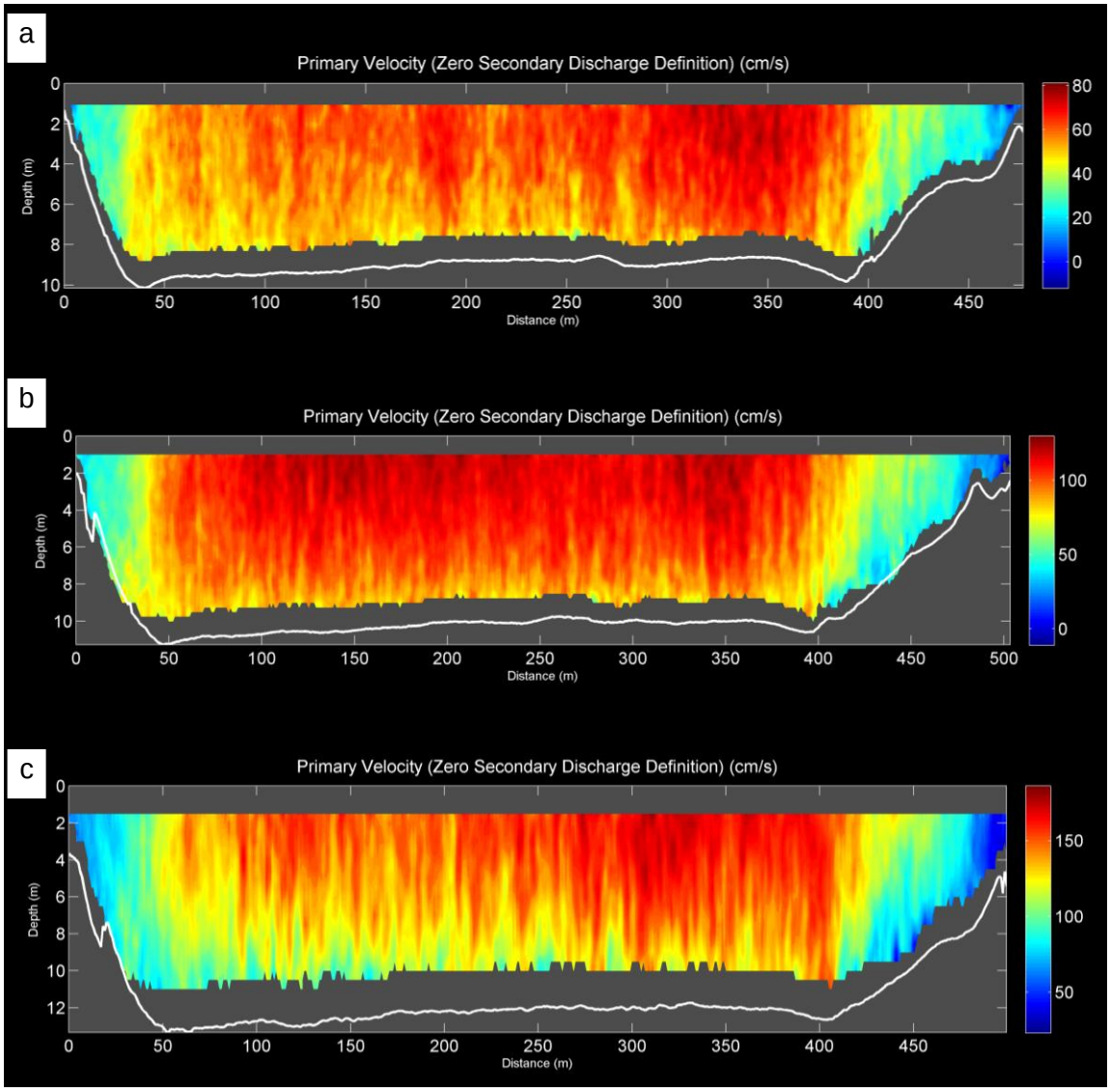

Figure 11: Primary velocity cross-sections from downward-looking aDcp transects. a. April 15, 2010 low flow conditions. b. May 19, 2010 rising flow conditions. c. June 28, 2010 peak flow conditions. Data were processed using VMT software. Note velocity scales differ for each plot. See Figures A-7 – A 12 for all the primary velocity cross-sections.

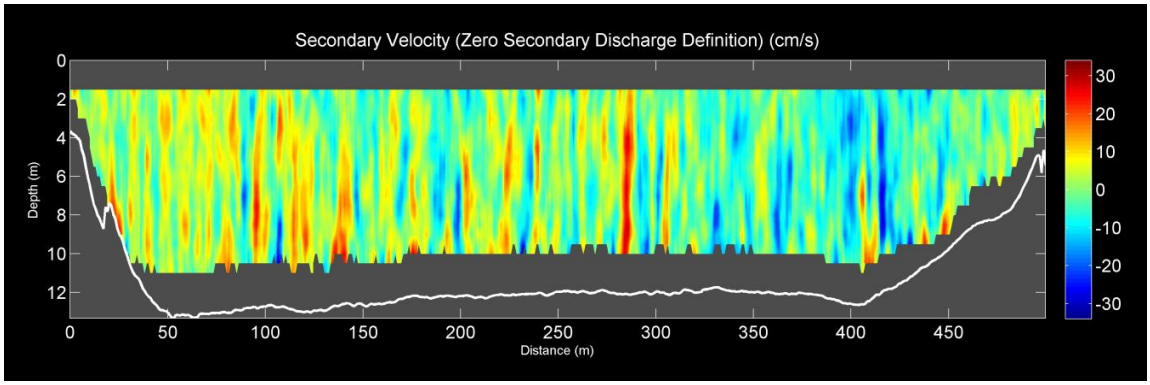

Figure 12: Secondary velocity cross-section for the peak flow conditions of June 28, 2010. See Figures A-7 – A-12 for all secondary velocity cross-sections.

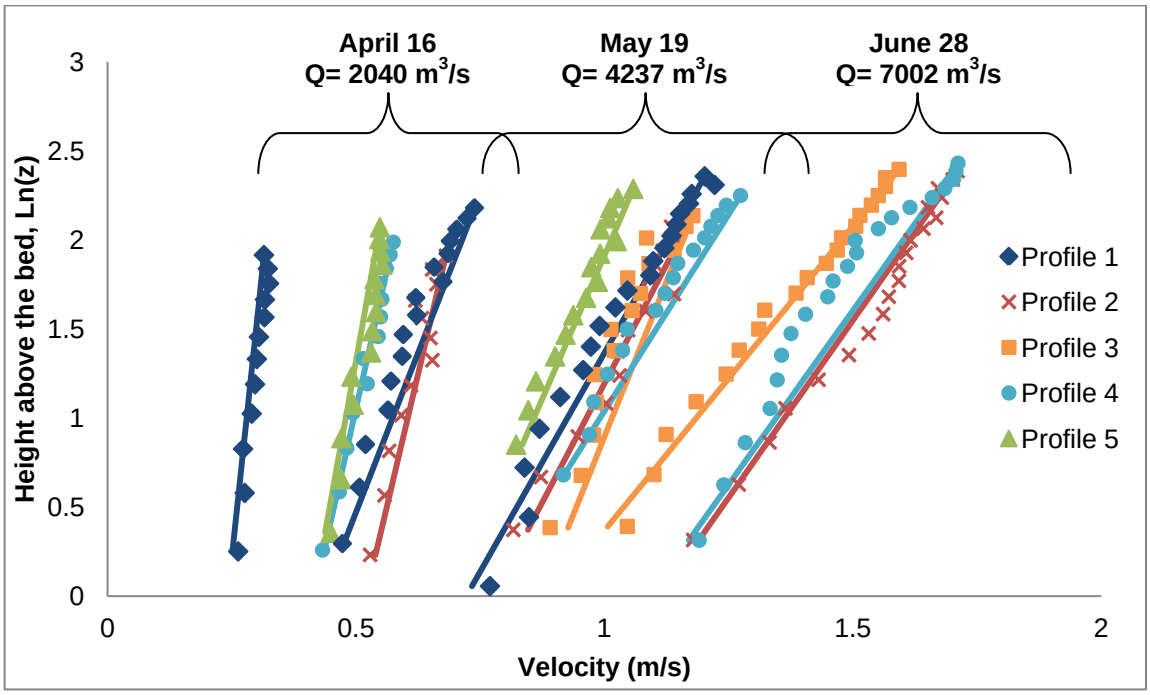

Figure 13: Velocity profiles for April 16 low flows, rising flows on May 19, and peak flows on June 28, 2010. The data points are the measured velocities and the solid lines are calculated from theory. See Figure A-13 for the velocity profiles for all campaigns.

2.4.2 Bed Material

Table 4 shows the mean, median and standard deviation of the bed material grain-size for each profile during the latter five sampling campaigns. No bed samples

were obtained in the first campaign. Bed material generally ranged from medium to coarse sand. At profiles 3, 4, and 5 there was a minor change in grain-size distribution through time and so the centre Profile 3 is displayed here (Figure 14). At these locations, bed material consisted of medium sand, with a mean that ranged from 230 to 380 microns. The change in the mean grain-size was 32%, 7.6% and 38% at sites 3, 4 and 5 respectively, through the sampling campaigns.

At profile 1, in the shallower portion of the channel where there are generally lower flows, the change in bed-material grain-size through the freshet was greater than at other profiles (Figure 15). Here, bed material coarsened through the freshet as the mean size ranged from fine sand on May 19 to medium gravel on June 28 and August 3. This implies that higher flows associated with the freshet entrained finer particles on the bed that were carried out of the reach. The difference between the mean grain-size of the May 19 and June 27 samples was great at 10.7 mm. The bed material sample from August 3, during the falling limb of the hydrograph was coarser than during pre-peak conditions but finer than at the peak with a mean grain-size of 7.60 mm.

The difference between the maximum and minimum mean grain-sizes at profile 2 was 1.12 mm. This coarsening did not occur between the rising (May 19) and peak flows (June 27) as expected from the pattern observed at Profile 1 (Figure 15). The largest mean grain-size was associated with the June 7 sample and finest on August 3.

Table 4: Selected bed-material grain-size statistics by profile and sampling campaign. Grain-sizes are stated in units of microns (μm). Note: the geometric mean and standard deviations are listed.

Profile	Statistic	May 19	May 27	Jun 07	Jun 27	Aug 03
1	Mean	144.9	162.7	492.9	10790	7596
	Std Dev	1.421	1.506	7.376	2.496	2.857
	D_{50}	110.3	163.7	161.1	12040	10120
2	Mean	910.4	707.6	1704	719.8	582.5
	Std Dev	2.126	1.949	3.818	2.107	1.683
	D_{50}	822.1	643.7	1001	607.5	546.7
3	Mean	363.4	381.8	369	374.4	257.1
	Std Dev	1.328	1.326	1.467	1.317	1.287
	D_{50}	378.3	393.8	366.7	382.7	263.6
4	Mean	317.7	291.9	297.6	299.6	293.5
	Std Dev	1.346	1.289	1.295	1.3	1.27
	D_{50}	318.1	296.1	299.6	300.4	295.4
5	Mean	262.9	231.9	283	256	374.9
	Std Dev	1.327	1.348	1.325	1.263	1.286
	D_{50}	276.5	239.6	288.4	270.1	387

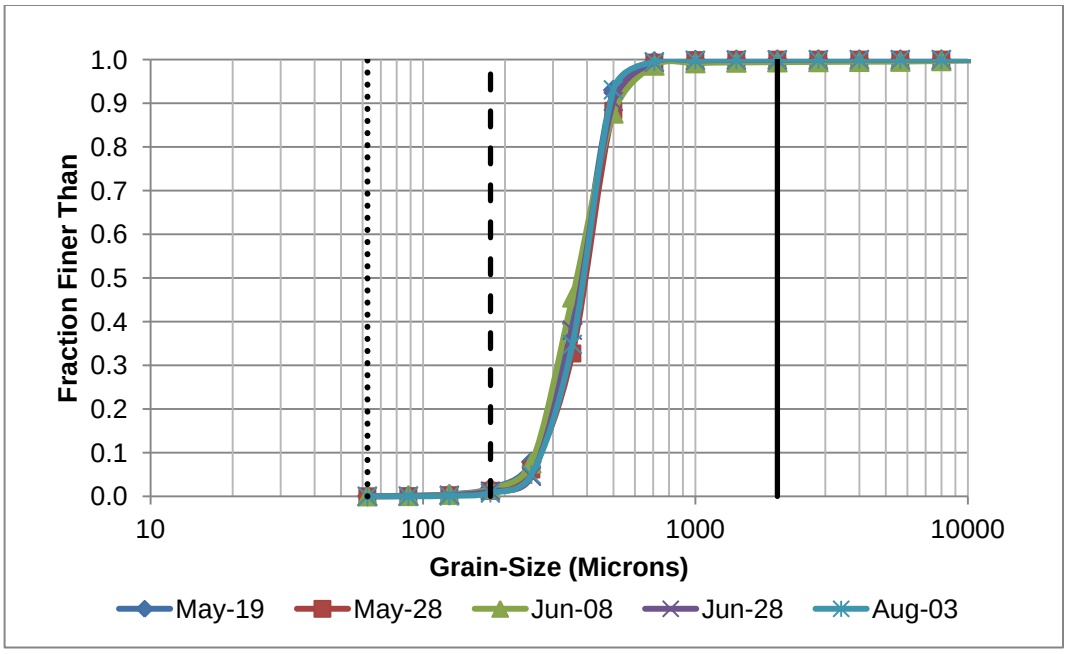

Figure 14: Profile 3 bed-material grain-size distribution for five sampling campaigns over the 2010 freshet. Solid line: gravel-sand division, dashed line: bed- wash material load division at 177 microns, dotted line: sand-silt division. See Figure A-14 for distributions for all profile locations.

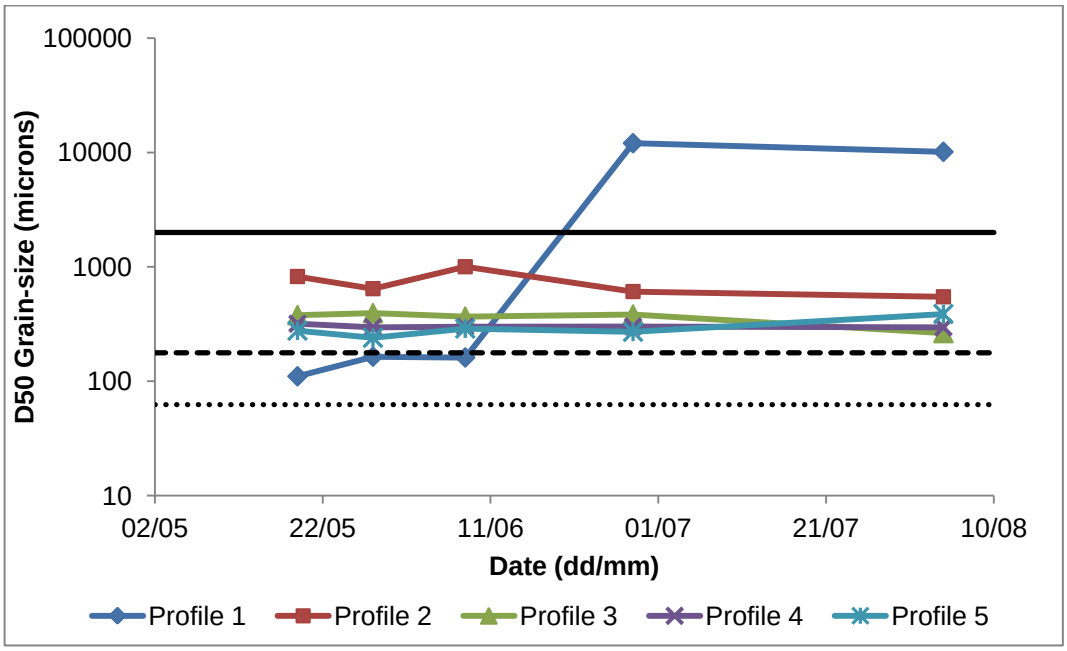

Figure 15: D_{50} bed-material grain-size for five sampling campaigns and 5 profile locations across the channel over the 2010 freshet. Solid line: gravel-sand division, dashed line: bed-wash material load division at 177 microns, dotted line: sand-silt division. See Figure A-15 for mean bed-material grain-size.

2.4.3 Suspended sediment concentration and flux

The LISST-Portable measures volumetric concentration in µL/L. As noted above, the instrument manufacturer recommends a conversion factor of 2.65, based on the density of clastic sediment, to convert to mass per volume concentrations. Figure 16 shows the filtered suspended sediment concentration (mg/L) plotted against the volumetric LISST concentrations (µL/L). Linear regression forced through the origin suggests that the conversion factor is actually 1.67 for this data set. Using a conversion factor of 2.65 over-estimates the sediment concentrations observed during the freshet (Figure 17 and Figure 18). The LISST results with this alternate conversion factor still tend to over-estimate sediment concentration during low flows (Figure 18 a), but improve during rising flows in mid-May (Figure 18 d). During peak flows in late June, the situation is the opposite and the 1.67 conversion factor leads to an underestimation from the LISST (Figure 18 g).

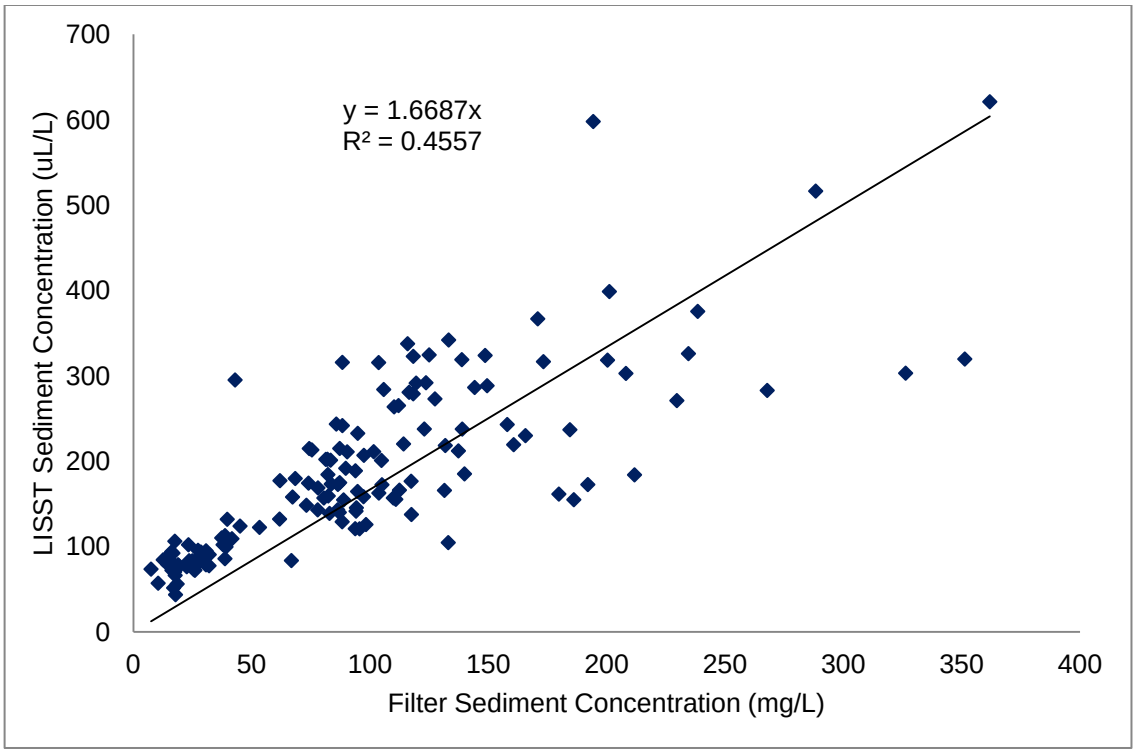

Figure 16: Filter suspended sediment concentration (mg/L) vs. LISST concentrations (µL/L).

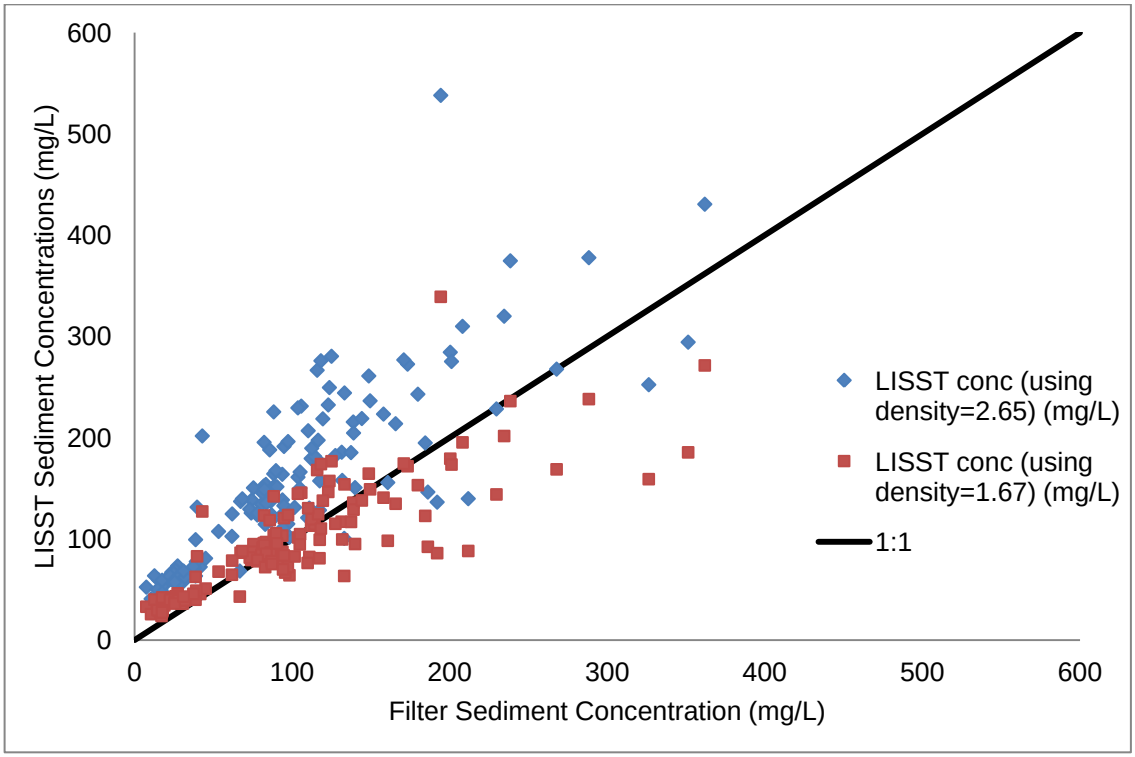

Figure 17: Filter sediment concentrations versus LISST concentrations in mg/L calculated using densities 2.65 and 1.67.

There are a number of possible reasons for the disagreement between the conversion factors. It could be the presence of particulate organic matter (POM) captured in the samples. However, combustion removed approximately 5% of the mass, suggesting this is not the case. Another reason for differences in density could be flocculation (Sequoia Scientific, 2010) that could result in a decrease in sediment concentrations. But, flocculation is typically stronger in saline waters than in fresh water and is more prevalent for clay particles. The cross-section at Mission is affected by tides, but this is a backwater effect and there is no saline water penetration. The fine fraction of sediment load in the Fraser is dominated by silt-sized particles. While I cannot rule out flocculation as the reason for the difference in the conversion factor, it is unlikely to produce the observed effect. A possible reason for the difference may be error caused by sediment loss during the process of running samples through the LISST-Portable device, where particles may have been trapped and therefore not included in the filter measurement. There was no obvious release of sediment during sample processing from the LISST, so this also seems unlikely. In light of this, it does seem likely that the volumetric concentration measured by the LISST is simply biased relative to the mass concentration due to different measurement principles.

Due to the discrepancy between the LISST and filter method concentrations and the uncertainty surrounding the LISST mass concentrations, the filter concentrations are used for the remainder of the calculations while only the grain-size distributions from the LISST are employed. This gives us accurate suspended sediment flux measurements, but the grain-size specific measurements may be biased.

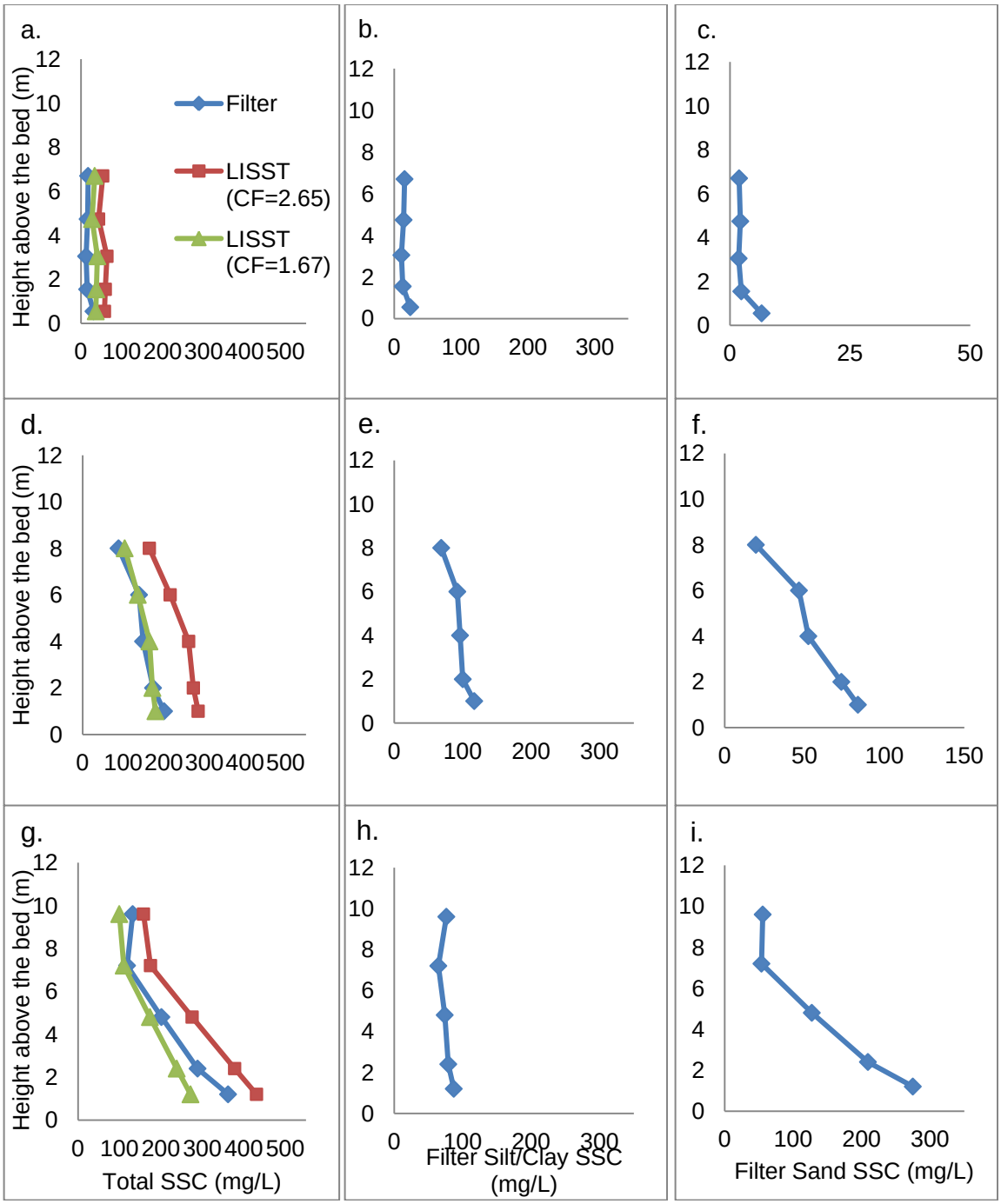

Figure 18: Profile 4 sediment concentration for the (a-c) April 15-16, 2010, (d-f) May 18-19, 2010 and (g-i) June 27-28, 2010 sampling campaigns. a, d, g are total SSC profiles from the traditional filter method and LISST-Portable method using conversion factors (CF) of 2.65 and 1.67. b, e, h are filtered silt/clay concentrations and c, f, i are the filtered sand concentrations. See Figures A-1 – A-6 for all concentration profiles.

Figure 18 shows that total SSC are dominated by fine sediment during low flows and that coarse sediment concentrations increase with higher flows. During rising and peak flows, a mix of coarse and fine particles is in suspension. Silt/clay concentrations are relatively uniform throughout the water column; while the coarser sand profiles are similar to total SSC and profiles show patterns of increasing concentration towards the bed. Low flows (April and August campaigns) are the exception as total SSC is dominated by finer silt and clay particles and sand concentrations vary less through the water column, implying that only the finest sand is present.

Suspended sediment median grain-size (D_{50}) varied both across the channel and throughout the water column over the freshet (Figure 19). During the April 15-16, D_{50} ranged from approximately 14-21 microns. During the rising flows sampled on May 18-19 and May 27-28, median grain-size was slightly larger ranging from 15- 47 microns, with the exception of a single sample on May 28 at profile 3 taken at 0.2h which had a D_{50} of 101 microns. Samples during June 7-8 varied from about 21 to 162 microns and during the peak flows recorded on June 27-28 ranged from approximately 21- 201 microns. Suspended sediment during post-freshet flows on August 3-4 had a D_{50} that ranges from 18-66 microns. Sediment at profile 1 always remained fine (<63 microns) and at profile 2 all sediment was fine except during the peak flow conditions of June 28. Sediment in the upper portion of the water column, above 0.6h, was always fine, across the channel.

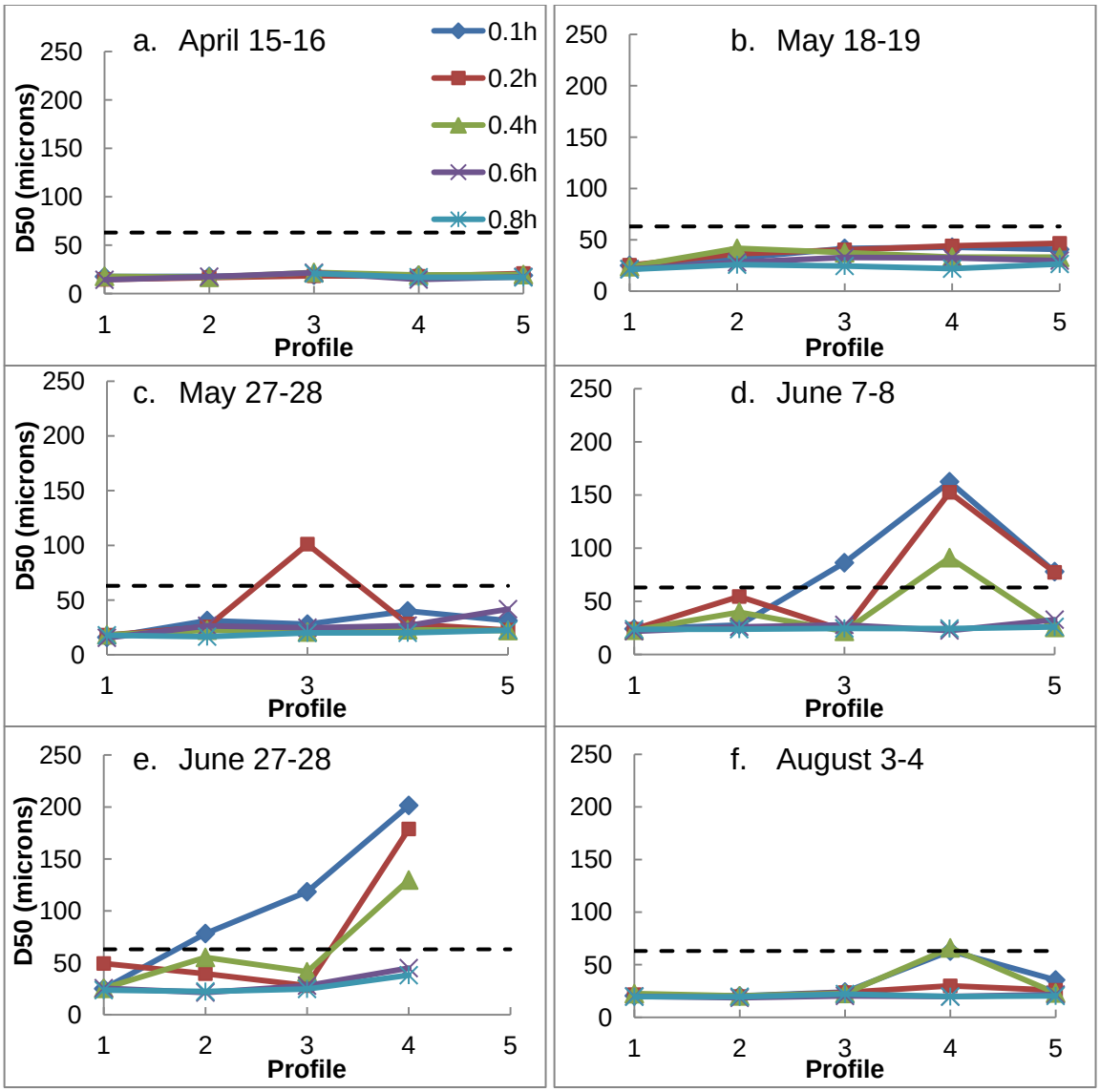

Figure 19: Suspended sediment grain-size (D_{50}) cross-channel and water column: April - August (a-f). Profile 4 that always yields the largest D_{50}, except for the May 27 profile 3 (c.). The dashed line signifies the sand-silt division at 63 microns.

The suspended sediment concentration profiles were plotted with the Rouse profile for each location across the channel and for all sediment sampling campaigns. Figure 20 compares the calculated Rouse profiles and the measured concentration profiles. Overall, the measured concentration profiles display much greater profile-profile variation across the channel than the theoretically calculated Rouse profiles. Profiles 3 and 4 are overrepresented by the theoretical Rouse profiles while profiles 1

and 2 are under represented. Profile 5 is overrepresented during lower flows and underrepresented during higher flows, though it is important to note that there is no measured concentration profile data for the peak flows at this location.

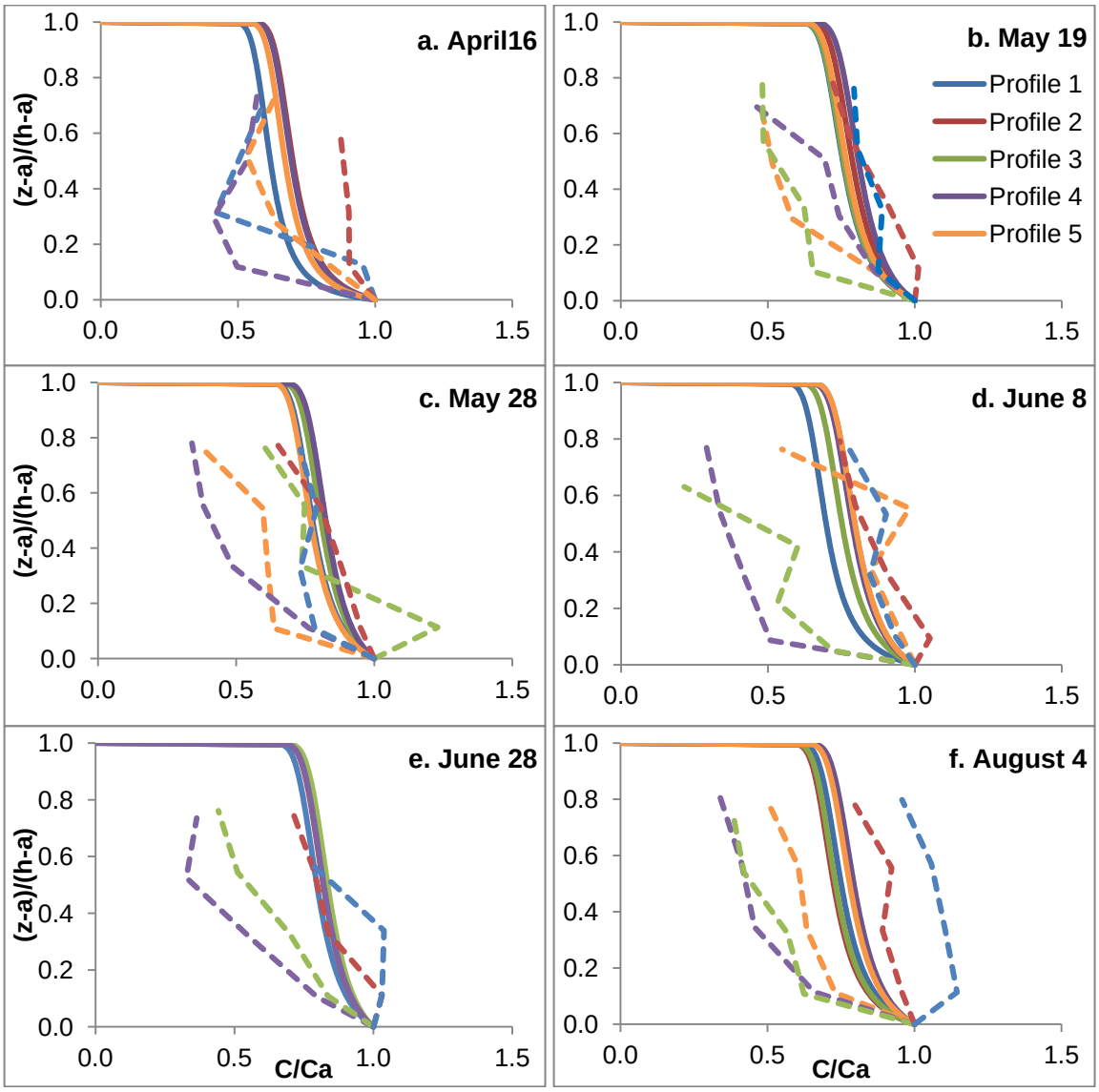

Figure 20: Suspended sediment concentration profiles. Dashed lines are sampling data points and solid lines are fit to the Rouse profile.

The sediment load at Mission is primarily fine sediment; however, a significant portion is coarser sand particles. Suspended sediment flux closely follows discharge through the freshet though there is some deviation in late May and early June when the

total sediment flux increased at the end of May, decreased in early June and increased to a maximum at the end of June (Figure 21). The peaks in total and sand flux coincide with peak measurements of discharge. However, the peak in the silt/clay portion occurred in late May prior to the peak in total sediment flux and corresponds with the increase in total flux (Figure 22 and Figure 23).

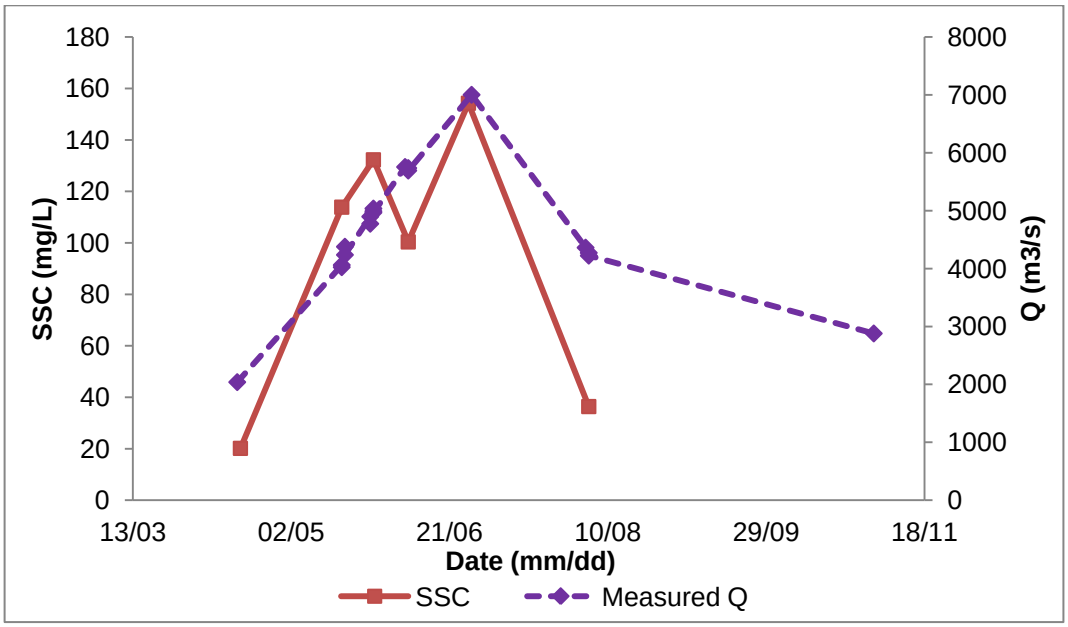

Figure 21: Channel-averaged total SSC and discharge at Mission. The points are joined with lines to show the observed seasonal pattern.

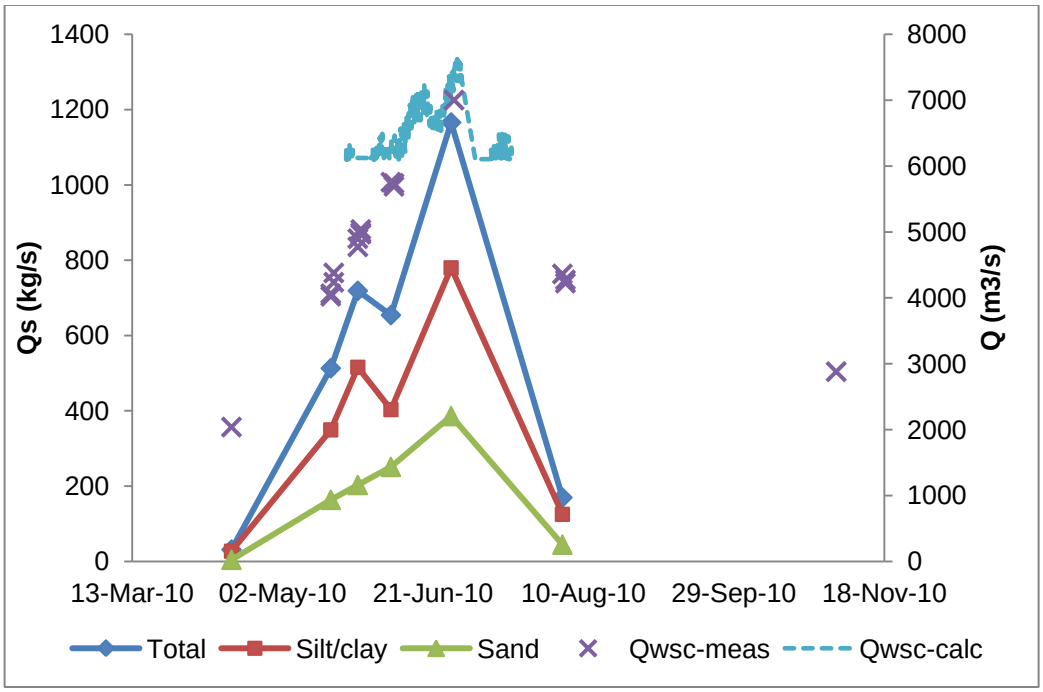

Figure 22: Suspended sediment flux (total, silt/clay, and sand), measured discharge and flow record at Mission. The points are joined with lines to show the observed seasonal pattern.

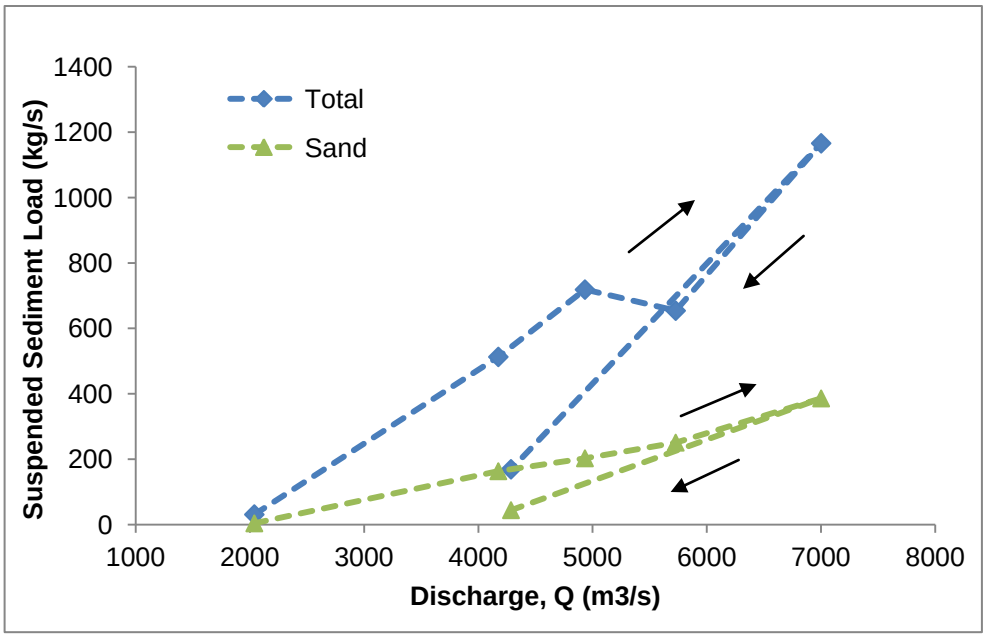

Figure 23: Daily suspended sediment load over a range of discharge conditions. Points are joined to illustrate hysteresis. Arrows show direction of hysteresis loop.

2.5 Discussion

2.5.1 Characteristics of suspended sediment flux in the reach

The variability in flow affects the SSC and flux across the channel. Flow is greatest in the centre left of the channel indicating the position of the thalweg and significantly lower near the right bank (looking downstream). This suggests that there is a larger sediment flux through the centre-left than the centre right portion of the channel. The centre SSC profile 3 is located in the thalweg and all particle sizes of the suspended load are transported through there, which makes it a good indicator for total channel SSC via the K-factor approach. Profile 4 is also located in the thalweg and so one would expect profile 4 to correlate well with channel SSC and flux but profiles 1 and 5 are located in low flow zones and therefore would not be good indicators. Profile 2 is not the ideal location for the K-factor approach as it is in the centre-right of the channel where less flow occurs.

Sediment flux and grain-size vary throughout the freshet. At low flows in April through late May, the majority of the suspended load is fine silt-clay. The daily load ranged from approximately 2700 tonnes in April to 62000 tonnes in late May. At higher flows, sand is also present in the suspended load. In early June, the daily suspended-sand load was over 21000 tonnes and reached over 33000 tonnes at peak flows in late June. It appears an approximate threshold for significant sand suspension in the reach may be 5700 m^3/s, which occurred during the June 8 campaign when increased amounts of sand were found in suspension.

Figure 24 compares bed and suspended material (at 0.1h) at the centre profile 3 over the freshet. The overlap in grain-size suggests that sand in suspension is in fact bed material in the reach. During low-moderate flows on May 18-19, May 27-28 and August 3-4, sand greater than 177 microns represented 15%, 16%, and 10%,

respectively, of suspended material. During the high and peak flows of the June 7-8, 2010 and June 27-28 campaigns, suspended material consisted of 36% and 41%, respectively, sand greater than 177 microns. This implies that bed material suspension occurred rather than wash load from upstream sources. A 177-micron division point was chosen to separate bed and wash material as less than 2% of bed material particles are smaller than 177 microns. The grain-size of 177 microns is also consistent with the bed-wash load material division-point described in historical records (McLean and Church, 1986).

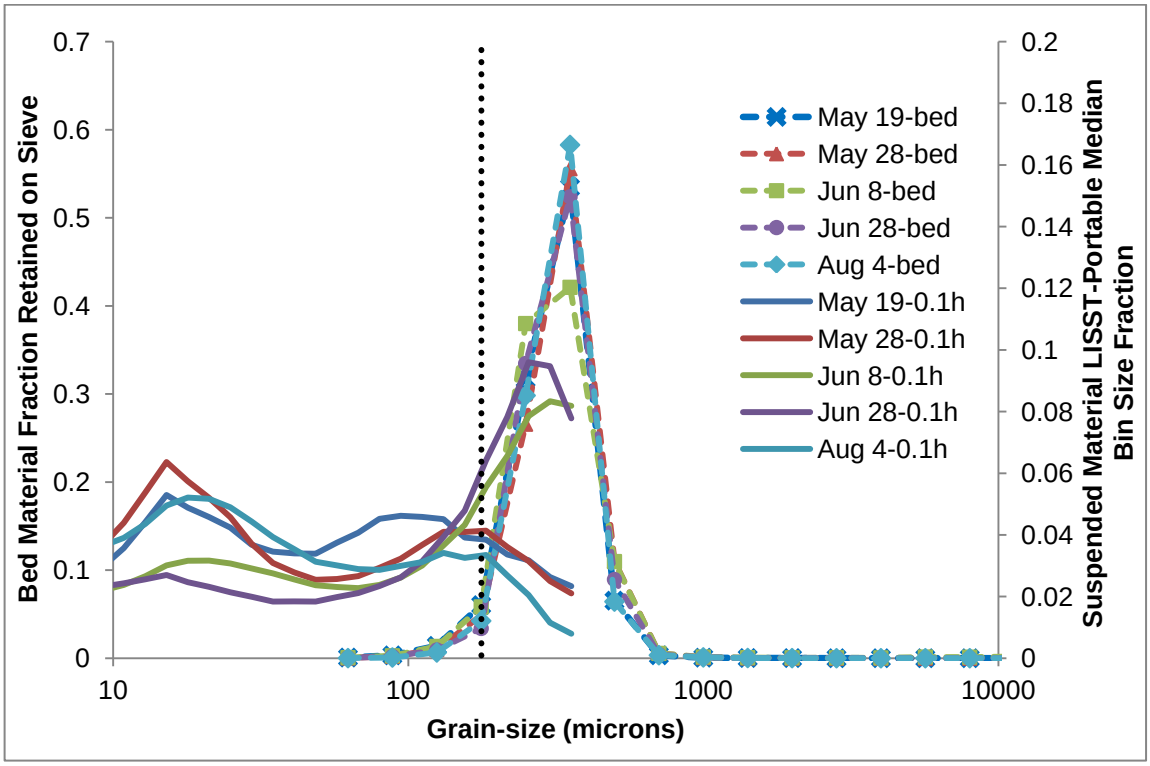

Figure 24: A comparison of bed material and LISST-Portable suspended material (at 0.1h in the water column) grain-size for the centre profile 3. Note: axes have different scales to highlight trends and the dotted line is the 177-micron wash-bed material division point.

It is common in rivers for peaks in sediment flux to lead the hydrograph, resulting in a clockwise hysteresis effect (Humphries et al., 2012). There appears to be a strong

clockwise hysteresis effect in the wash load (silt/clay) component suggesting that fine sediment is entrained as flows are rising and depleted as peak flows are reached (Humphries et al., 2012). This is displayed in the steeper relation between sediment flux and flow on the rising limb than the falling limb. A clockwise hysteresis is also evident in the sand fraction, but it is less pronounced than for the finer sediment. This suggests that sand is less supply-limited than finer sediment because it is entrained from the bed, while silt/clay is supplied only from upstream sources.

Another interesting result is that the total sediment flux peaked twice (Figure 22), once before the peak is water discharge and then again at peak flows. The wash load (silt/clay) has this same pattern, but the sand load peaked only at high flows. This suggests that the sand is supplied from the bed, or it becomes wash load when flow reached a threshold and sand is blown out of upstream storage channels.

2.5.2 Can we model suspended sediment transport in the reach with available theory?

Four ways have been proposed to define the variation in fluid diffusivity with depth (eq. 3-6) that can be used to derive 4 equations to model sediment concentration profiles (eq. 7-10). The velocity profiles in the reach are log-linear with height above the bed suggesting the parabolic distribution (eq. 5) is the correct equation to use. Integration of the parabolic representation of diffusivity (ε) yields the Rouse equation for sediment transport (eq 7).

However, the Rouse equation does not predict the vertical distribution of the sediment flux well (Figure 20). There is a similarity in the overall shape, but measured profiles display more variation both across the channel and through the water column than the Rouse profiles predict. Generally, Rouse theory overestimates concentrations higher in the column, however the fit between the observed and theory appears to

depend on the flow conditions and the location along the cross-section in the channel. This implies SSC and flux in the reach cannot be modelled without continuous monitoring across the channel.

2.5.3 Evaluation of historical records

In Figure 25, 2010 concentration profiles during peak flows conditions (Q=7002 m^3/s) are plotted with 1986 concentration profiles obtained during comparable daily flow (Q=7150 m^3/s; ~2% difference in discharge). In 1986, concentrations at the surface ranged from 250 to 350 mg/L and from over 400 to over 1700 mg/L at the bed. It is important to note that an additional two samples were obtained, one closer to the bed and one closer to the surface, during the 1986 sampling. In 2010, our highest measurement was at 0.9h and lowest at 0.1h. In 1986, concentrations near the surface (0.9h) were between 330 and 450 mg/L, while near the bed (0.1h) they 380 and 830 mg/L. Profiles from 2010, ranged from under 100 to just over 200 mg/L near the surface, and from 100 to near 400 mg/L near the bed. Both years display similar cross-channel variation of increasing concentrations from profile 1 location to profile 4 (Figure 25).

Suspended sediment concentrations were significantly lower in 2010 than in 1986 (Figure 25). There are a number of potential reasons for this difference. Perhaps the sequence of seasonal flows is a factor. For example, in 2007 peak daily flows were high (11,800 m^3/s), which can clear out sediment stored in the channel. In 2008 and 2009, the flows were low to moderate (10,900 m^3/s and 8770 m^3/s, respectively), so sediment may have moved back into storage. The lower concentrations in 2010 could also be a result of sediment being stored in the back channel and sloughs resulting in a decreased flux. Alternatively, the sequence of flows in the 1980s could have led to increased concentrations because storage areas were filled and suspended sediment

was transported downstream. Another reason may be that the channel is aggrading at Mission, which is important to monitor in the future.

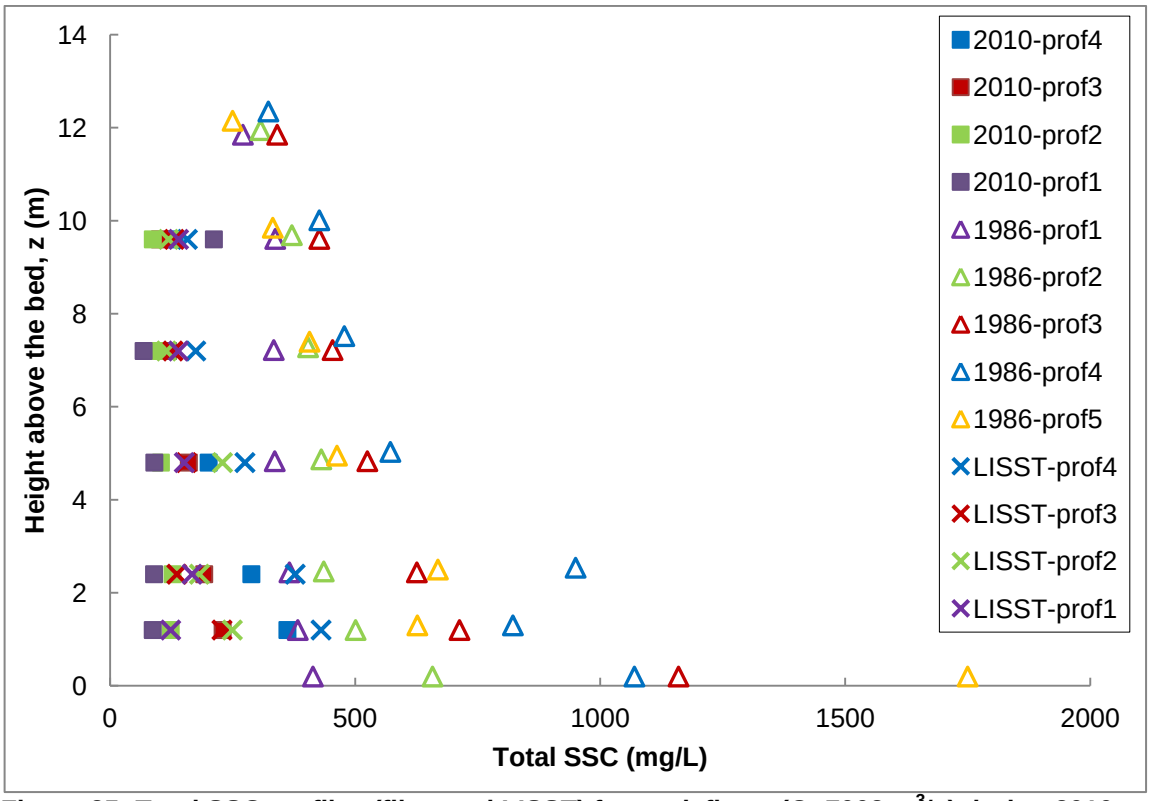

Figure 25: Total SSC profiles (filter and LISST) for peak flows (Q=7002 m^3/s) during 2010 and 1986 (Q=7150 m^3/s) discharge flows.

Historic and 2010 K-factors as a function of discharge are shown in Figure 26. There were sufficient data available for only 1984, 1985, and 1986. In their 1986 investigation, McLean and Church (1986) found the K-factor at Mission varied systematically: higher at low flows and becoming noticeably lower at higher discharges. High K-factor values during low flow conditions are due to the difference in sediment source. During low flows, sediment in suspension is wash load supplied from upstream sources distributed across the channel, increasing the K-factor ratio. During high flows, bed material becomes entrained in the flow, decreasing the ratio of cross-sectional average concentration to single-vertical depth-averaged concentration. The 2010 K-factor data change in a similar manner (Figure 26). However, the average K-factors

appear to have increased over time. The K-factor ranged from approximately one to almost 1.6 during low flows and from 0.6 to 0.8 for high flows. It increased from 1984 to 1986 from approximately 0.8 to 0.9 and from 1986 to 2010 from 0.9 to 1.0. The K-factor varied greatly, but the pattern displayed in 1984-1986 holds and so the K-factor method is still an appropriate approach. The 2010 K-factor is the highest in the available record and so the K-factor value appears to be different. This suggests that conditions may be changing at Mission and that continuous monitoring of sediment flux is needed because historic records may be only somewhat representative of current conditions.

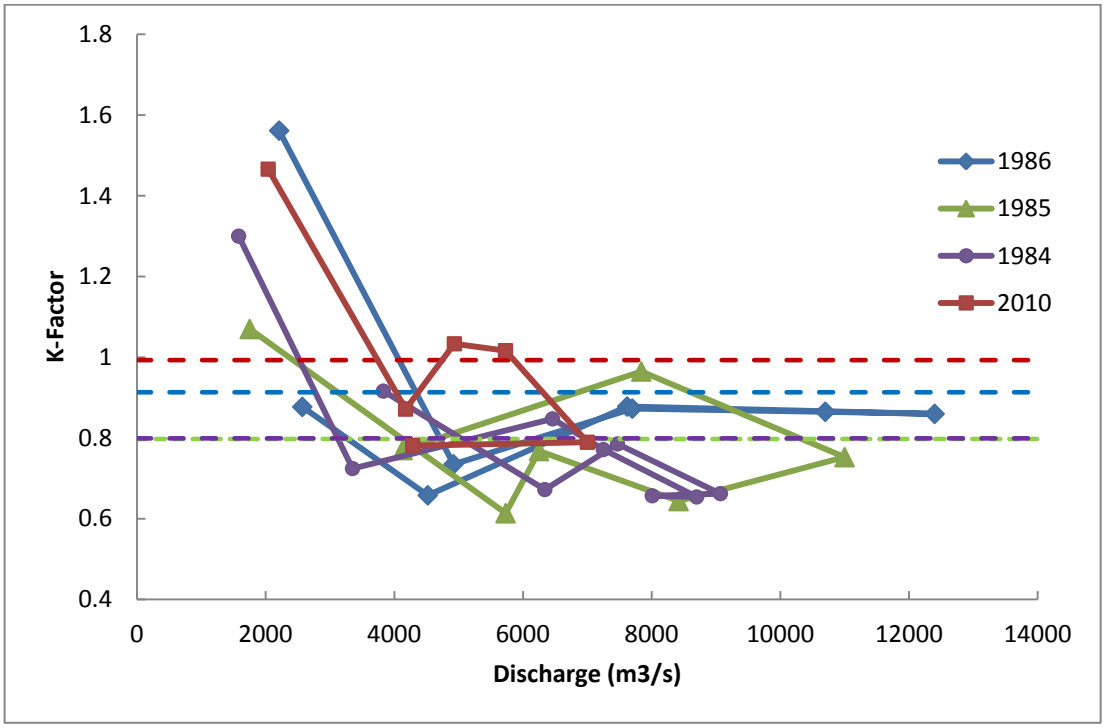

Figure 26: Current and historic K-factor with discharge. The dashed lines are the year's average K-factor. (Data source: WSC, http://www.wateroffice.ec.gc.ca/index_e.html, accessed Nov. 2011)

The relation between daily total SSC and discharge, separated into pre- and post-peak conditions, displays seasonal hysteresis (Figure 27). It is difficult to detect if the current rating curve is different from the historic rating curve because there is only one year of data. But the relation for the 2010 data appears steeper on the rising limb

and falling limb. Continued observations for at least a few more years are needed to determine if 2010 is indeed an aberration. The lack of agreement between modelling based on Rouse equation and observed distribution of sediment concentration, further suggests continuous measurements are needed to appraise dredging requirements and to guide river management practices.

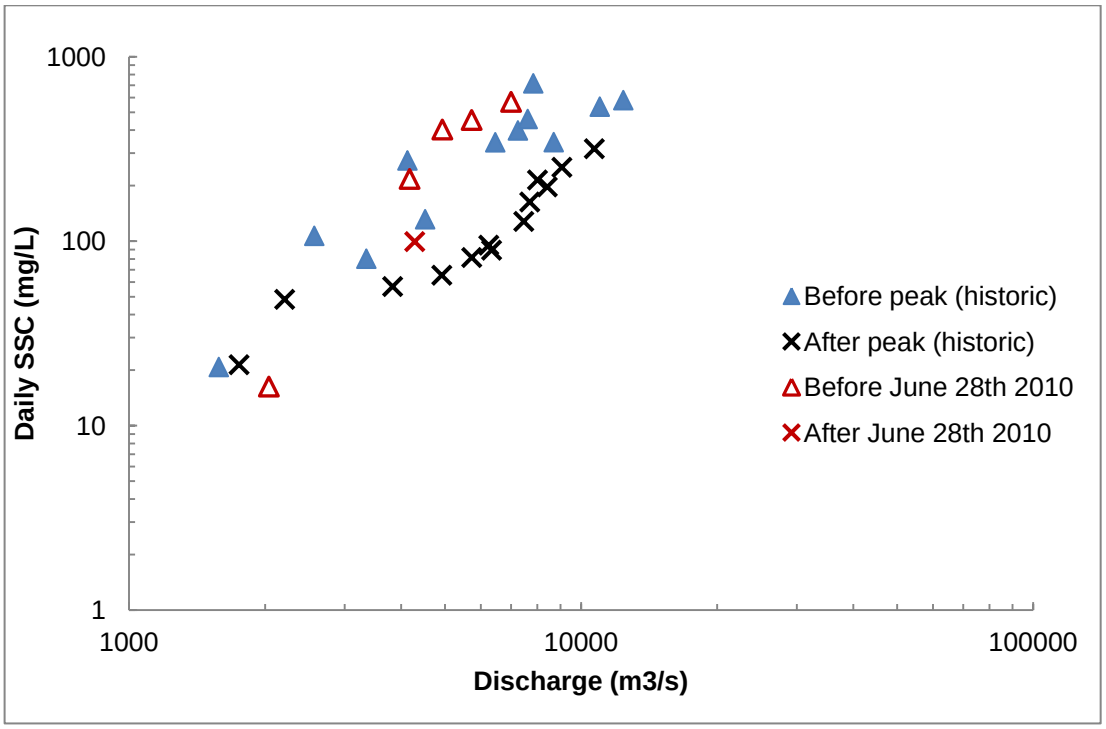

Figure 27: Historic and 2010 seasonal hysteresis in daily average total SSC with discharge. Historic data consists of the years 1984, 1985, 1986 (data source: www.wateroffice.ec.gc.ca, accessed March 2011.)

2.6 Conclusion

Suspended sediment concentration, bed material, velocity and discharge were measured on the Fraser River at Mission gauge over the 2010 freshet. Total suspended sediment concentrations were obtained and flux was calculated from isokinetic, filtered, bottle samples. Flux was broken into coarser sand-sized particles and finer silt-clay fractions using grain-size distributions obtained from a LISST-Portable. The estimates of concentration and flux were compared with historical records based on sediment rating curves from the Water Survey of Canada's 1965-1986 sediment monitoring program. The results demonstrate that:

1. A discrepancy exists between sediment concentrations reported by the LISST-Portable and those found via traditional filtering methods. The manufacturer suggests that measured volumetric sediment concentrations can be converted to mass per volume concentrations using a conversion factor of 2.65. This work shows a conversion factor of 1.67 is more appropriate for the Fraser River at Mission.

2. The daily load of silt/clay at Mission in 2010 was approximately 2700 tonnes per day at low flows (~2000 m^3/s) and 67000 tonnes per day at peak flow (~7000 m^3/s). Most of the transport is fine silt and clay, which are supply-limited, so continuous monitoring of sediment concentrations and grain-size is required.

3. There is a hysteresis effect in the sediment flux. Grain-size discrimination reveals a strong hysteresis for silt-clay, but a weaker effect for sand.

4. During high flows, 36% - 41% of suspended material is sand greater than 177 microns. A 177-micron bed-wash material division point implies that bed material suspension occurred rather than wash load from upstream sources. The grain-size division point of 177 microns is consistent with the bed-wash load material division-point described in historical records.

5. Concentrations in 2010 are significantly lower than the historic 1986 records, suggesting further observations are needed at Mission to maintain the rating curve.

6. The K-factor, which is the relation between sediment flux in the centre of the channel and the total flux, displayed a similar hysteresis with discharge in 2010 to the historical record, but was greater in magnitude.

7. Modelling based on Rouse equation does not match the observed distribution of sediment concentrations, which suggests continuous and current measurements are needed to appraise dredging requirements and to guide river management practices.

3: Hydroacoustics

3.1 Introduction

Our ability to predict the timing and quantity of suspended sediment transport is limited because fine sand, silt and clay delivery are supply-limited, requiring empirical modelling approaches of limited temporal stability. A solution would be the development of continuous monitoring techniques capable of tracking sediment concentrations and grain-size. The sediment budget for lower Fraser River currently is based on historical sediment rating curves developed from data collected from 1965-1986 by the Water Survey of Canada. Re-establishing the sediment-monitoring program using hydroacoustics is explored by evaluating the use of a 300 kHz side-looking acoustic Doppler current profiler (aDcp), mounted just downstream of the sand-gravel transition at Mission. I also evaluate a downward-looking 600 kHz aDcp measuring vertical profiles. The instruments are assessed for accuracy in sensing total concentration, as well as discriminating between sand and silt-clay grain-sizes.

3.2 Methods

3.2.1 Deployment

3.2.1.1 600 kHz downward-looking aDcp

A downward-facing 600 kHz Teledyne RD Instruments Workhorse Rio Grande aDcp (V-aDcp) was used to capture vertical profiles at five positions across the channel (Figure 29). The V-aDcp was deployed from a 19-ft launch and was connected to a laptop onboard; data were streamed and logged through WinRiver software. A Trimble GPS rover operated in Real Time Kinematic mode was used for aDcp positioning. Measurements of acoustic signal intensity and velocity through the water column as well as, depth were recorded at ~1 Hz. The downward orientation of the aDcp allowed velocity profiles to be obtained for the purpose of suspended sediment flux calculations.

Sampling was conducted during six two-day campaigns during the 2010 freshet: April 15-16, May 18-19, May 27-28, June 7-8, June 27-28, and August 3-4. The sampling was scheduled to ensure the rise, peak and fall of the hydrograph were captured. Samples were taken approaching low tide to avoid tidal influences on flow.

3.2.1.2 300 kHz side-looking aDcp

A horizontally-oriented 300 kHz ChannelMaster H-aDcp (Figure 28), manufactured by Teledyne RD Instruments, was mounted on the Mission Harbour dock just upstream of the Mission railway bridge (Figure 28). The dock and ADCP is located on the right side of channel (looking downstream) within the study cross-section shown in Figure 5. The aDcp was set to collect data in 128 bins, each two metres in length. It was selected for its superior range in large rivers and collected data to its maximum range of 259 m across the channel with a 3-metre blanking distance (Figure 29). It was mounted with a 1.2-degree tilt downward to detect movement near the bed. The aDcp

emits pulses of acoustic energy in a beam with a spread angle of 2.2 degrees. The instrument reports velocity calculated from observed Doppler shifts in signal frequency, as well as acoustic backscatter that is reflected back to the instrument by particulate matter in the flow, temperature, stage, and pressure.

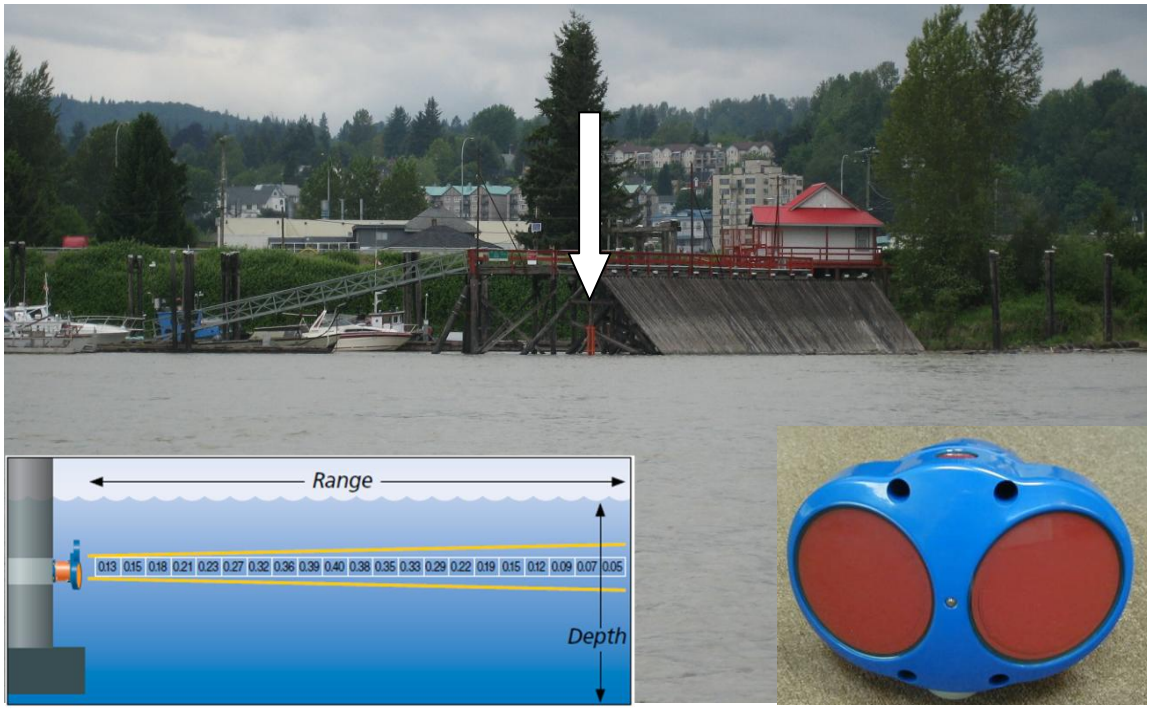

Figure 28: H-aDcp location in Fraser River at Mission (arrow). Inset images: ChannelMaster H-aDcp and example set-up from Teledyne RD Instruments image source: http://www.rdinstruments.com/channelmaster.aspx, accessed March 30, 2010. Numbers are observed velocities.

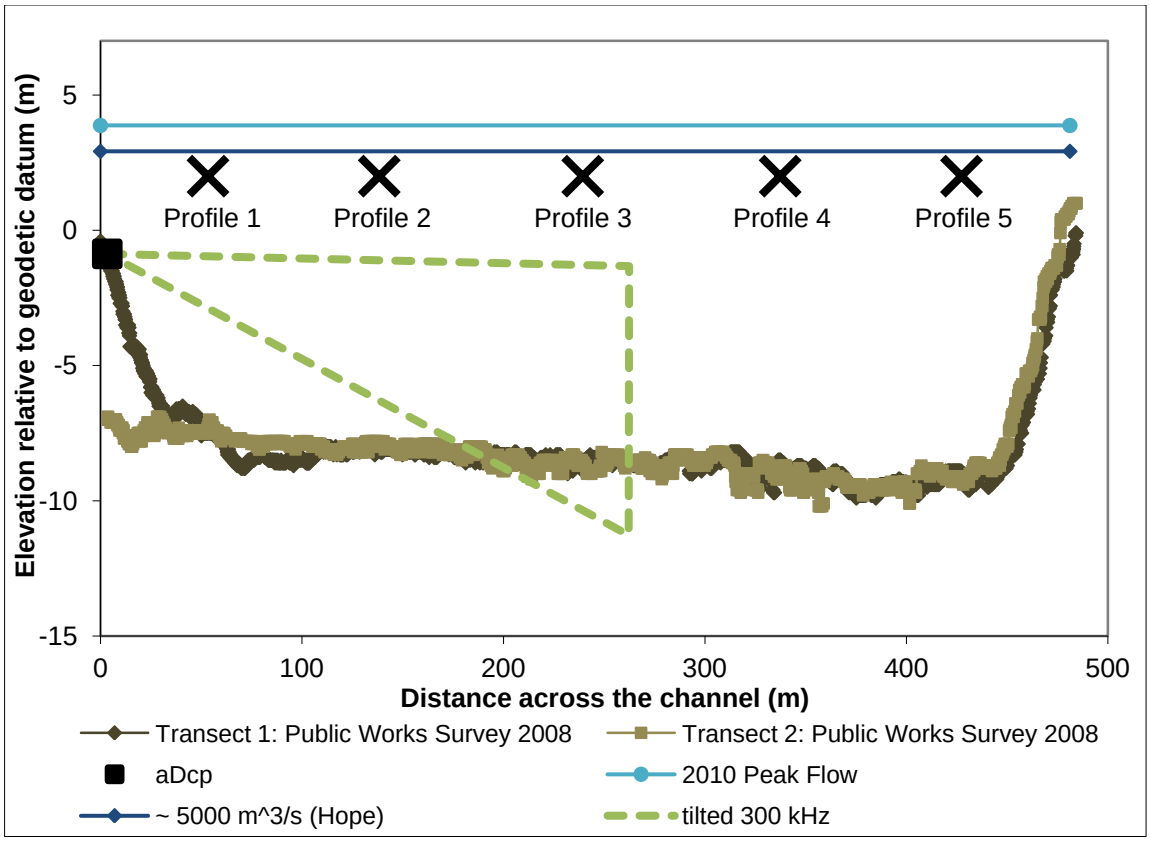

Figure 29: The aDcp mounting and beam position, profile locations in the channel relative to 2010 Mission water level (peak and when flow at Hope was ~5000 m^3/s), and bed elevation. When flow at Hope reaches approximately 5000 m^3/s, significant bed material suspension occurs (McLean et al., 1999). Beam shape appears asymmetric due to difference in the vertical and horizontal scales.

The data were logged to a computer on the dock (Figure 30) at approximately 0.2 Hz. Data can be averaged and viewed in the instrument's accompanying Channel Master software WinH-aDcp. The instrument began collecting data on April 12, 2010 and ran almost continuously until August 9, 2010, with the exception of a power outage on June 26, 2010. There were minor interruptions throughout the summer due to local power failures. From August to November 2010, the aDcp and computer were powered by a battery charged by solar panels. As the days shortened, the amount of time the solar power kept the battery charged declined. So data were collected intermittently (Table 5 lists data collection dates).

Figure 30: Work station for aDcp housing the computer controlling the instrument and logging data.

Table 5: Horizontal aDcp data collection times

Horizontal aDcp Data Collection Times
April 12- June 26, 2010
June 27- August 9, 2010
August 19-31, 2010
September 16-25, 2010
October 7-14, 2010
October 21-26, 2010
October 28, 2010
November 1-3, 2010

3.2.2 Calibration and supplementary measurements

In order to calibrate the aDcps, suspended sediment samples were collected using a P63 sampler co-located with the acoustic sensors. The P63 sampler was

deployed from the same launch as the 600 kHz aDcp, two metres away on the opposite side of the vessel. Point-integrated suspended sediment samples were obtained at distances and depths across the channel aligned with the horizontally-oriented aDcp beam. The precise lateral position and vertical position of each sample were vital for co-location of physical sediment sample and the acoustic beam. Vertical position of the P63 samples was controlled by a motorized winch and depths below the water surface were measured using a manual USGS B-reel, also attached to the sampler. The boat's location in the cross-section from the aDcp was measured using a laser distance meter. These positions were marked on electronic marine navigation charts, allowing for reoccupation of the same vertical profile locations during each campaign.

Suspended sediment bottle sampling for the 600 kHz instrument's calibration was conducted simultaneously with the aDcp profiles at five verticals across the channel. The P63 sampling consisted of point samples at five approximate depths: 0.1h, 0.2h, 0.4h, 0.6h and 0.8h, where h is flow depth. This was less strictly followed during low stage and flow conditions in April, where sometimes only 4 points in the water column were sampled and so sampling depths differed from the aforementioned procedure. During the June 27-28 campaign, only four vertical profiles (profiles 1, 2, 3, 4) were collected because the winch for the electric motor broke; no data were collected at profile 5. Samples were processed for grain-size distribution using a LISST-Portable, by Sequoia Scientific and filtered for a measure of total SSC. For more information on the bottle sampling, see section 2.2.1.

During each sampling campaign, the Water Survey of Canada obtained several discharge measurements. A final supplementary measurement was also taken on November 2, 2010. Data were collected with a Teledyne RD Instruments downward-looking 1200 kHz aDcp, except for June 28 when peak flows had depths beyond the

range of the 1200 kHz instrument and so a 600 kHz instrument was used. For each measurement, four cross-stream transects were obtained approaching low tide.

3.2.3 Data Processing

The processing procedure is based on a locally calibrated sonar equation:

$$B = 0.43A + 2log_{10}(R) = 2\alpha_w R = 2\alpha_s R \quad (22)$$

where B is range-normalized backscatter, in decibels (dB); A is amplitude of the signal strength, in counts; 0.43 is a default scale factor (if otherwise unknown); R is distance, m along beam; α_w is water absorption coefficient, dB/m; and α_s is sediment attenuation coefficient, dB/m. The aDcp reports amplitude of acoustic signal strength (A) as echo intensity (EI) in counts. Following a methodology developed by Topping et al. (2007) at the USGS, EI is converted into measured backscatter (MB) in decibels, with corrections for both water absorption and sediment attenuation producing water-corrected backscatter (WCB) and sediment-corrected backscatter (SWCB). The first step is to convert EI to MB

$$MB = sf * EI \quad (23)$$

where sf is the instrument and beam specific scale factor. Next, WCB is calculated as

$$WCB = MB + 20log_{10}(R) + 2\alpha_w R \quad (24)$$

where α_w is the water absorption coefficient computed assuming zero salinity from

$$\alpha_w = 8.686 * 3.38x10^{-6}\frac{f^2}{f_T} \quad (25)$$

$$f_T = 21.9x10^{\left(6-\frac{1520}{T+273}\right)} \quad (26)$$

f is the frequency of the aDcp and T is the water temperature in degrees Celsius. SWCB is calculated by correcting for two-way sediment attenuation losses

$$SWCB = WCB + 2\alpha_s R \quad (27)$$

where α_s is the sediment attenuation coefficient computed as follows:

$$\alpha_s = -\frac{1}{2} S_{WCB,R} \quad (28)$$

where $S_{WCB,R}$ denotes the slope of the least-squares linear regression between WCB and R. Topping et al. (2007) and Wright et al. (2010) have argued that WCB can be related to total sediment concentration, SWCB to sand concentration, and silt-clay concentrations to sediment attenuation coefficient.

Correlation curves were developed from simple linear regression, corrected using the reduced major axis method (Mark and Church, 1977) between bottle sample SSC and measures of corrected backscatter and the sediment attenuation coefficient.

Bin-by-bin correlations with the point samples were examined for both instruments (only the bins from the aDcp that corresponded to the bottle sampling points were used in the correlation curve). The bin-by-bin method of calibration is a deviation from the Topping et al. (2007) procedure designed to test an alternate approach. The correlation equations were used to calculate estimations of SSC from aDcp WCB and/or SWCB. H-aDcp backscatter measures are semi-continuous and so were averaged daily before further analysis.

3.3 Results

3.3.1 aDcp calibrations

3.3.1.1 V-aDcp

The downward-looking aDcp collected vertical profiles at 5 locations across the channel over the rising, peak and falling stages of the hydrograph. Vertical backscatter profiles increased towards the bed during all 6 sampling campaigns (Figure 31 a-e). The

backscatter signal was highest during peak flows on June 27-28 and lowest during pre- and post-freshet flows recorded on April 15-16 and August 3-4.

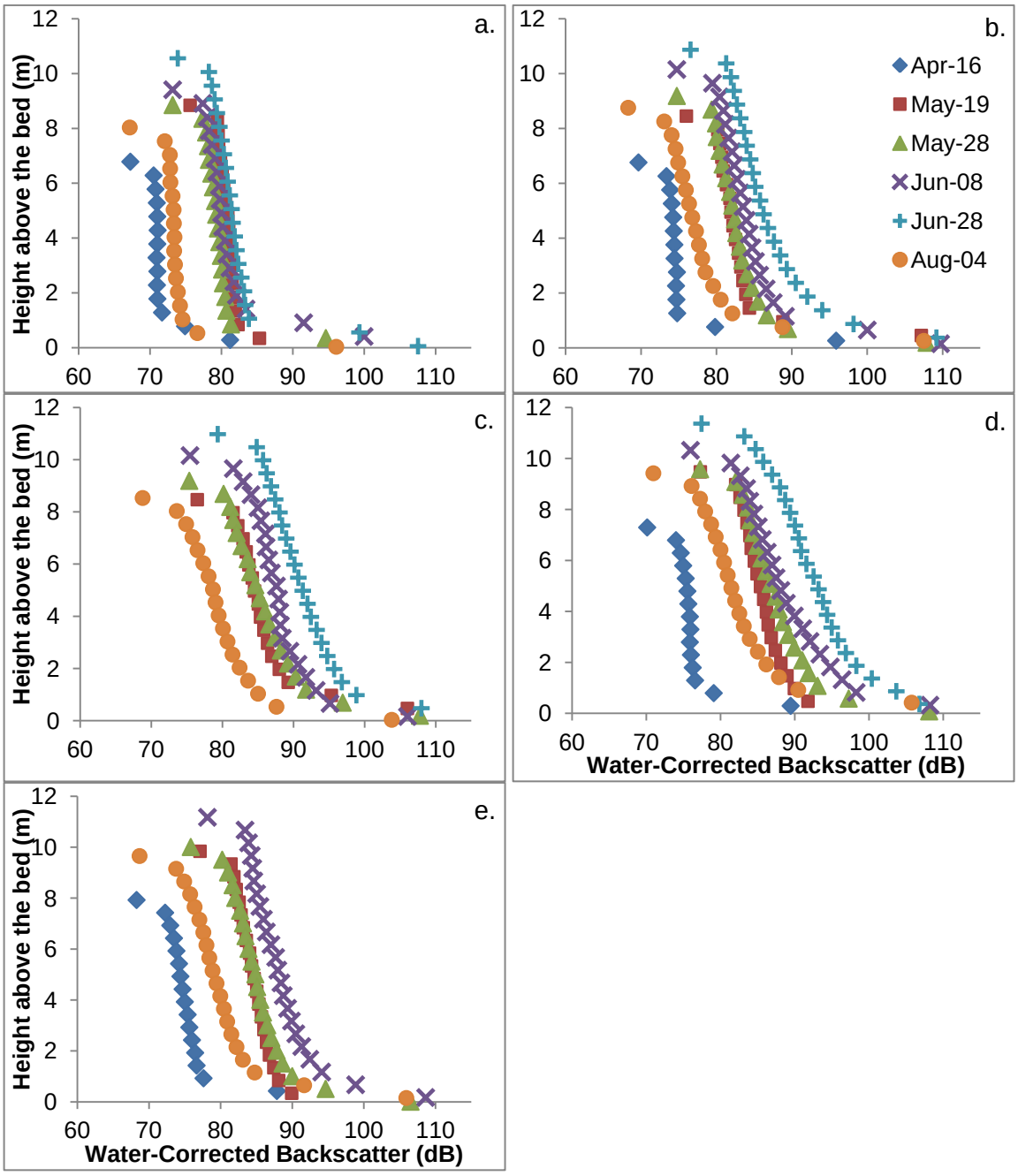

Figure 31: Water-corrected backscatter profiles over the 2010 freshet for a. profile 1, b. profile 2, c. profile 3, d. profile 4, and e. profile 5. See Figure B-1 for SWCB profiles.

The 600 kHz instrument was successfully calibrated following the Topping et al. (2007) method. Total SSC from conventional bottle sampling samples were positively correlated (R^2=0.724) with water-corrected backscatter (Figure 32a) and sand SSC with sediment-corrected backscatter (R^2= 0.856) (Figure 32b). Poor correlations (R^2=3x10-5) were found between silt-clay concentration and sediment attenuation coefficient (Figure 32c). The calibrations are summarized in Table 6.

Table 6: Summary of calibration equations and corresponding statistics. All calibrations were calculated using simple linear regression. If calibrations were used, they were then corrected using the reduced major axis (functional) method. R^2 is the coefficient of determination, a goodness-of-fit measure, and standard error is the estimate of standard deviation of the underlying errors. Standard error of regression and slope describe the uncertainty of the regression calibration (Reg.) and the slope, respectively.

aDcp	Independent Variable	Dependent Variable	Slope	Intercept	R^2	Standard error of Reg.	Standard error of slope	Func. Slope	Func. Intercept
V-aDcp	WCB	Log_{10}(Total SSC)	0.0491	-2.19	0.724	0.190	$2.64x10^{-3}$	0.0577	-2.90
	SWCB	Log_{10}(Sand SSC)	0.0865	-5.61	0.856	0.200	$3.09x10^{-3}$	0.0935	-6.17
	Sediment Attenuation	Silt-clay SSC	-3.70	61.0	$3.00x10^{-5}$	37.1	56.5	N/A	N/A
H-aDcp	WCB	Log_{10}(Total SSC)	0.00600	1.24	0.027	0.280	$4.82x10^{-3}$	N/A	N/A
	SWCB	Log_{10}(Sand SSC)	-0.0440	6.40	0.237	0.330	0.0200	N/A	N/A
	WCB	Log_{10}(Total SSC)	0.111	-7.99	0.870	0.170	0.0200	0.119	-8.69

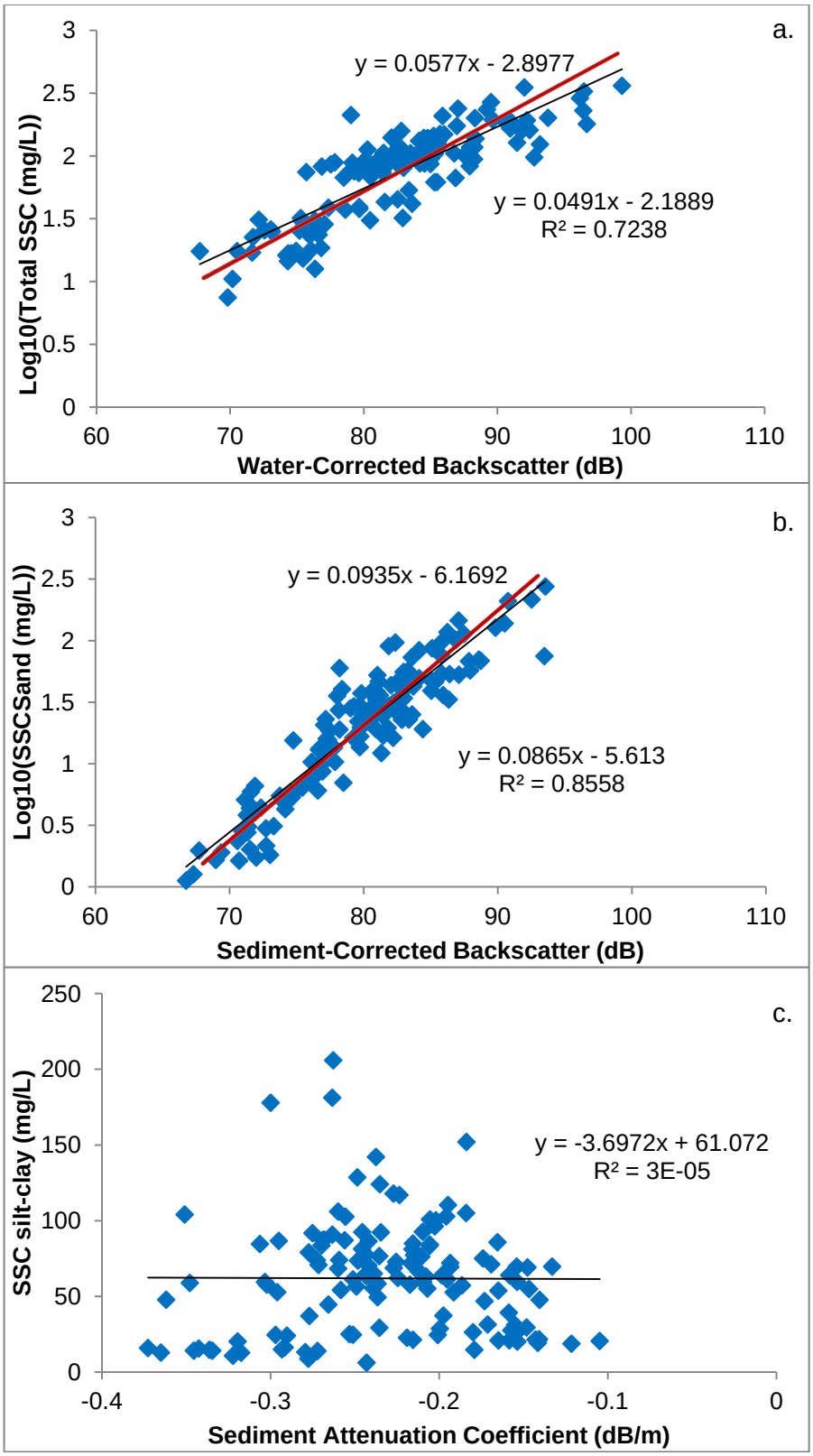

Figure 32: V-aDcp calibration curve, bin-by-bin correlation between a. total SSC and WCB, b. sand SSC and SWCB, c. silt-clay SSC and sediment attenuation coefficient. The black line is the simple linear regression line and the red line is the adjusted functional relation.

3.3.1.2 H-aDcp

The H-aDcp's almost continuous measurements of water-corrected backscatter cross-channel profiles through time are shown in Figure 33. Instantaneous backscatter (MB, WCB, SWCB) profiles display similar patterns during the peak flows on June 28, 2010 (Figure 34). The signal decreases away from the instrument for the first 60 m along the beam, increases from 60 m to about 130 m, and then decreases again to the end of the beam range. The initial bin-by-bin calibration utilizing the full length of the acoustic beam was unsuccessful. The WCB-SSC calibration is poor and only 2.7% of the variability in SSC is explained by WCB (Figure 35a). The SWCB calibration is negative (Figure 35b). The calibration between the sediment attenuation coefficient and sediment concentration was not pursued due to the discouraging negative SWCB correlation.

Backscatter should decline moving away from the instrument due to the attenuation of the acoustic signal from the water and sediment in the water. The trend evident in all backscatter profiles (Figure 33 and Figure 34) is unexpected and a possible explanation for the poor correlations (Figure 35). It is important to note that given the bin-by-bin approach is a deviation from the Topping et al. (2007) method and that sediment concentration does not vary greatly at one height in the water column (where the instrument samples), it was not expected to be successful.

However, it is clear that EI does increase and decrease with discharge (Figure 36). This change in EI suggests a coherent relation exists between SSC and the acoustic signal and so an alternate approach was explored. Examination of the acoustic beam spread across the channel suggests that the bed should have caused interference at ~180 m from the transducer (Figure 29). The increasing trend from 60-130 m

however, suggests that the beam may have hit the bed or the water surface much closer to the transducer.

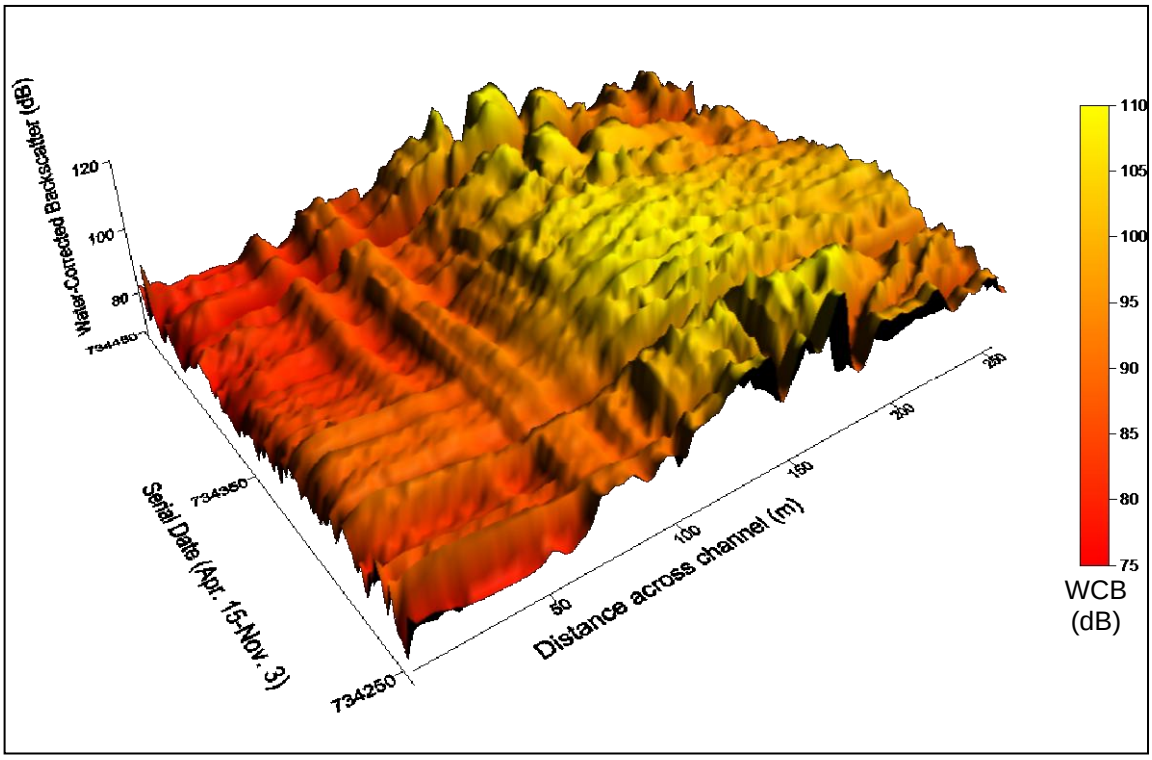

Figure 33: Hourly water-corrected backscatter. The serial date represents the whole and fractional number of days from the reference to start date Jan-01- 0000 00:00:00, 734243 is April 15, 2010 and 734445 is November 3, 2010.

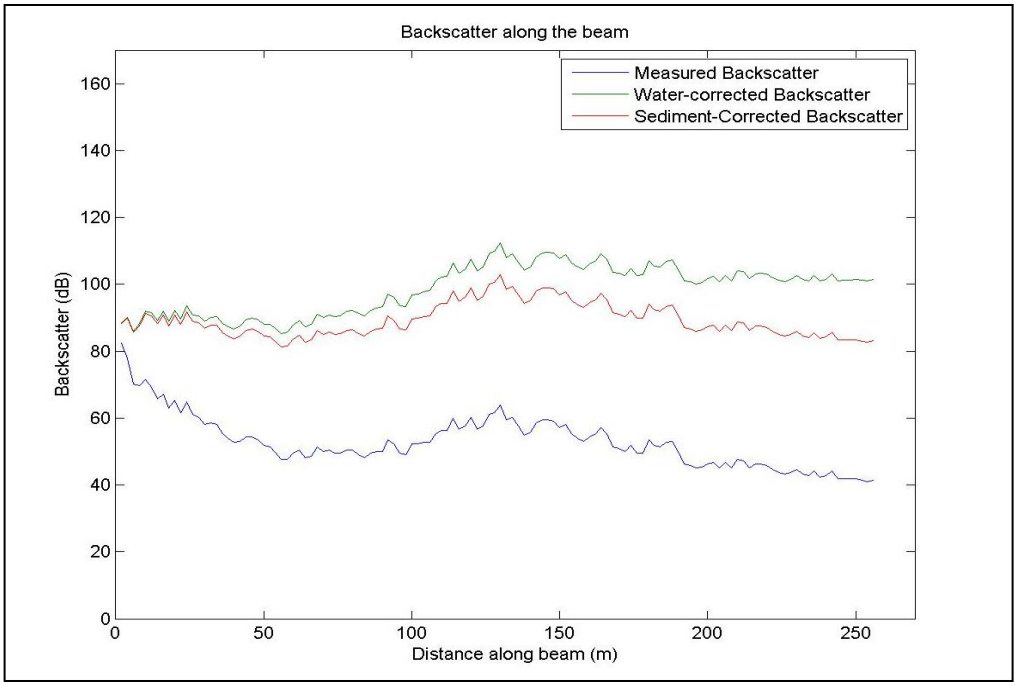

Figure 34: Instantaneous backscatter profiles across the aDcp beam from June 28, 2010 peak flows.

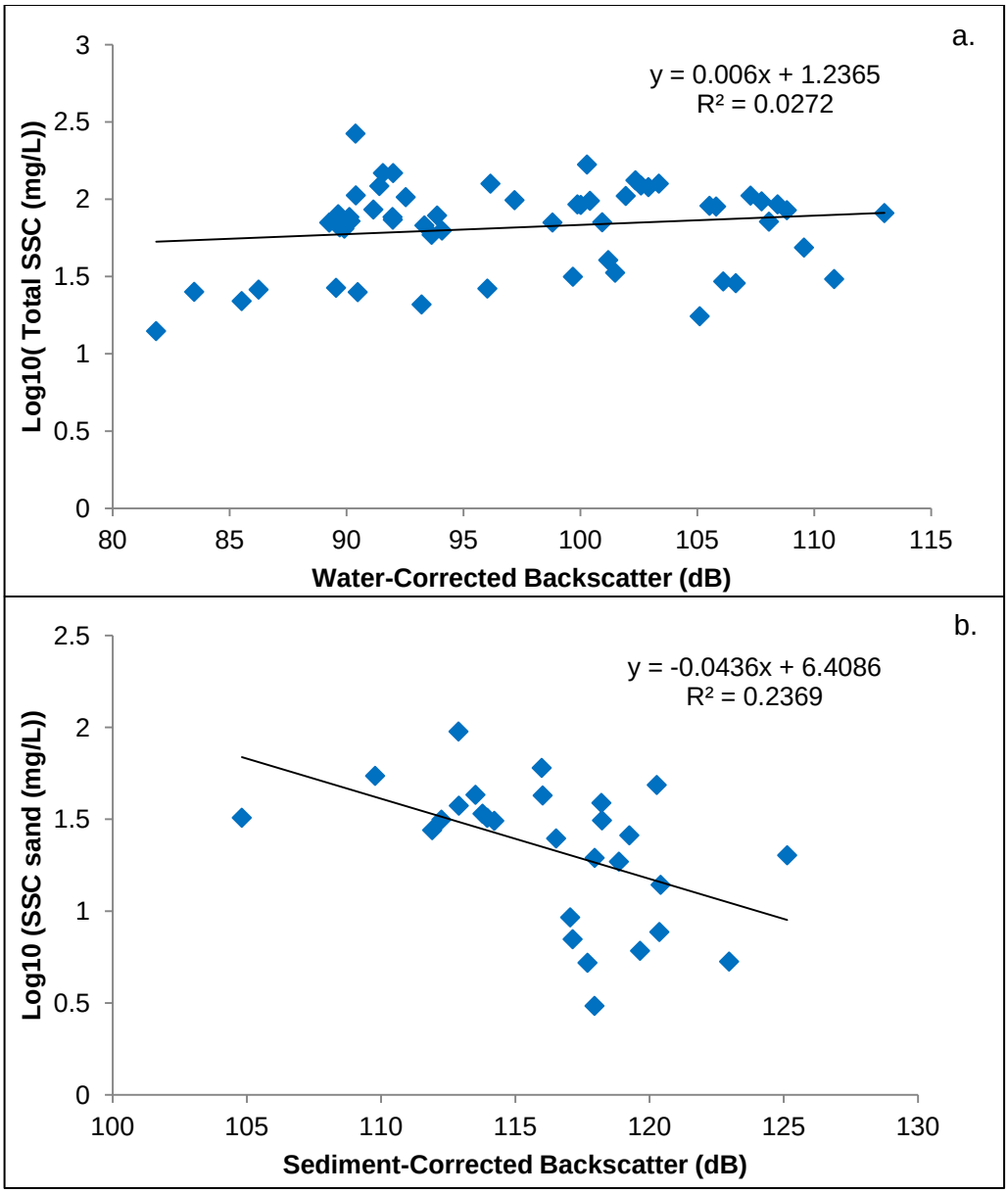

Figure 35: H-aDcp bin-by-bin correlation calibration curves. a. Total SSC and WCB, b. sand SSC and SWCB.

In light of this observation, the acoustic data for only the first 60m (30 bins) of the beam, the area before the disturbance in the signal, were utilized in a new calibration. This range of the profile has the expected decreasing trend in backscatter with distance. Rather than calibrating backscatter at a particular bin against individual bottle samples at the same location, I used an average backscatter along the beam length and the

average bottle sample SSC from 3 sediment samples collected within the first 60m of the beam in keeping with the Topping et al. (2007) method.

The WCB was averaged over the bottle-sampling time and then averaged across the first 30 bins (60 m) of the aDcp beam profile. The concentration was a weighted average of total concentration (c_{60m}) of the three bottle samples collected within the beam range of 60 m

$$c_{60m} = \frac{\sum c_i w_i}{\sum w_i}, \tag{29}$$

where c_i is the concentration of the sample and w_i is the width of the flow (within the beam range of 60 m) the sample represents. The resulting calibration is shown in Figure 37 and yields a strong positive correlation between total SSC and WCB, with an R^2 of 0.8704 and p-value of 6.6×10^{-3}.

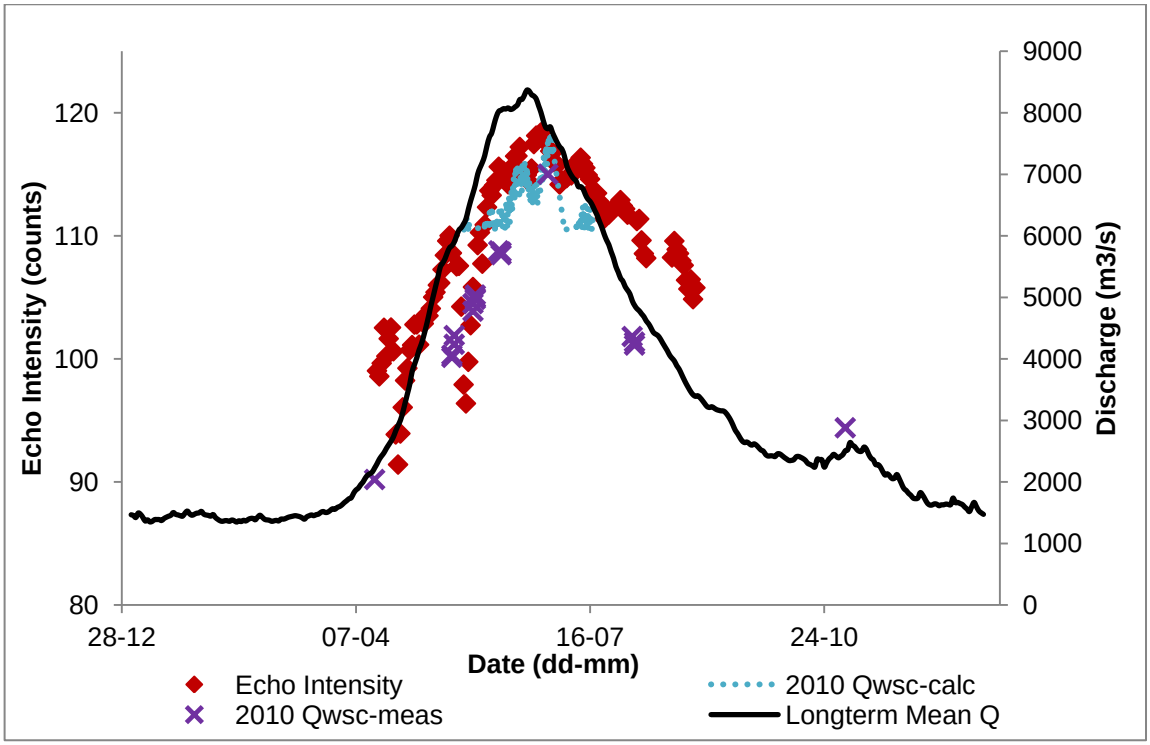

Figure 36: Average daily echo intensity with discharge over the freshet.

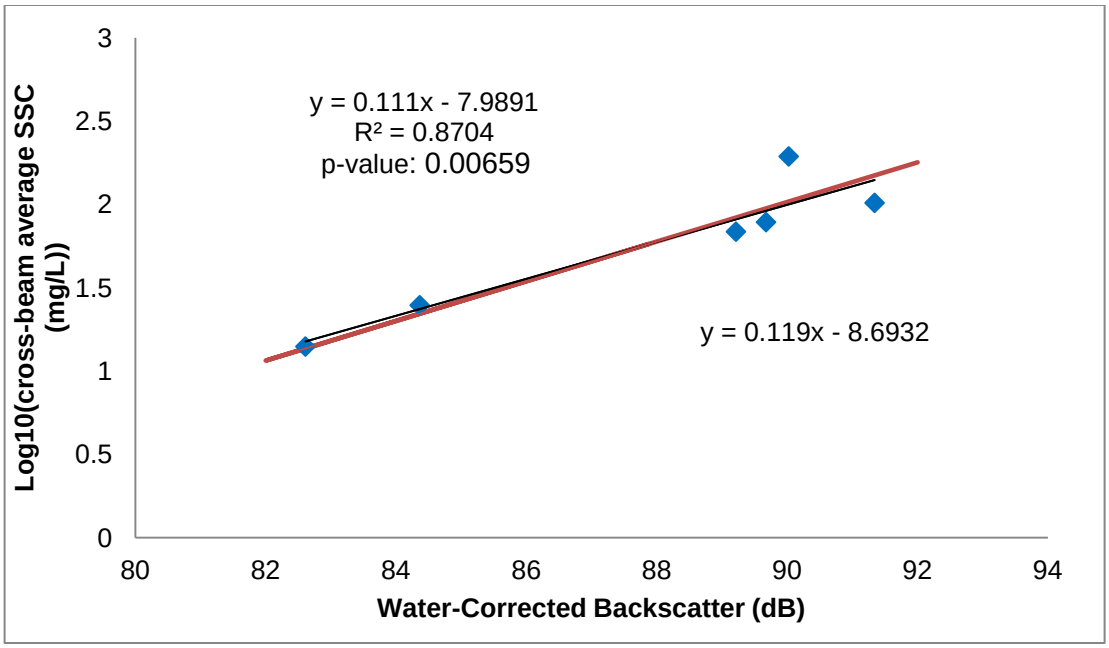

Figure 37: Total SSC calibration curve, beam-averaged correlation with WCB. Linear regression in black line (expression above data) and functional regression in red (expression below data).

3.3.2 Suspended sediment load at Mission

The total sediment flux moving through the channel was calculated from the sum of the sediment flux moving through 5 panels of the cross-section, each with a width that is a fraction of the total channel. In order to calculate the total sediment concentration, we must depth-average and width-average measured concentrations. Different approaches must be taken in depth-averaging the vertical aDcp concentrations and the bottle sampled concentrations because the velocity determines how much water is sampled. Point-integrated bottle samples have different fill times, which accomplished the necessary velocity-weighting. The aDcp concentration estimates need to be velocity-weighted.

3.3.2.1 Bottle samples and V-aDcp

The depth-averaged concentration for each bottle sampling campaign was calculated as

$$c_j = \frac{\sum c_i d_i}{\sum d_i}, \quad (30)$$

where c_i is the concentration, d_i is the portion of the water column each sample represents, and j is 1-5 profiles. Depth-averaged profiles were then width-averaged for a channel-averaged estimate of SSC, c_T

$$c_T = \frac{\sum c_j w_j}{\sum w_j}, \quad (31)$$

where c_j is the depth-averaged profile concentration, w_j is the portion of the channel width the profile represents.

Concentration profiles from the V-aDcp were depth-averaged and velocity-weighted using

$$c_j = \frac{\sum c_i \mathrm{u}_i d_i}{\sum u_i d_i}, \quad (32)$$

as above, c_i is the concentration at a given elevation above the bed (from the aDcp bin), d_i is the portion of the water column each bin represents and u_i is the velocity from the aDcp bin. Channel- averaged concentration is calculated using equation 31.

Estimates of suspended sediment flux were calculated the same way for both bottle sample and V-aDcp concentrations. Some care must be taken in calculating the sediment flux through a panel, q_{s_j}. This sediment flux cannot be calculated from the product of c_j and u_j, the depth-averaged velocity and h, because

$$q_{s_j} = \left(c_j u_j + c^{'} u^{'}\right) h \quad (33)$$

where c' is the deviation of an at-a-point concentration from the depth averaged concentration ($c^{'} = c_j - c_i$) and u' is the deviation of an at-a-point velocity from the depth average ($u^{'} = u_j - u_i$). As such, the sediment flux through a panel must be calculated as $q_{s_j} = (cu)_j d$ or

$$q_{s_j} = \sum c_i u_i d_i. \quad (34)$$

Panels are summed for an estimate of total flux, Q_s:

$$q_{sT} = Q_s = \sum q_{s_j} w_j. \quad (35)$$

The V-aDcp total SSC profile predictions underestimate total SSC observations during low-moderate flows (Figure 38a) and overestimate it during high flow conditions (Figure 38b). Predictions of total suspended sediment load (Figure 39a, Figure 40a) display a trend similar to total SSC, while suspended sand load is consistently overestimated throughout the range of flow conditions (Figure 39b, Figure 40b). Both V-aDcp predictions and bottle sampling estimates of sediment load show seasonal hysteresis and peaks in sediment concentration and flux coincide with peak water discharge.

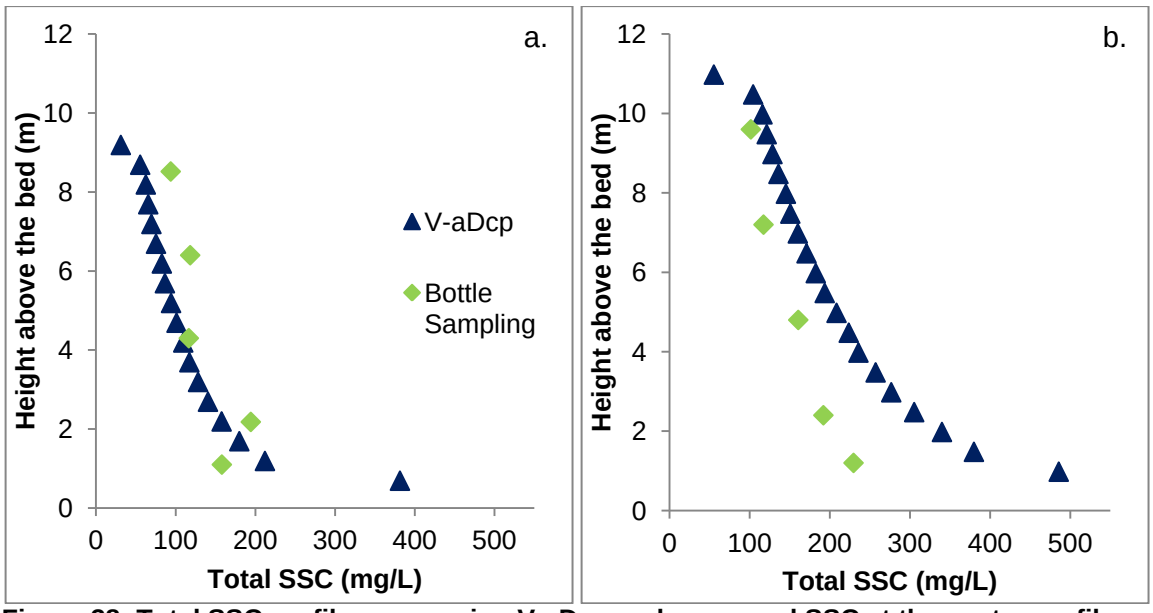

Figure 38: Total SSC profiles comparing V-aDcp and measured SSC at the centre profile during a. May 27 rising flows and b. June 28 peak flows.

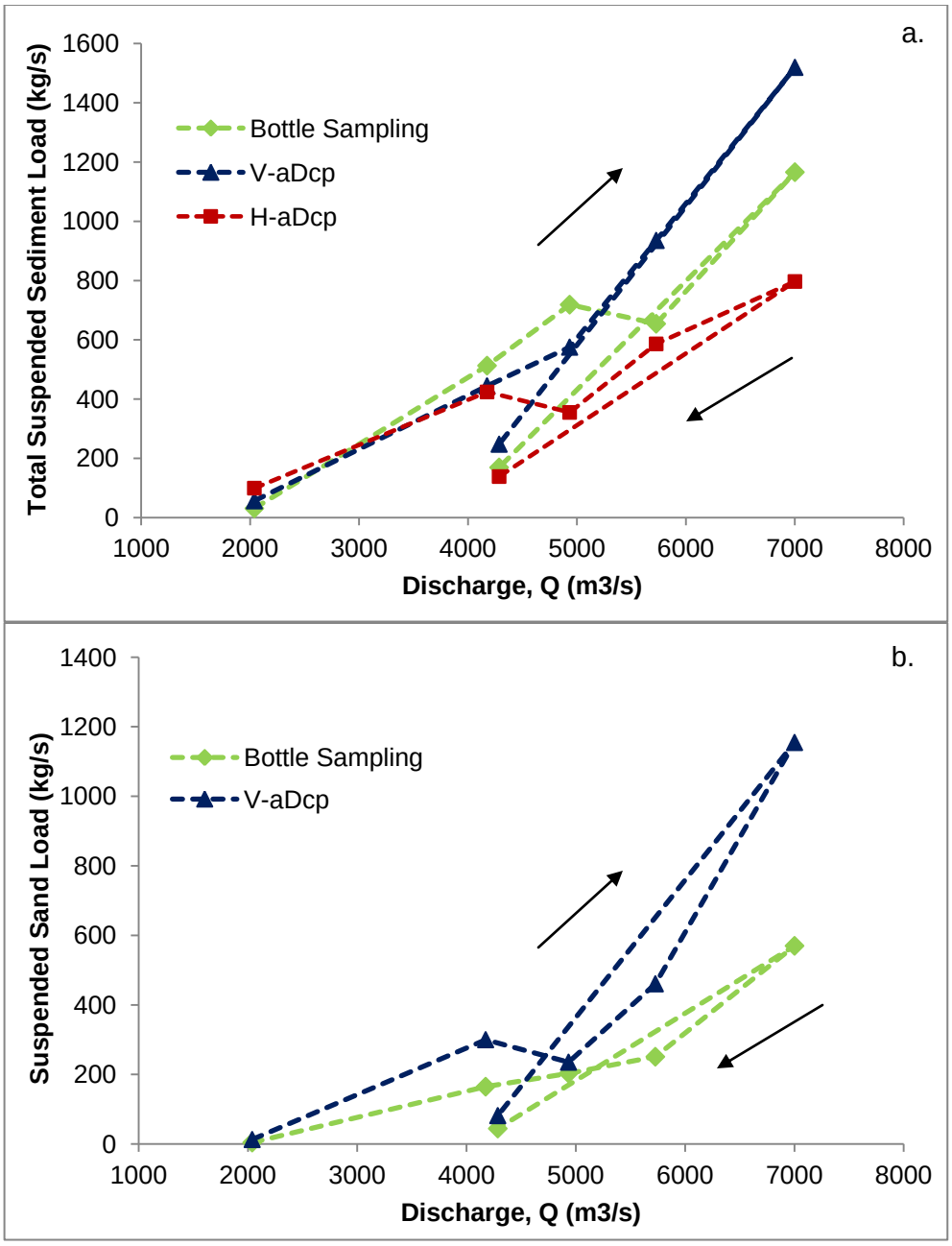

Figure 39: Daily suspended sediment load with discharge, comparing aDcp and observed bottle sampling estimates: a. total load, b. sand load. Points are joined to illustrate hysteresis.

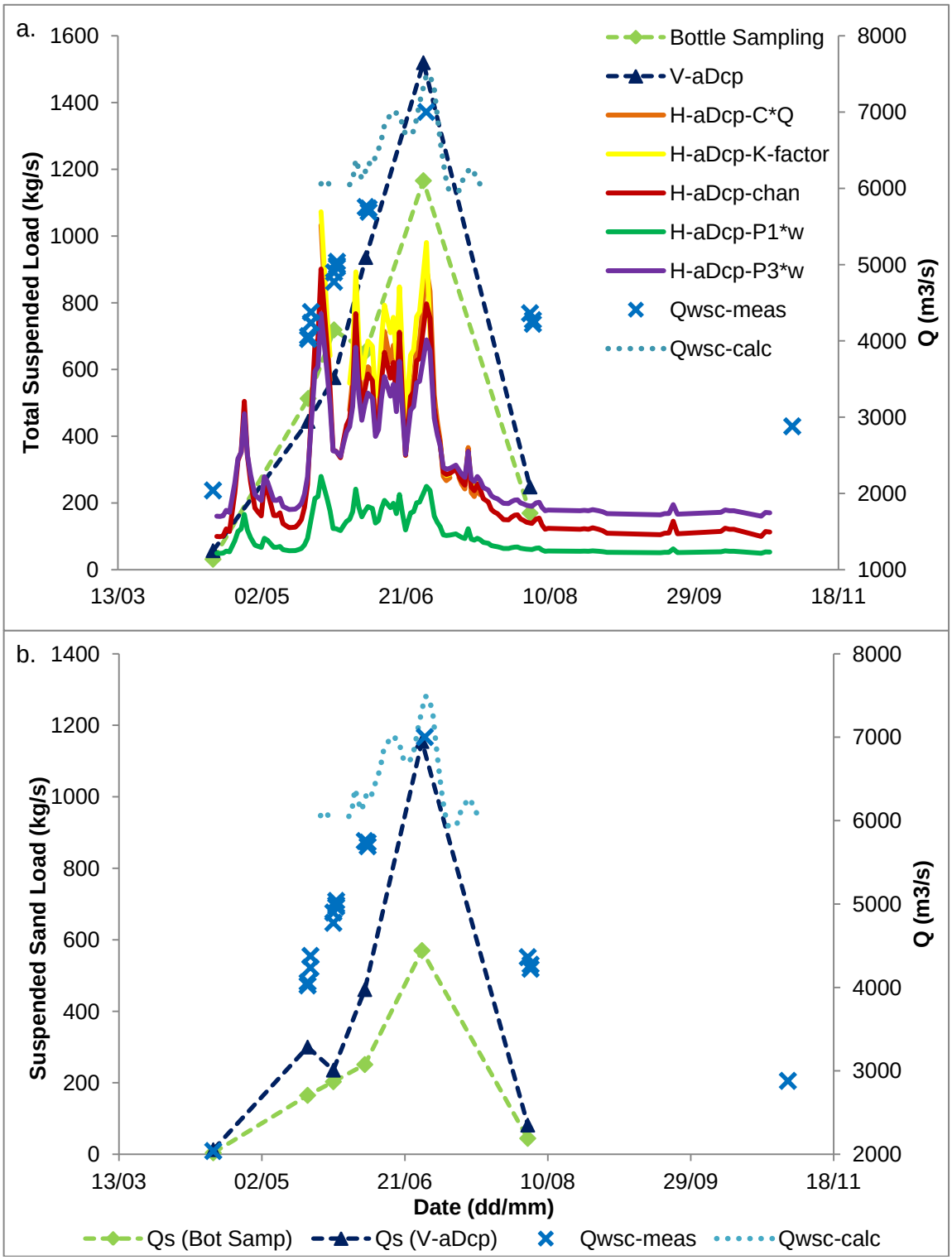

Figure 40: Suspended sediment load and discharge with time, comparison of aDcp estimates and observed bottle sampling methods: a. total load, b. sand load. The points are joined with lines to show the observed seasonal pattern.

3.3.2.2 H-aDcp

In order to calculate the sediment load at Mission, the mean sediment concentration in the beam must be calculated from the calibrated WCB data. Velocity does not vary greatly through the horizontal profile so the average concentration, <*c*>, along the first 60 m of the beam (30 bins) does not need to be velocity weighted and the mean concentration is calculated as:

$$< c >= \frac{\sum c_i}{30} \quad (36)$$

where c_i is the concentration in *i*=1 to 30 bins.

In order to calculate the channel-averaged suspended sediment concentration, the correlation between this H-aDcp beam concentration, <*c*>, and the channel-averaged concentration from the bottle sampling, c_T was used (Figure 41 a). The correlation is strong and has a R^2 of 0.6136. Tidal influence was evident in hourly-averaged total SSC for all H-aDcp data (Figure 42) and so the data were averaged daily to reduce variability. The relation was used to estimate daily channel concentration for the H-aDcp sampling period of April 15- October 25, 2010 (H-aDcp-chan) (Figure 43).

I also examined the relation between <*c*> and profile 1 concentration and profile 3 concentration (Figure 41b&c, Table 7). Profile 1 is located on the right side of the channel. I chose it because it is within the H-aDcp beam range and is most likely to be correlated with the H-aDcp beam concentration. Profile 3 is significant because it is located in the centre of the channel and has potential to be used with the K-factor method of estimating channel-averaged concentration (McLean and Church, 1986). Profile 1 and 3 depth-averaged concentrations were both positively correlated to H-aDcp <*c*>. Profile 1 has a lower R^2 value (0.4951) than the channel relation (0.6136), but a higher R^2 than the profile 3 relation (0.4078) (Table 7). Table 7 summarizes the

correlations between H-aDcp cone SSC (Beam SSC) and flux (qcone) and channel, profile 1 and profile 3 SSC (SSC chan, SSC P1, SSC P3) and flux (qs-chan, qs-P1, qs-P3).

Table 7: Summary of H-aDcp cone SSC and flux correlations with bottle sampling channel and profile SSC and flux.

aDcp	Independent Variable	Dependent Variable	Slope	Intercept	R^2	Standard error of Reg	Standard error of slope
H-aDcp	Beam SSC	SSC chan	0.81	29.7	0.614	36.1	0.300
	Beam SSC	SSC P1	0.49	31.8	0.495	41.2	0.510
	Beam SSC	SSC P3	0.59	49.2	0.408	40.9	0.480
H-aDcp	qcone (kg/sm)	qs-P1	4.20	0.0980	0.647	0.0300	0.060
	qcone (kg/sm)	qs-P3	11.1	0.323	0.592	0.0300	0.030
	qcone (kg/s)	qs-chan	115	90.4	0.575	298	49.7

Daily concentrations for profile 1 (H-aDcp-P1) and profile 3 (H-aDcp-P3) were calculated from the regressions (Figure 43 a). H-aDcp-P1 and H-aDcp-chan followed each other closely during low flows and H-aDcp-P3 and channel SSC estimates were higher during increased flows. The H-aDcp-chan and H-aDcp-P1 always underestimate the bottle sampling channel concentration, while H-aDcp-P3 overestimated channel concentration at low flows but is a better estimate throughout the rest of the flow stages (Figure 43b). All H-aDcp SSC estimates peak in late May rather than at the end of June like the bottle samples and coinciding with the peak in discharge.

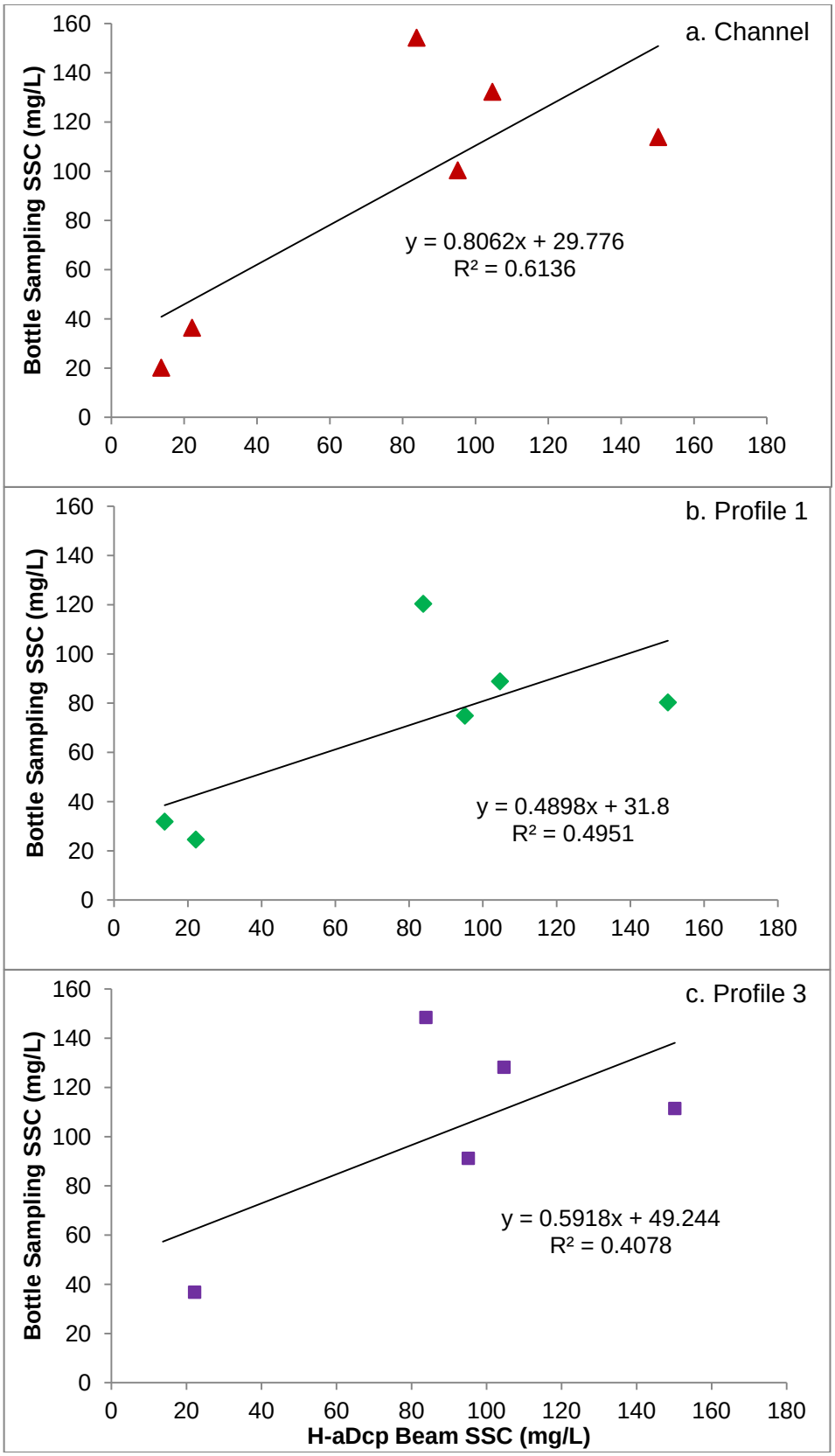

Figure 41: Correlation between H-aDcp beam SSC and depth-averaged a. channel, b. profile 1 and c. profile 3 SSC, see also Table 7.

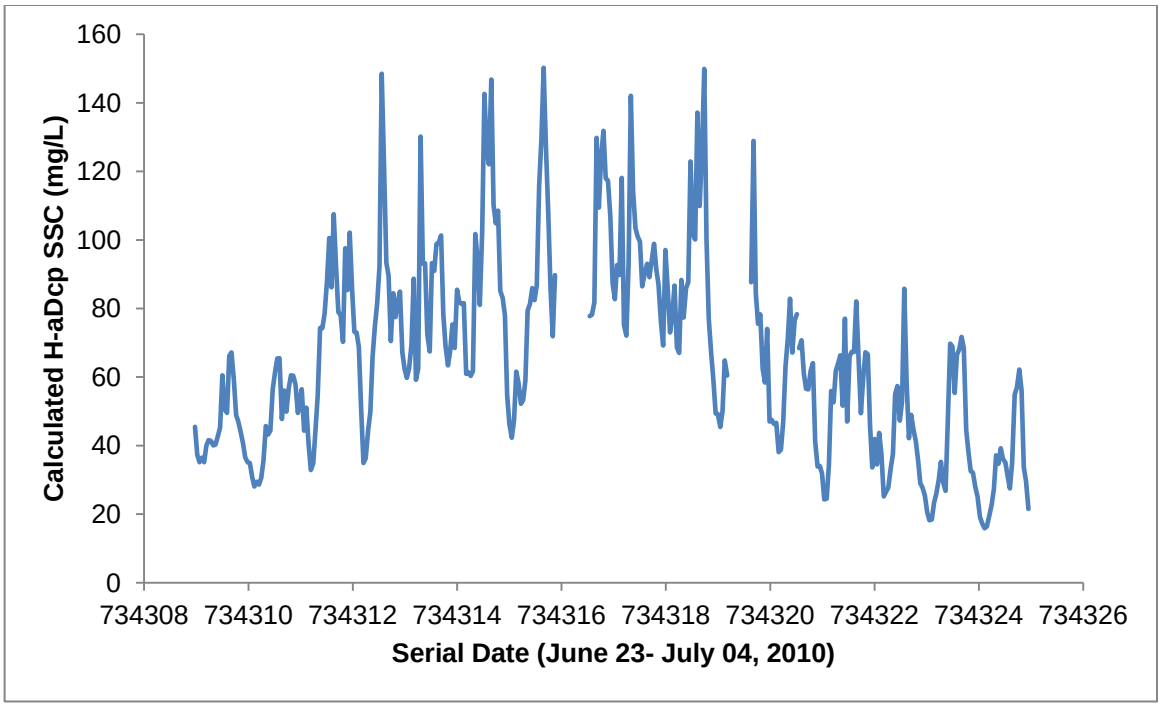

Figure 42: Hourly-averaged aDcp total SSC displays tidal oscillations.

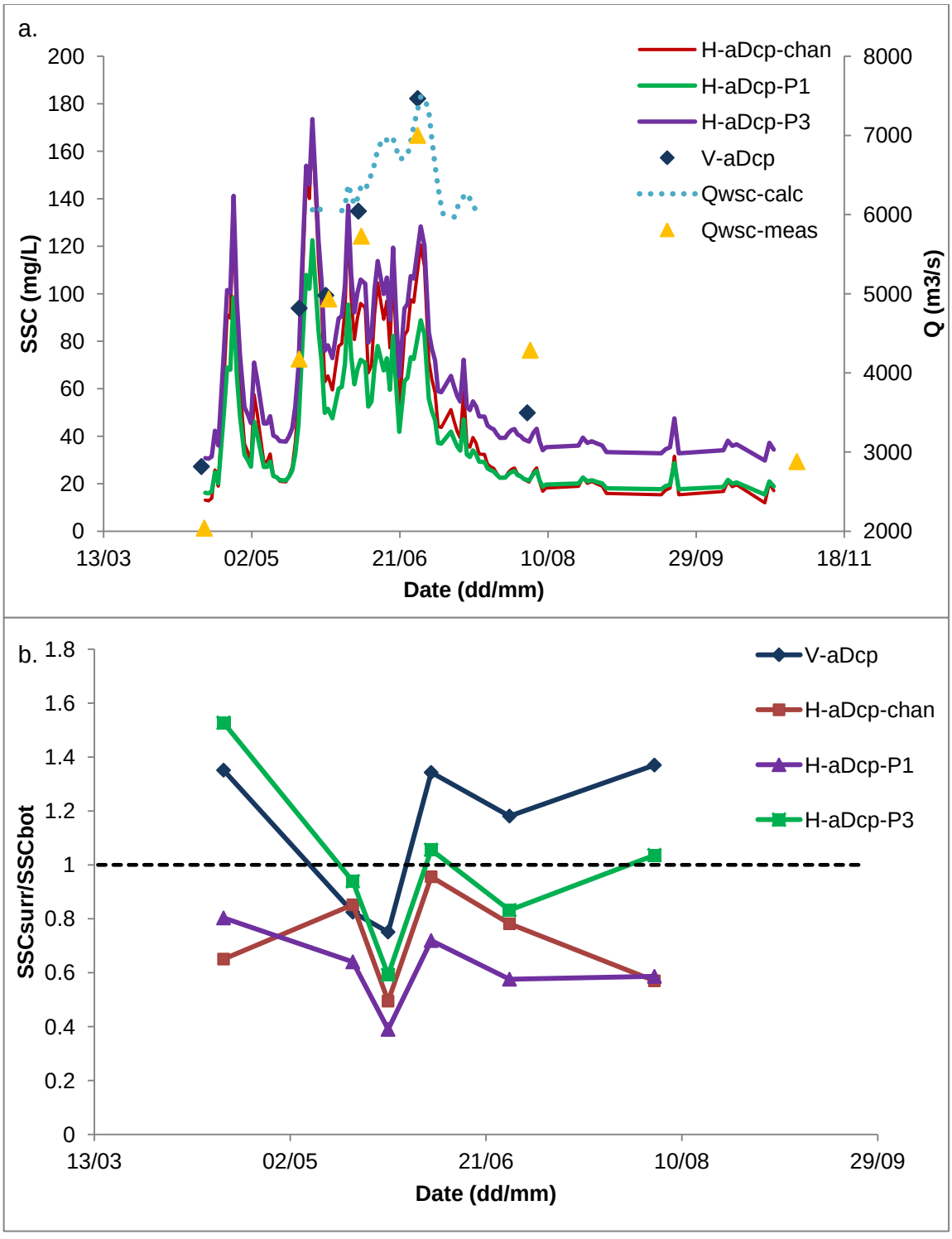

Figure 43: a. Channel-averaged, profile 1 and profile 3 depth-averaged SSC from H-aDcp measurements averaged daily and SSC from V-aDcp averaged over sampling period. Also plotted is 2010 WSC measured Q averaged over the sampling period (Qwsc-meas) and streamflow data calculated from the rating curve when flow is over 5000 m^3/s at Hope (Qwsc-calc) b. The ratio of channel-averaged SSC for surrogate H-aDcp (channel, profile 1 and profile 3) and V-aDcp and bottle sampling.

Flux within the beam cone of the aDcp was calculated as:

$$q_{cone} = < c > * < u > * Area_{2D\ slice\ of\ cone}, \quad (37)$$

where <u> is the average velocity along the first 60 m (30 bins), and

$$Area_{2D\ slice\ of cone} = \frac{1}{2} * \left(30bins * \frac{2m}{bin}\right) * beam\ height. \quad (38)$$

For correlation with measurements at profiles 1 and 3, the averaged beam height was used instead of the area of the 2D cone slice. Flux per unit width, in kg/sm, was calculated as

$$q_{cone-w} = < c > * < v > * 1/2(beam\ height). \quad (39)$$

Bottle sample channel flux, from equation 31, was correlated with H-aDcp cone flux, as calculated in equation 35 (Figure 44a). These relations between H-aDcp and bottle sampling flux were used to estimate the daily flux for the channel over the H-aDcp sampling period (Figure 45a).

I also examined the relation between $q_{cone\text{-}w}$ and profile 1 flux and profile 3 flux. In order to calculate the total flux in the channel, the depth-averaged fluxes at profiles 1 and 3 from the bottle sampling (equation 34) were correlated with H-aDcp cone flux (equation 37). Sediment flux in the aDcp beam (in kg/sm) and at profiles 1 and 3 were positively correlated (R^2=0.6465, R^2=0.5921, respectively) (Figure 44b). Similarly to channel flux, daily flux was estimated for profile 1 and profile 3 (Figure 45a). Channel flux was estimated from profiles 1 and 3 by multiplying the profile flux (kg/sm) by the channel width, W

$$Q_s = q_{cone-w} * W. \quad (40)$$

In addition, I calculated sediment flux following the method used in McLean & Church (1986). Channel-averaged depth-averaged SSC from the H-aDcp was multiplied

by discharge (averaged for the same time 24-hour period), resulting in suspended sediment flux (kg/s), $Q_{s\text{-}C*Q}$,

$$Q_{s-C*Q} = c_T * Q_{wsc-calc}, \quad (41)$$

where c_T is the daily channel-averaged SSC (kg/m^3) relation and $Q_{wsc\text{-}calc}$ is the daily discharge (m^3/s) from Water Survey of Canada records. I also used the K-factor methodology developed by WSC and reported in McLean & Church (1986). The method uses the depth integrated SSC measured at profile 3, c_3, to calculate the channel-averaged SSC. Multiplying the channel-averaged concentration by the discharge gives the sediment discharge:

$$Q_{sK} = c_3 * K * Q_{wsc-calc}, \quad (42)$$

where c_3 is the profile 3 concentration from the aDcp, and K is the K-factor (McLean & Church, 1986, earlier developed and adopted by WSC). For these calculations, I used a K-factor of 1.03 for May 22 - June 6, 1.02 for June 7 - June 26 and 0.79 for June 27 - July 16. Note that the flow record calculated by the WSC ($Q_{wsc\text{-}calc}$) at Mission is available only when water discharge reaches over 5000 m^3/s at Hope and so flux estimates are for May 22- July 16, 2010.

Estimates of total suspended sediment flux are displayed in Figure 40a. H-aDcp flux estimates display similar trends with a peak occurring in late May before the peak water discharge at the end of June. Profile 3 (H-aDcp-P3*w) and channel (H-aDcp-chan) estimates are higher than profile 1 (H-aDcp-P1*w) and follow each other closely during the rising stage of the hydrograph (Figure 40a). The flux resulting from the product of H-aDcp-C*Q gives higher estimates than those from H-aDcp-chan. Ratios of surrogate sediment flux (Qs-surr) from the various methods listed above to bottle sampling flux (Qs-bot) are compared in Figure 46. Channel flux estimates show a trend

similar to that of the channel SSC estimates. Most flux estimates overestimate the April flux by between 2 and 5 times the bottle sampling results (Qs-bot). For the remainder of the observed flow conditions, surrogate fluxes underestimate the flux with ratios between 0.45 and near 1. Also similar to channel SSC estimates, the V-aDcp overestimates June and August flows, while the H-aDcp-P1 almost consistently underestimates channel flux.

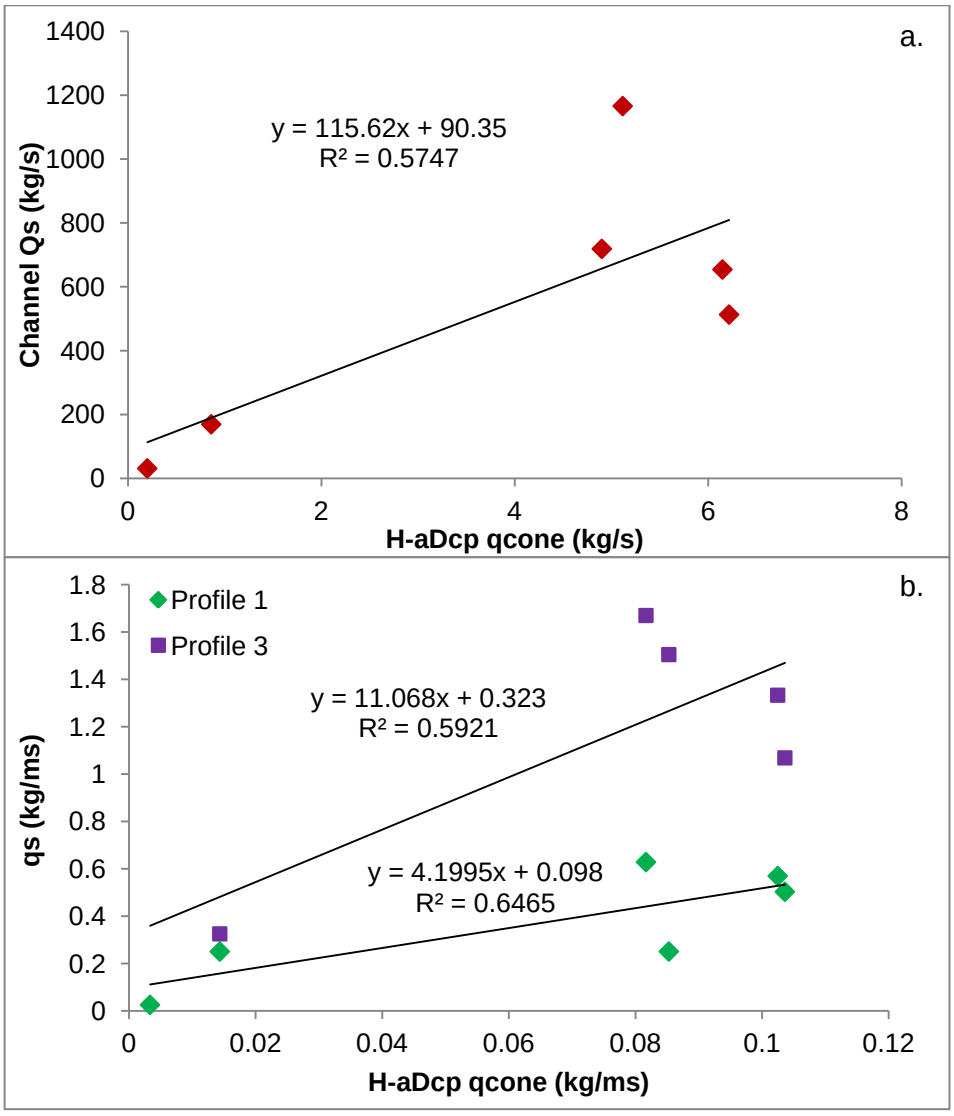

Figure 44: a. Correlation between H-aDcp cone flux (qcone) and measured channel flux (kg/s) b. Correlation between H-aDcp qcone and profile 1 and 3 measured flux (kg/sm).

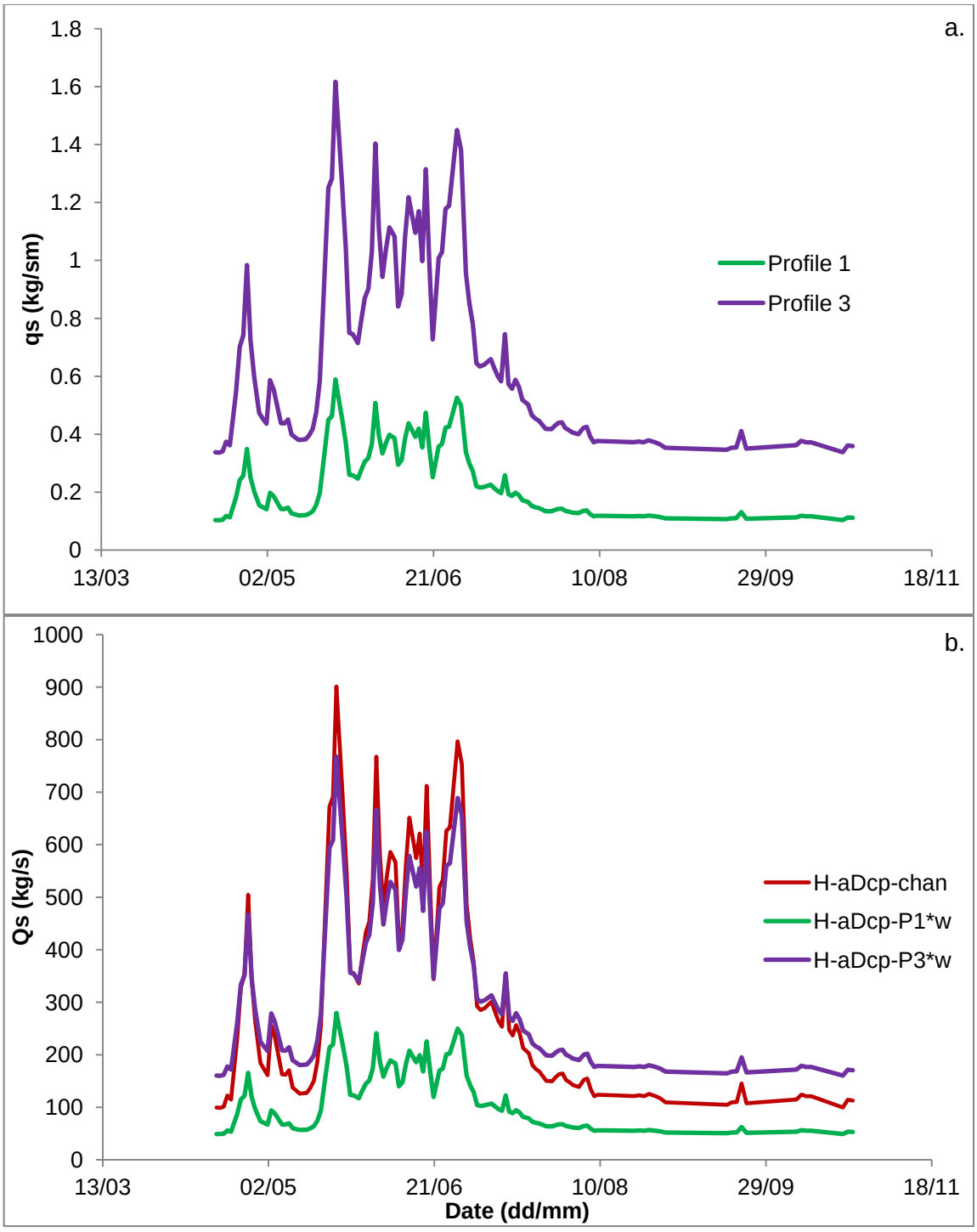

Figure 45: a. Profile 1 and profile 3 flux from the relations between H-aDcp qcone and measured profile flux. b. Channel flux estimated from relation between qcone and measured flux (H-aDcp-chan, H-aDcp-P1*w, H-aDcp-P3*w; see Figure 44).

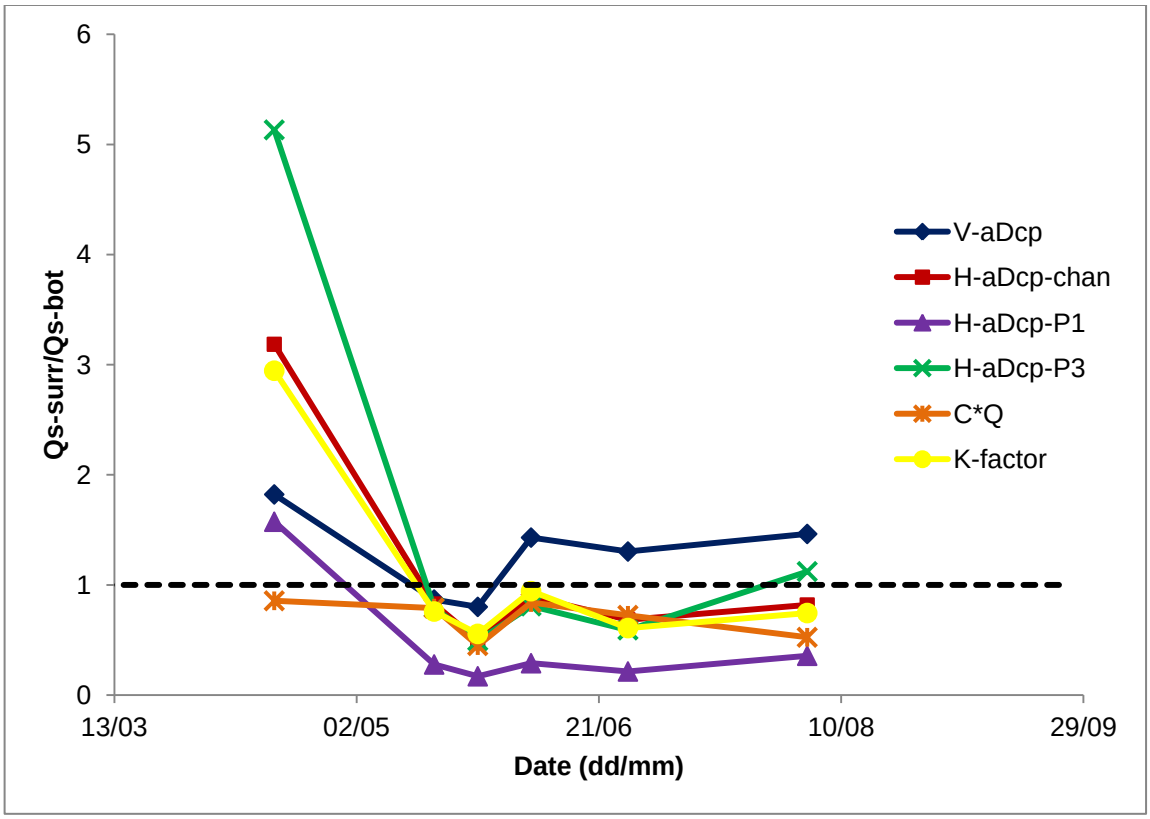

Figure 46: Ratio between surrogate flux (V-aDcp, H-aDcp-chan, H-aDcp-P1, H-aDcp-P3, C*Q, K-factor) and bottle sample flux. C*Q and K-factor are calculated using Qwsc-meas rather than Qwsc-calc so that the data could be calculated for individual campaigns. Dashed line is ratio one.

3.4 Discussion

3.4.1 Can a 600 kHz downward-looking aDcp be used to sense SSC and flux?

In keeping with Topping et al. (2007), the 600 kHz instrument was calibrated successfully with correlations for total SSC-WCB , R^2=0.7238 (Figure 32a) and sand SSC- SWCB, R^2=0.8558 (Figure 32b) , though a bin-by-bin relation was utilized. However, there does appear to be a bias in that the aDcp underestimates SSC during low-moderate flows and overestimates during high flows. I suspect that this bias may be due to a strong gradient in grain-size throughout the water column at higher flows, which can affect calibrations because backscatter and attenuation depend on particle size as

well as concentration (Wright & Topping, 2009). This argues for depth-averaging rather than bin-by-bin calibration, and/or perhaps, a separate calibration for the rising versus falling limbs of the hydrograph.

In contrast with Topping et al. (2007), a poor correlation existed between fine silt-clay concentrations and sediment attenuation coefficient (Figure 32c). This may be due to differences in SSC. In the Grand Canyon (Topping et al., 2007), suspended sediment concentrations were 2 to 3 orders of magnitude larger than concentrations observed in the Fraser River, suggesting sediment attenuation coefficient may not be a suitable surrogate for silt-clay concentrations in the Fraser River.

3.4.2 Can a 300 kHz side-looking aDcp be used to sense SSC and flux?

When the full length of the beam was used, the total SSC-WCB correlation (Figure 35a) was weak (R^2=0.027) and the sand SSC-SWCB correlation (Figure 35b) was weak (R^2=0.237) and negative, which is contrary to the results from literature (Topping et al., 2007; Wright &Topping, 2009). This is likely due to the pattern in signal across the channel (Figure 33) and the bin-by-bin approach initially used for the correlation. The pattern in acoustic signal may be a result of the beam grazing the bed of the channel or water surface, though from the cross-section diagram, the bed seems more likely. However, the truncated and averaged WCB signal was successfully calibrated with total SSC, with a goodness of fit R^2=0.8704. Overall, the H-aDcp estimates of total suspended sediment flux increased with discharge. Grain-size discriminating calibrations may be improved with more data points and the use of multiple H-aDcps of varying frequencies (Wright & Topping, 2009).

It is important to consider the location of the aDcp within the channel and how the data within this range may affect estimates for the entire channel. The location of the

channel in which this instrument collected data (nearest to profile 1) was characterized by little variation in grain-size of suspended sediment throughout the freshet (section 2.4.3 Figure 19). The average D_{50} was 21 microns and varied by only 35 microns with a minimum of 14 microns during low flows in April and a maximum of 49 microns peak flows in late June. The peak of silt-clay concentration occurred on May 27-28 and the peak in sand (and total SSC) was measured on June 27-28. This means it is possible that if the H-aDcp captures only fines in this part of the channel, then the peak in silt-clay overestimates total concentration and the peak in sand is underestimated in this location of the channel. This carries through to the estimates of channel SSC and flux.

Assuming that the bottle sampling measures of concentration and calculations of flux are an accurate representation of channel flux, most methods (all except C*Q) overestimated channel-averaged flux during the low April flows and underestimated it during the rising and falling limbs of the hydrograph. Although profile 1 is located within the aDcp beam range and flux was correlated with H-aDcp cone flux (R^2 of 0.6465), this method consistently underestimated channel flux suggesting Profile 1 location may not be an appropriate surrogate.

The flux calculated from the C*Q method had the smallest deviation from the bottle sampling flux (ratios vary by 0.4) across the sampling periods. It is interesting that the product of channel-averaged SSC and discharge (both C*Q and K-factor) result in similar estimates of channel flux because this multiplication method does not take into the account the covariance of SSC and velocity.

Profile 3 (at the centre of the channel) concentrations closely follow channel concentrations and are useful for calculations in the K-factor method, which relates profile 3 to the channel SSC. Profile 3 flux follows a similar trend and, with the exception

of April 16 estimates, may be the most appropriate method for estimating channel flux without requiring measures along the cross-section.

3.4.3 Advantages and limitations of instrumentation and methods

The 300 kHz H-aDcp has a higher goodness of fit (R^2= 0.8704) between total SSC and WCB than the downward-looking 600 kHz aDcp (R^2=0.7238). This may arise from the difference in calibration methods (cross-beam averaged versus bin-by-bin points) or due to the strong gradient in grain-size in the vertical water column observed by the downward-looking aDcp at high flows that is not present in the horizontal profile. Side-looking instruments have an advantage of providing continuous measurements of SSC, and subsequently suspended sediment flux as they can be mounted permanently. The horizontal orientation allows for cross-channel measurements versus the at-a-point vertical profiles and daily sediment loads from the downward-looking aDcp, but estimates from the relation between H-aDcp and centre profile 3 demonstrate measures at one location may be sufficient for estimating channel flux.

Though it measures across the channel, a disadvantage of the H-aDcp is that it measures at just one height in the water column and therefore, other factors, including gradients in vertical SSC, should be considered and may introduce additional error. Another problem encountered with the H-aDcp is that it interferes with the bed and/or water surface when projected far out into the channel. Sand discrimination available from the V-aDcp is an advantage over the H-aDcp, again arguing for multiple frequencies and more data points. Wright & Topping (2009) state that, in general, for low concentrations, higher frequencies are better and for higher concentrations, lower frequencies are better. This suggests that higher frequency instruments may be more suitable for detecting sediment in rivers like the Fraser, with relatively low sediment

concentrations in comparison to the Colorado River where maximum concentrations are an order of magnitude greater.

Another issue arises when sampling within the beam. Due to the conical shape of the beam, the H-aDcp sampling volume gets larger with increasing distance from the instrument transducer. Hence, when a comparison is attempted with bottle sampling, the H-aDcp is sampling a much greater volume of water than the bottle samples capture. In this respect, the H-aDcp may be a better way to sample suspended sediment concentrations than conventional bottle sampling.

3.5 Conclusions

Suspended sediment concentration and flux were estimated using the Topping et al. (2007) method of converting an acoustic signal to SSC. Two instruments were evaluated: a permanently mounted 300 kHz side-looking aDcp and a 600 kHz downward-looking aDcp. The side-looking instrument provided continuous measurements across a section of the channel while the downward-looking instrument collected vertical profiles at 5 locations along the cross-section. The results demonstrate that:

1. V-aDcp can be bin-by-bin calibrated for total and sand SSC. Channel-averaged total SSC and flux were overestimated during low April and August flows and high June flows and underestimated during rising May flows. Channel-averaged sand SSC and flux estimates are consistently overestimated. This argues for depth-averaging or separate calibrations for rising and falling limbs of the hydrograph.

2. H-aDcp could not be bin-by-bin calibrated for sediment concentration.

3. H-aDcp can be range-average calibrated for total concentration. Grain-size discrimination may require higher frequency and multi-frequency instrumentation.

4. Profile 1 had a strong H-aDcp cone SSC correlation (R^2=0.6136) and flux correlation (R^2=0.6465) but consistently underestimated channel SSC and flux (except April 16 flux). This implies this profile 1 location, though located within H-aDcp beam range, is not a good surrogate for total channel SSC and flux.

5. With the exception of April 16, profile 3 SSC and flux were correlated with channel SSC (R^2=0.4078) and flux (R^2=0.5921). There was little variation from the bottle sampling results, suggesting profile 3 may provide the best channel flux estimates without sampling the entire cross-section.

6. The channel flux estimates from C*Q method vary the least from the bottle sampling flux, but require knowledge of channel-averaged SSC. The K-factor method, based on profile 3 concentrations, also provided estimates with little deviation from the bottle sampling SSC and flux.

7. An advantage of acoustic profiling is simultaneous measurement of velocity for sediment load calculations. V-aDcp provides at-a-point vertical profiles, but an H-aDcp can provide continuous measurements and is thus better suited to continuous monitoring of suspended sediment flux.

4: Conclusion

This research evaluated suspended sediment transport of the Fraser River at Mission, BC, by comparing current measures to historical records. Results indicate that 2010 concentrations were lower than 1986 records and that modelling based on the Rouse equation does not match the observed distribution of sediment concentration. This suggests continuous and current measurements are required to monitor suspended sediment transport.

The use of aDcps for monitoring of suspended sediment transport was evaluated. The successful calibration of the aDcps with suspended sediment samples provides evidence to support progress towards a methodology for monitoring that is continuous and requires minimal labour after the initial calibration. The results indicate that it is possible to estimate total suspended sediment flux using a 300 kHz H-aDcp in the Fraser River but that it might not be the most appropriate frequency for capturing the fine sediment. A higher frequency instrument may be better at sensing low sediment concentrations consisting of mostly fine sediment that dominates sediment transport in the Fraser River. A downward-looking 600 kHz aDcp was also calibrated; results argue for further testing of the sensitivity of higher frequency side-looking instruments. Multi frequency systems, requiring multiple instruments, may also provide grains-size discrimination.

The current estimates of suspended sediment transport provided by a multi-frequency aDcp deployment could contribute to improving the sediment budget that is required for understanding sediment delivery to navigation channels, and documenting the effects of sediment extraction and resulting sedimentation. The sediment budget

input is required for sensible management of the dredging of these navigation channels in the Fraser River. Applying sediment budget principles guides dredging planning so that, in the long term, sediment removals will not systematically change the river morphology in the estuary.

This research also has broader significance in fluvial geomorphology, sedimentology and channel stability because of the importance of sediment transport processes. Sediment transport processes have been recognized as an integral component of nutrient cycling, contaminant transport and aquatic habitat maintenance in river channels. The methods outlined for this project could be applied not only in the lower Fraser River but also in other large channels.

References

Blott, S.J., K. Pye. 2001. GRADISTAT: A Grain-size distribution and statistics package for the analysis of unconsolidated sediments. Earth Surface Processes and Landforms 26: 1237–1248.

Bridge, J., 2003. River and Floodplains: Forms, Processes, and Sedimentary Record. USA: Blackwell Science Ltd.

Church, M. 2006. Bed Material Transport and the Morphology of Alluvial River Channels. The Annual Review of Earth and Planetary Science. 34:325–54.

Church, M. 2007. Review of the lower Fraser River sediment budget: final report. Report to Fraser River Estuary Management Program, 26 July, 2007: 24pp.

Church, M., J.G. Venditti. 2008. Recommendations for the reestablishment of sediment transport observations at Mission City (WSC Station 08MH024): Final Report. Report to Fraser River Estuary Management Program, 28 November, 2008: 8pp + Appendices.

Dietrich, W.E. 1982. Settling velocity of natural particles. Water Resources Research, 18 (6): 1615-1626.

Gartner, J.W. (2004). Estimating suspended solids concentrations from backscatter intensity measured by acoustic Doppler current profiler in San Francisco Bay, California, Marine Geology, 211,169-187.

Komar, P.D. Sediment Transport by Floods, in Flood Geomorphology by V.R. Baker, R.C. Kochel, and P.C. Patton, p. 97-111, John Wiley & Sons, Inc., USA 1988.

Humphries, R., J. G. Venditti, L. S. Sklar, and J. K. Wooster (2012), Experimental evidence for the effect of hydrographs onsediment pulse dynamics in gravel-bedded rivers, Water Resour. Res., 48, W01533, doi:10.1029/2011WR010419.

Mark, D.M., M. Church. 1977. On the Misuse of Regression in Earth Science. Mathematical Geology, 9 (1):63-75.

McLean, D.G., M. Church. 1986. A Re-examination of sediment transport observations in the lower Fraser River. Environment Canada, Inland Waters Directorate, Water Survey of Canada Report: 52pp (+ Tables and Figures).

McLean, D.G., M.Church, B. Tassone. 1999. Sediment transport along lower Fraser River. 1. Measurements and hydraulic computations. Water Resources Research 35: 2533-2548.

Northwest Hydraulic Consultants (nhc). 2002. Review of lower Fraser River sediment budget: final report. Report prepared for the Dredge Management Advisory committee, Fraser River Estuary Management Program. 42pp + appendix.

Parker, G. 2004. 1D Sediment Transport Morphodynamics with applications to Rivers and Turbidity Currents. E-Book, November, 2004.

Sequoia Scientific, Inc. 2007. LISST Portable Excel Report Template. Version 3.

Sequoia Scientific, Inc. website. 2010. How do I convert the volume concentrations (VC) from the LISST to mass concentrations? Retrieved February 20, 2012. http://sequoiasci.com/Articles/ArticlePage.aspx?pageid=197

Teledyne RD Instruments. 1996. Acoustic Doppler Current Profiler Principles of Operation: a Practical Primer, second Edition for Broadband ADCPs.

Teledyne RD Instruments website, retrieved March 30, 2010. http://www.rdinstruments.com/channelmaster.aspx

Teledyne RD Instruments. 2006. Acoustic Doppler Current Profiler Principles of Operation: A Practical Primer, 3rd Edition.

Topping, D.J., S.A. Wright, T.S. Melis, D.M. Rubin, 2007. High-resolution measurements of suspended-sediment concentration and grain-size in the Colorado River in Grand Canyon using a multi-frequency acoustic system. Proceedings of the 10th International Symposium on River Sedimentation, August 1-4, 2007, Moscow, Russia. 3: 330-339.

Vanoni, V.A. 1946. Transportation of sediment by water. American Society of Civil Engineers. 3: 67-133.

van Rijn, L. 1993. Principles of Sediment Transport in Rivers, Estuaries and Coastal Seas Part I: Edition 1993. The Netherlands: Aqua Publications.

Venditti, J.G. 2010. Environmental Fluid and Sediment Dynamics Course Notes, unpublished.

Water Resources Branch. Sediment Data British Columbia 1986. Water Survey of Canada. Ottawa, 1988.

Wren, D.G., Barkdoll, B.D., Kuhnle, R.A., Derrow, R.W. 2000. Field techniques for suspended-sediment measurement. Journal of Hydraulic Engineering. 126 (2): 97-104.

Wright, S, G Parker. 2004. Flow resistance and suspended load in sand-bedded rivers: simplified stratification model. Journal of Hydraulic Engineering. 130:796-805.

Wright, S.A., and Topping, D.J. 2009. Evaluation of hydroacoustics for monitoring suspended-sediment transport in rivers, OSW Webinars.

Appendices

Appendix A.

Supplementary Sediment Sampling Program Results

Note: Discharge was provided by the Water Survey of Canada. November 2 , 2010 files are not available and so were not included in the appendix.

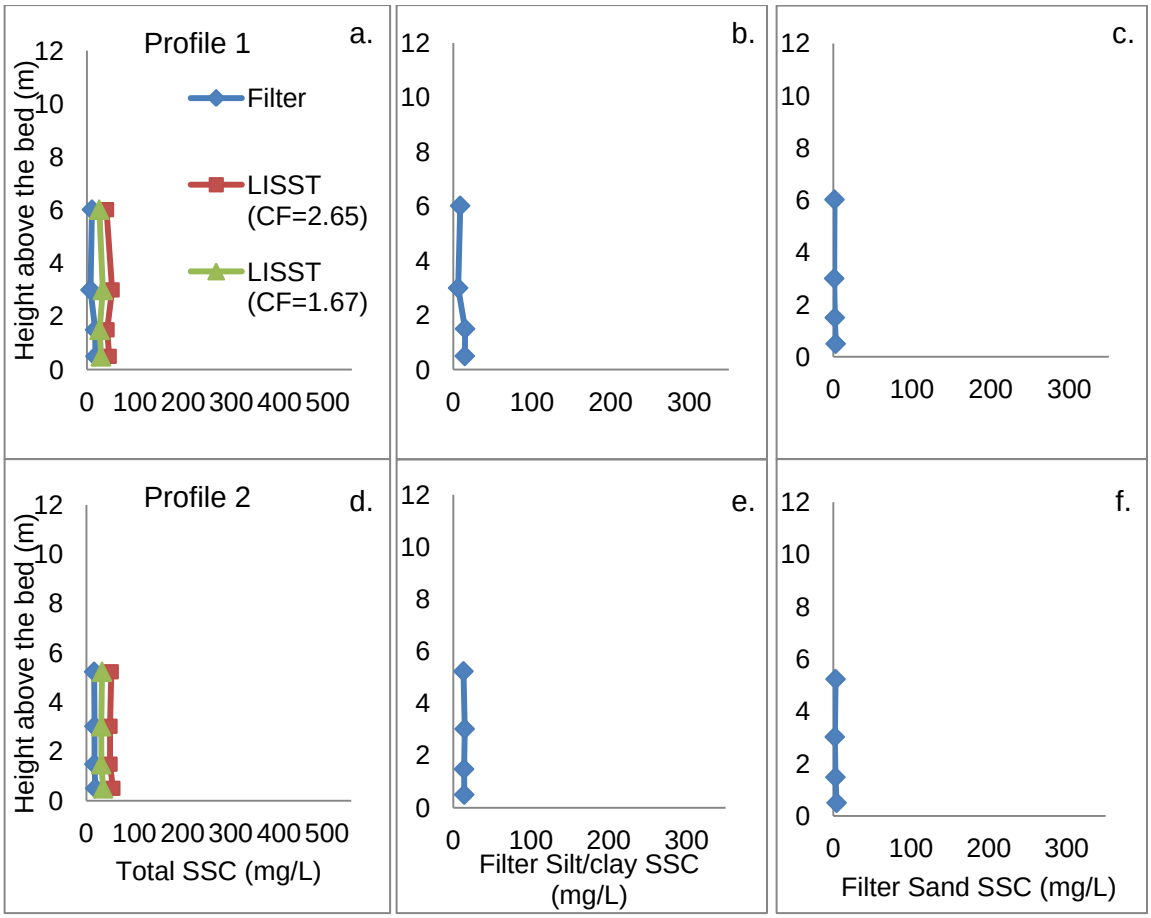

Figure A-1: April 15, 2010 sediment concentration for the (a-c) Profile 1, (d-f) Profile 2, (g-i) Profile 3 and (j-l) Profile 5. a, d, g, j are total SSC profiles from the traditional filter method and LISST-Portable method using conversion factors (CF) of 2.65 and 1.67. b, e, h, k are filtered silt/clay concentrations and c, f, i, l are the filtered sand.

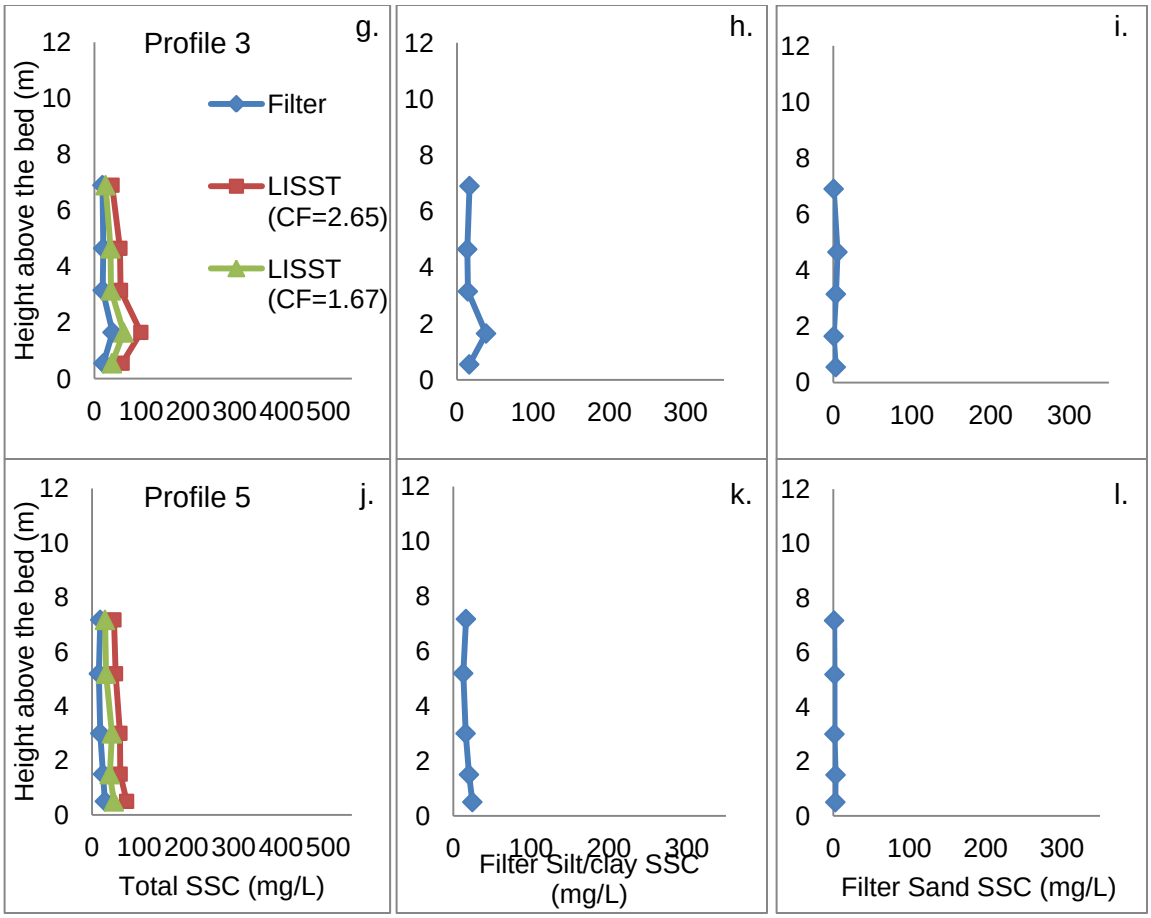

Figure A-1 continued.

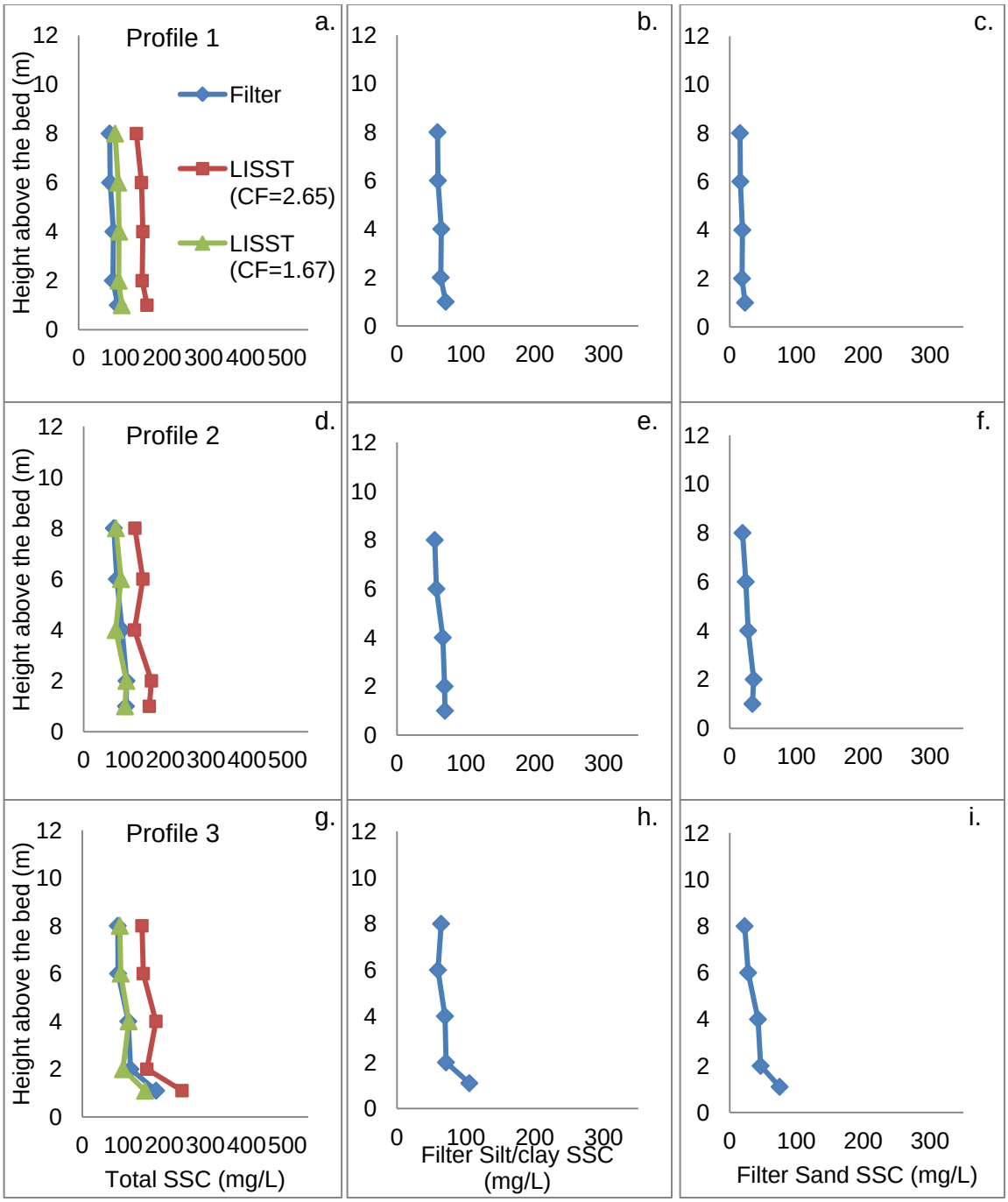

Figure A-2: May 19, 2010 sediment concentration for the (a-c) Profile 1, (d-f) Profile 2, (g-i) Profile 3 and (j-l) Profile 5. a, d, g, j are total SSC profiles from the traditional filter method and LISST-Portable method using conversion factors (CF) of 2.65 and 1.67. b, e, h, k are filtered silt/clay concentrations and c, f, i, l are the filtered sand.

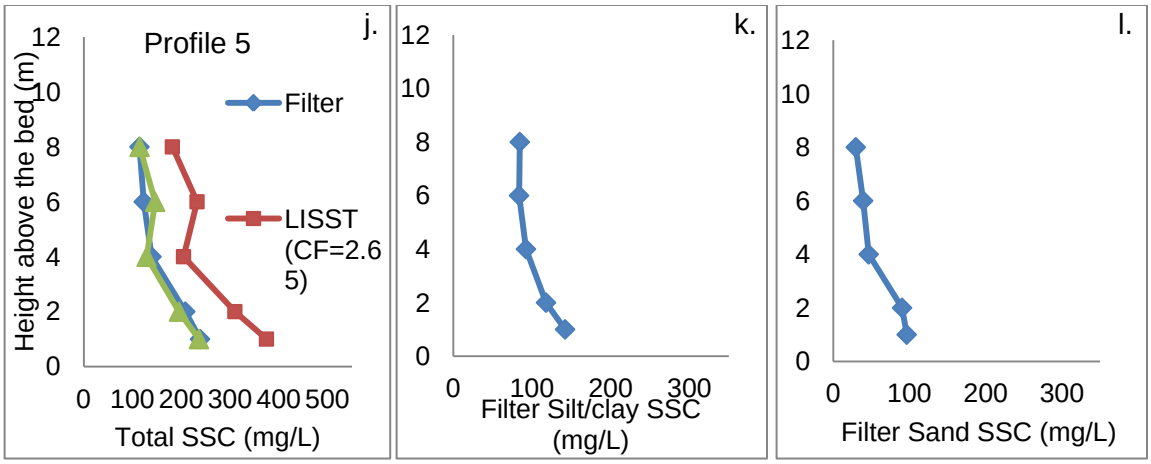

Figure A-2 continued.

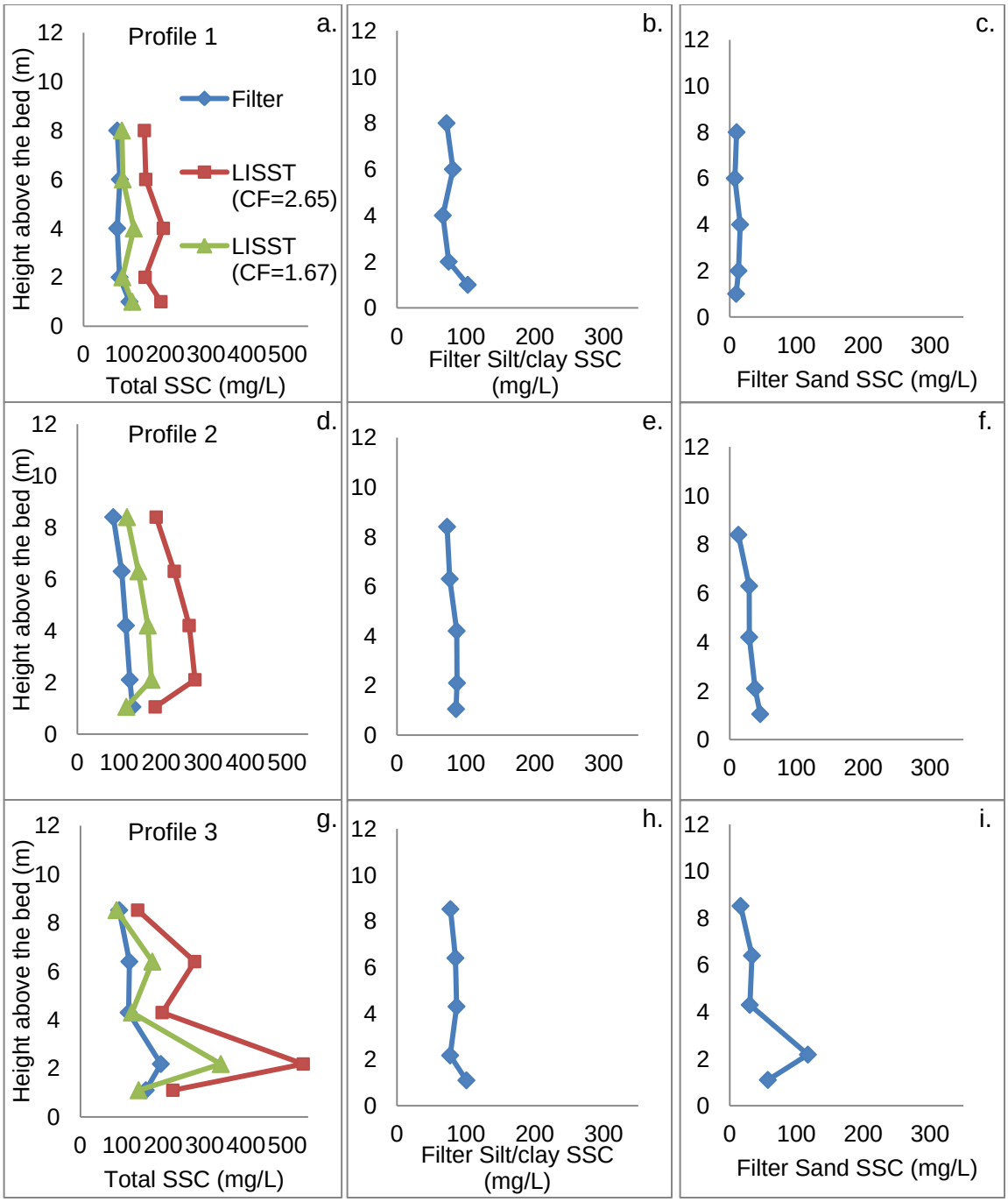

Figure A-3: May 28, 2010 sediment concentration for the (a-c) Profile 1, (d-f) Profile 2, (g-i) Profile 3, (j-l) Profile 4 and (m-o) Profile 5. a, d, g, j, m are total SSC profiles from the traditional filter method and LISST-Portable method using conversion factors (CF) of 2.65 and 1.67. b, e, h, k, n are filtered silt/clay concentrations and c, f, i, l, o are the filtered sand.

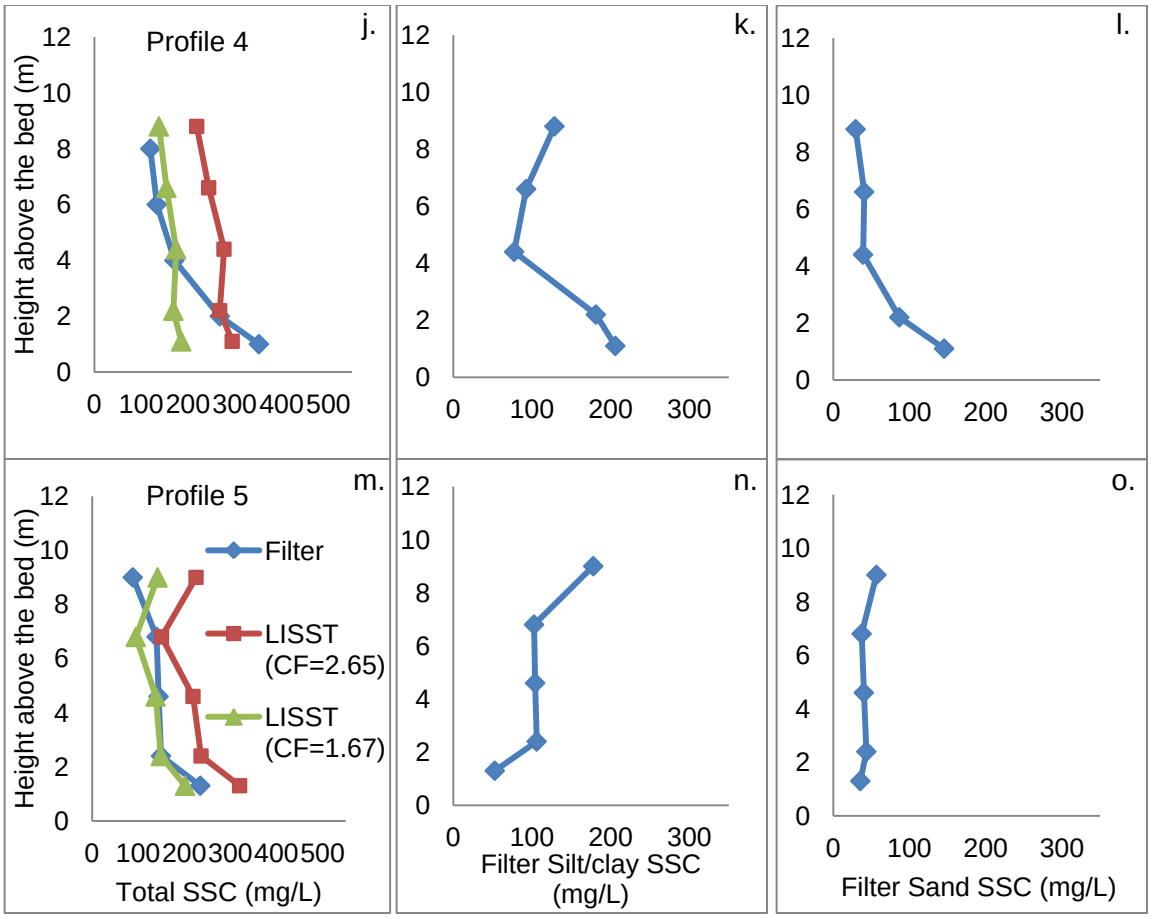

Figure A-3 continued.

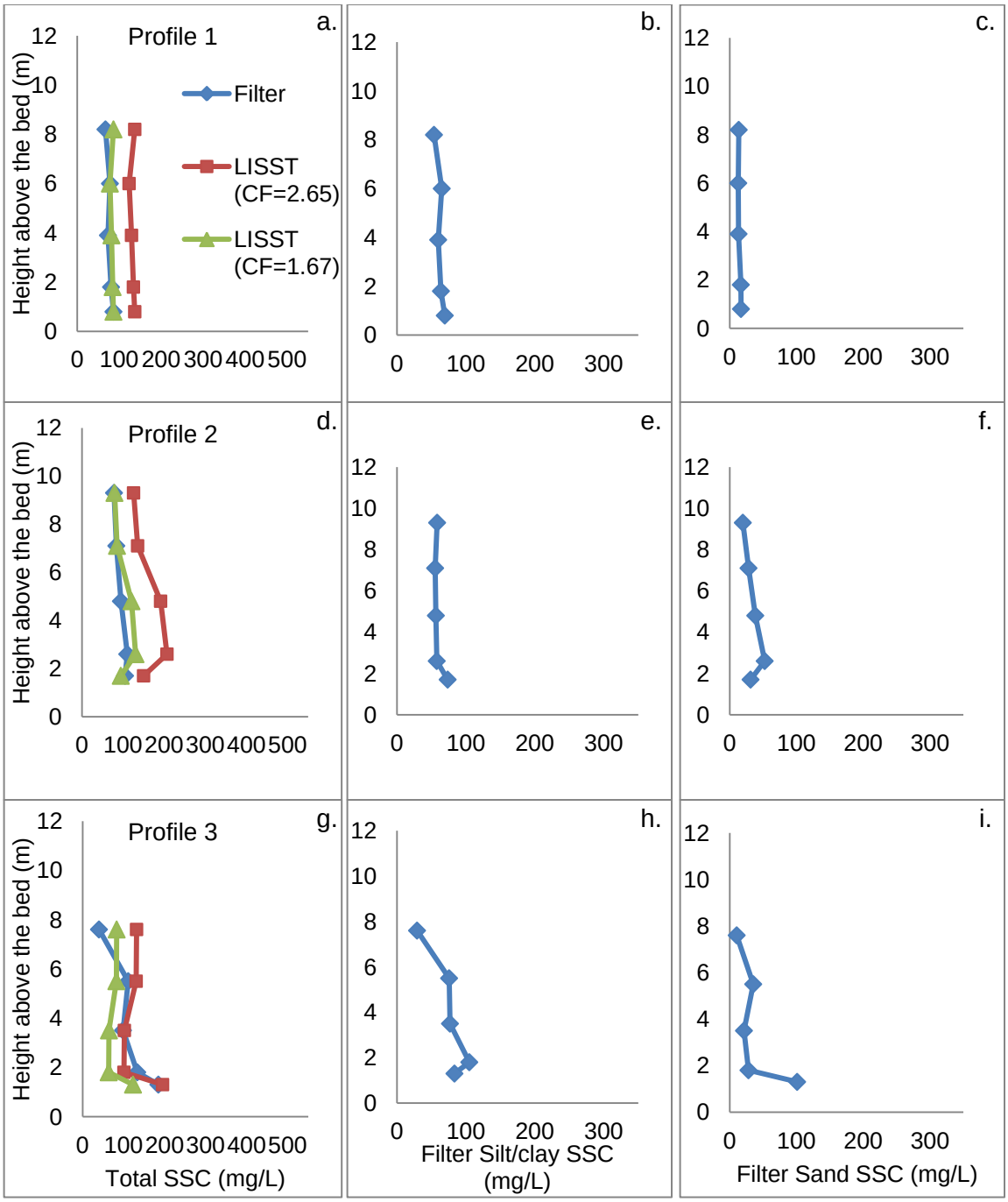

Figure A-4: June 8, 2010 sediment concentration for the (a-c) Profile 1, (d-f) Profile 2, (g-i) Profile 3, (j-l) Profile 4 and (m-o) Profile 5. a, d, g, j, m are total SSC profiles from the traditional filter method and LISST-Portable method using conversion factors (CF) of 2.65 and 1.67. b, e, h, k, n are filtered silt/clay concentrations and c, f, i, l, o are the filtered sand.

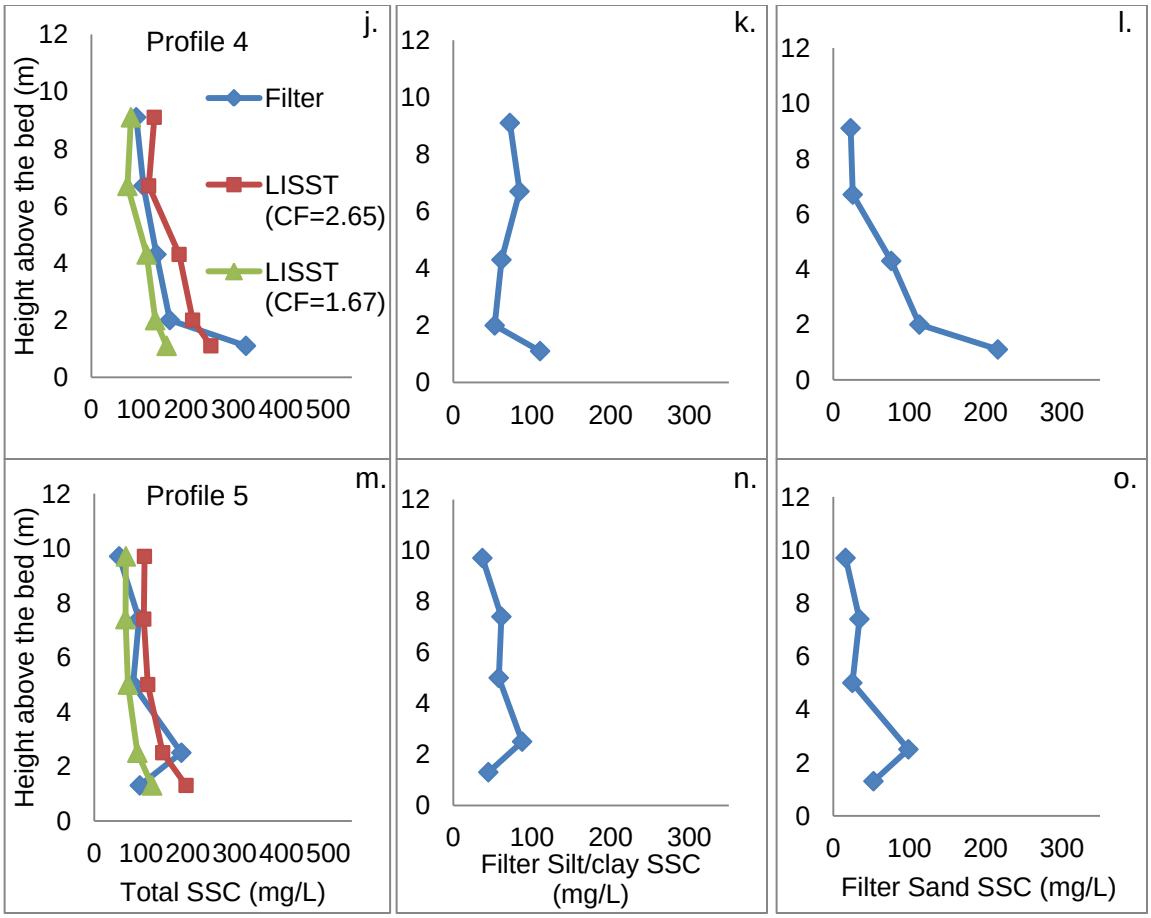

Figure A-4 continued.

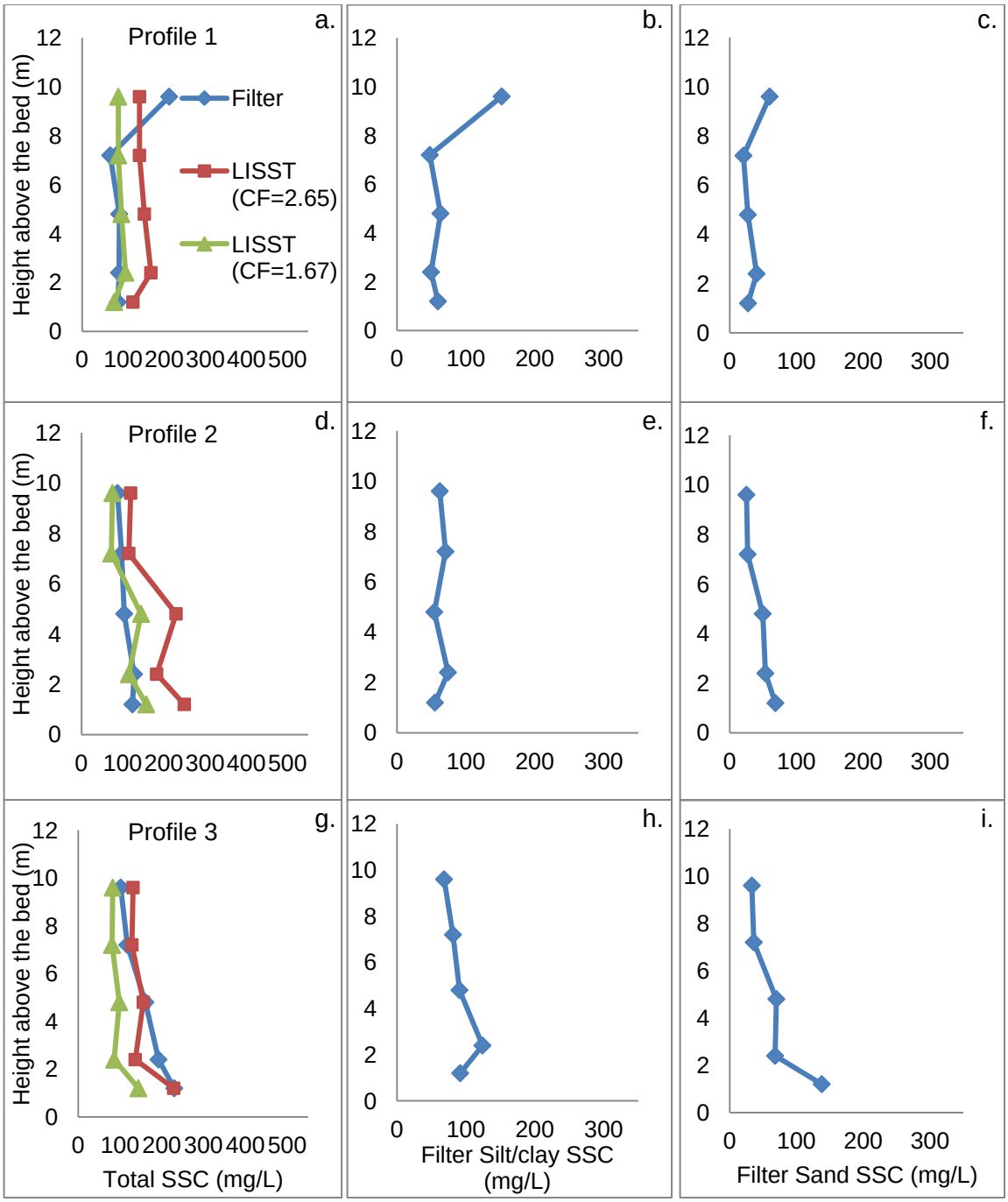

Figure A-5: June 28, 2010 sediment concentration for the (a-c) Profile 1, (d-f) Profile 2, (g-i) Profile 3. a, d, g are total SSC profiles from the traditional filter method and LISST-Portable method using conversion factors (CF) of 2.65 and 1.67. b, e, h are filtered silt/clay concentrations and c, f, I are the filtered sand.

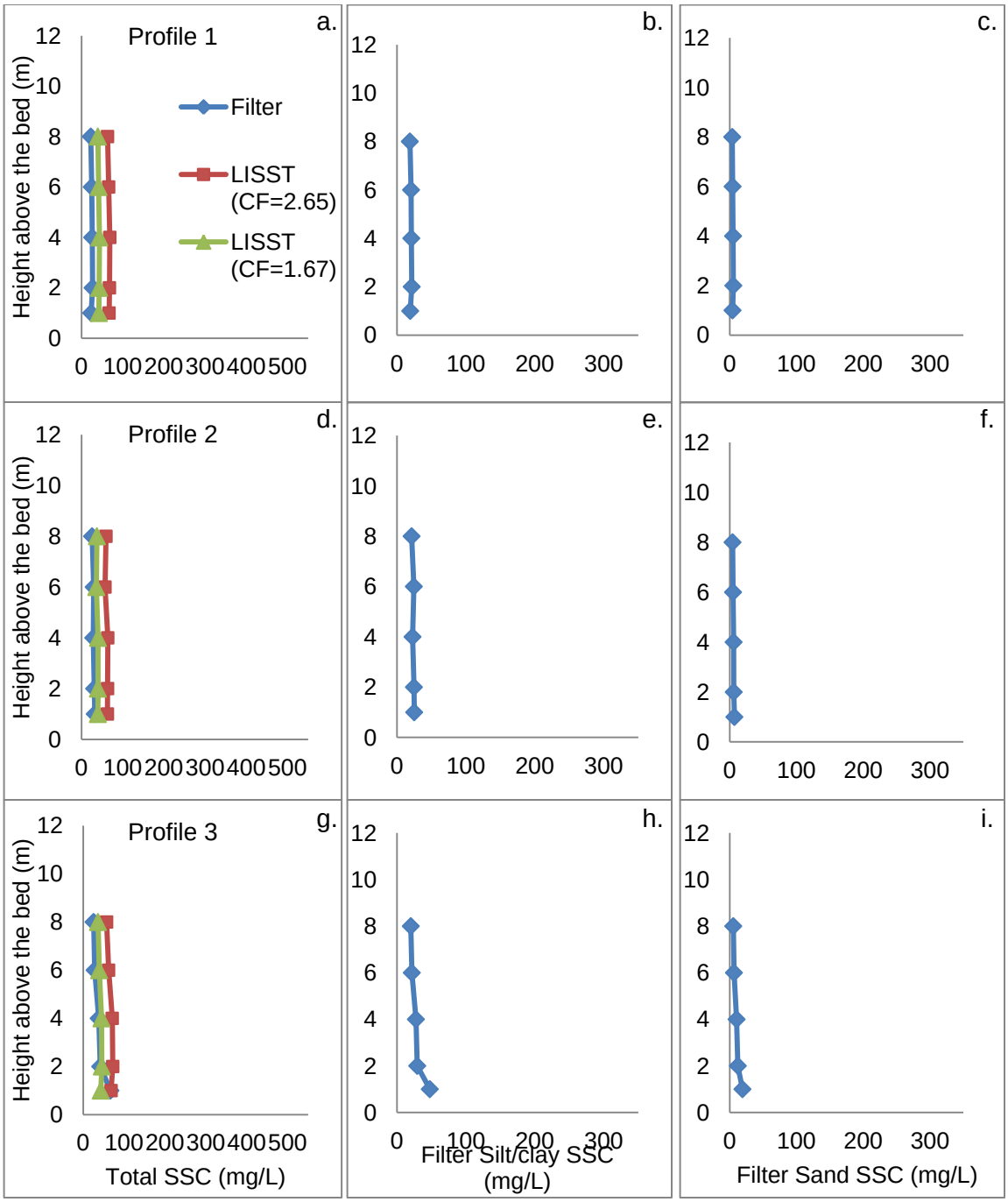

Figure A-6: August 4, 2010 sediment concentration for the (a-c) Profile 1, (d-f) Profile 2, (g-i) Profile 3, (j-l) Profile 4 and (m-o) Profile 5. a, d, g, j, m are total SSC profiles from the traditional filter method and LISST-Portable method using conversion factors (CF) of 2.65 and 1.67. b, e, h, k, n are filtered silt/clay concentrations and c, f, i, l, o are the filtered sand.

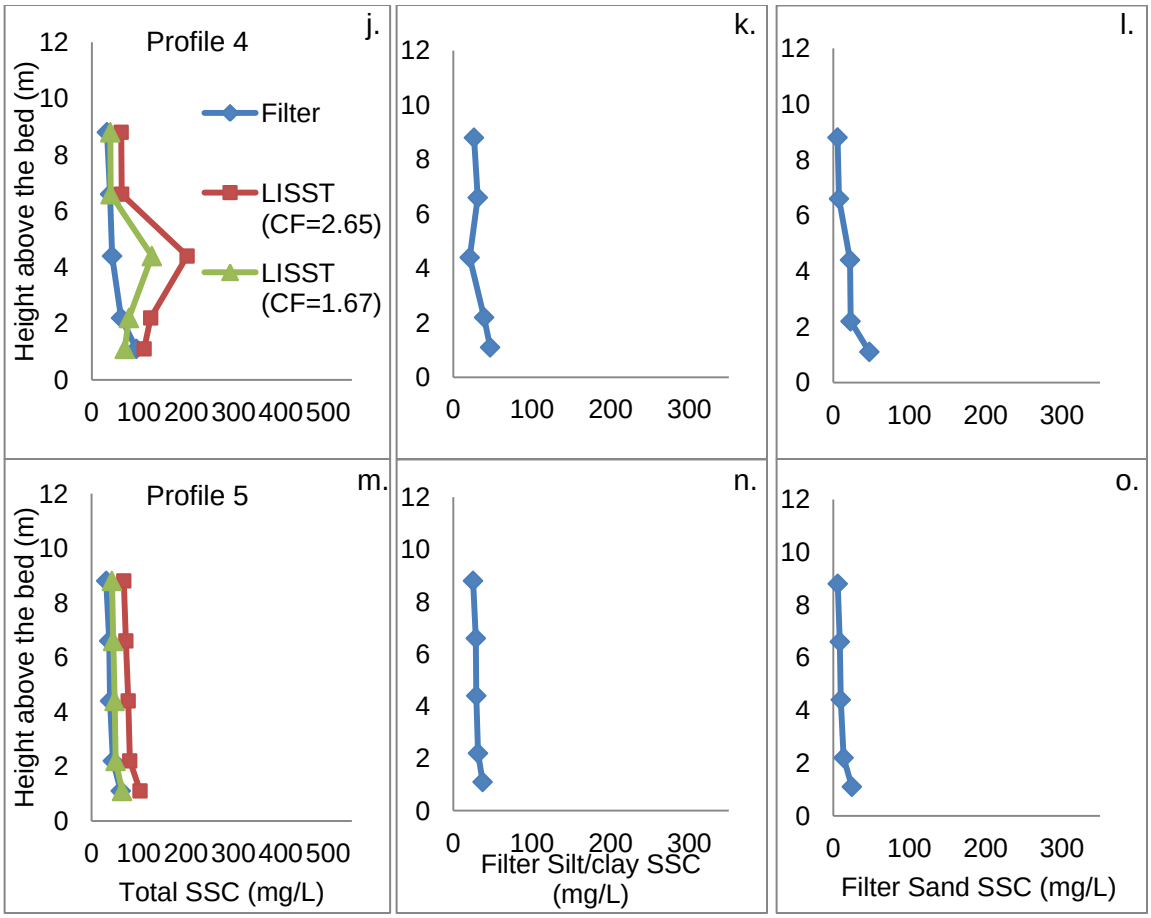

Figure A-6 concentration continued.

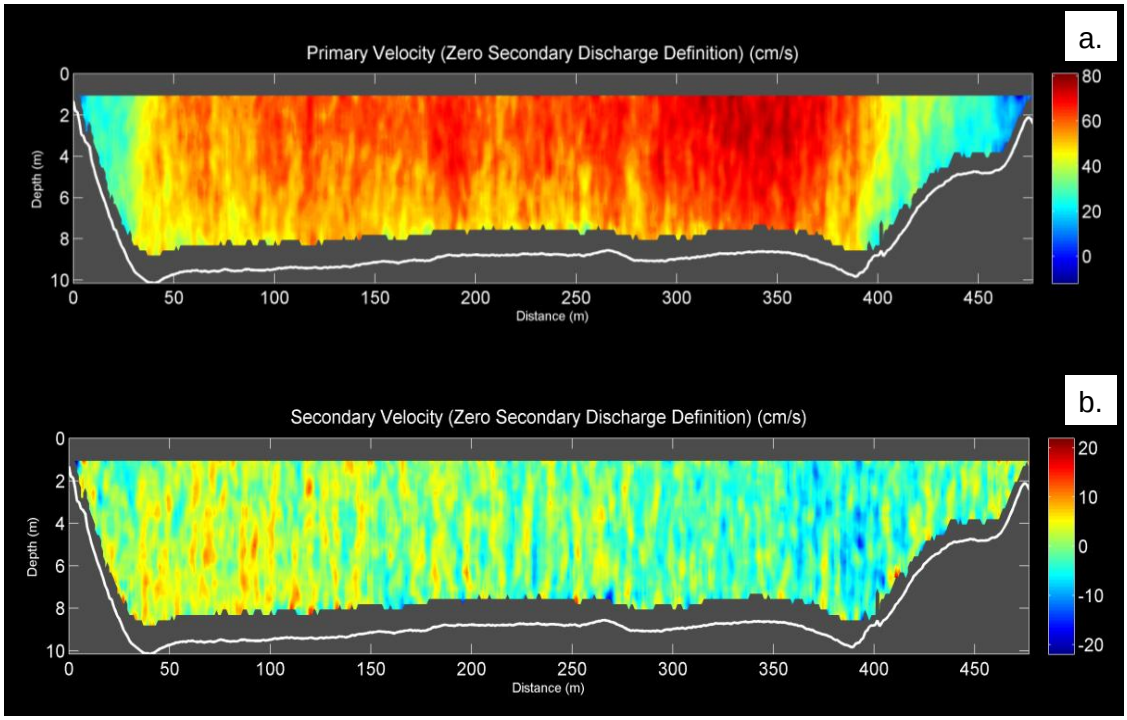

Figure A-7: April 15, 2010 velocity cross-sections from downward-looking aDcp transects a. primary and b. secondary velocity.

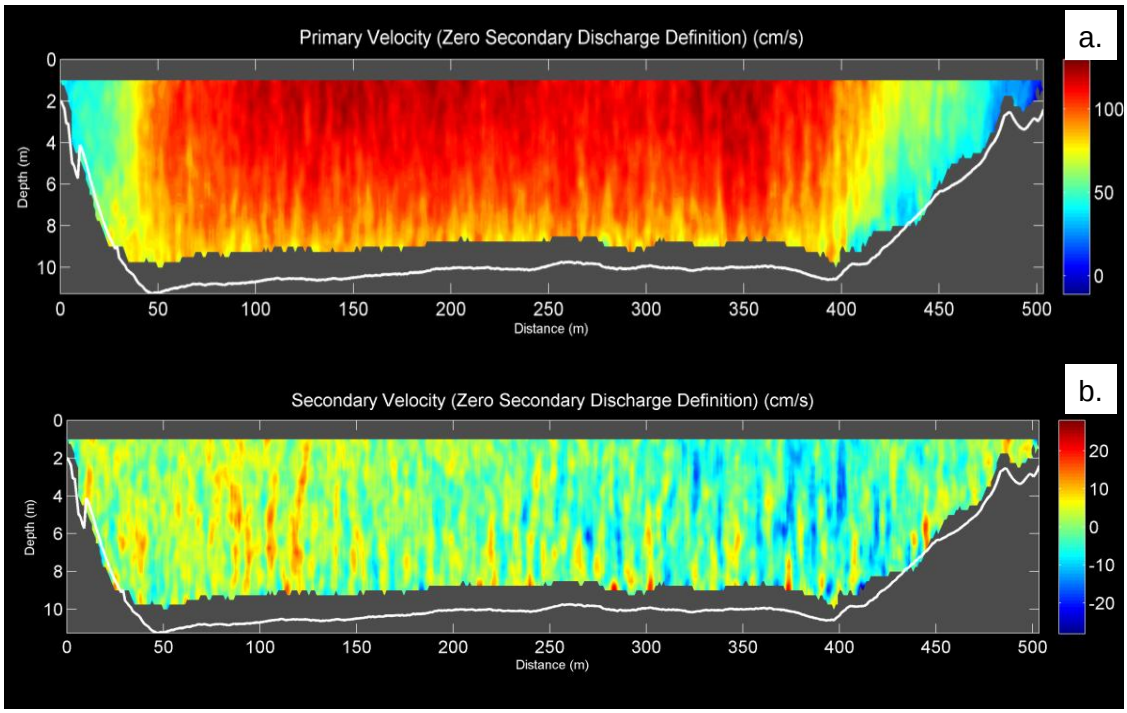

Figure A-8: May 19, 2010 velocity cross-sections from downward-looking aDcp transects a. primary and b. secondary velocity.

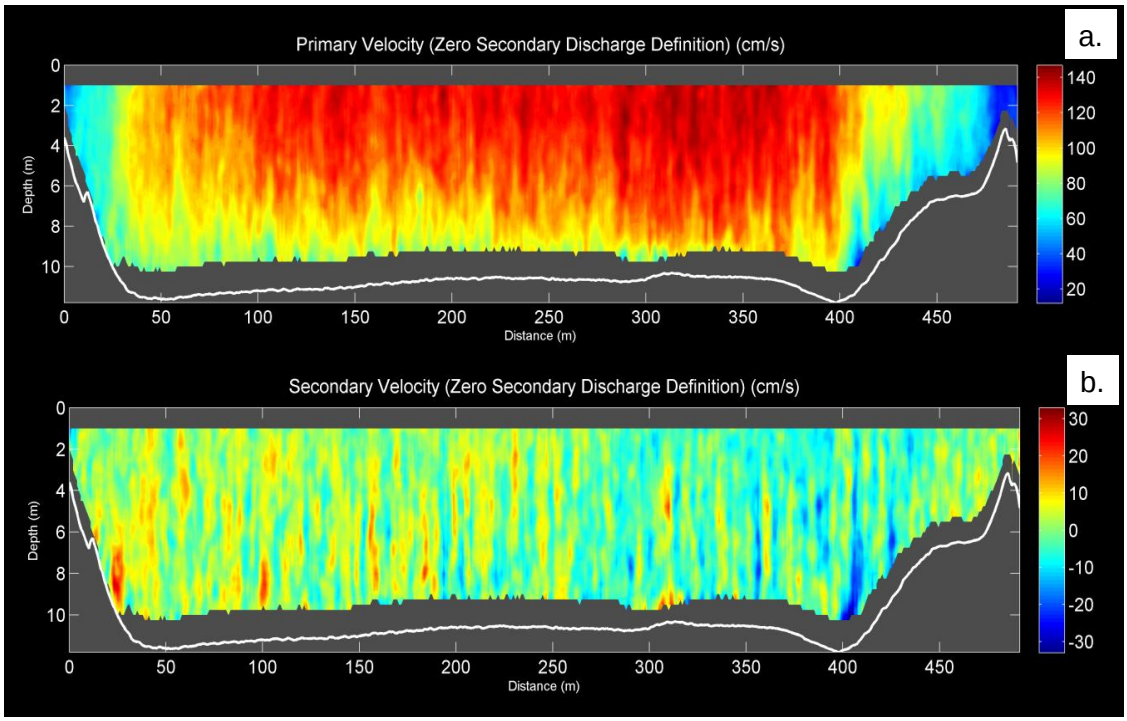

Figure A-9: May 28, 2010 velocity cross-sections from downward-looking aDcp transects a. primary and b. secondary velocity.

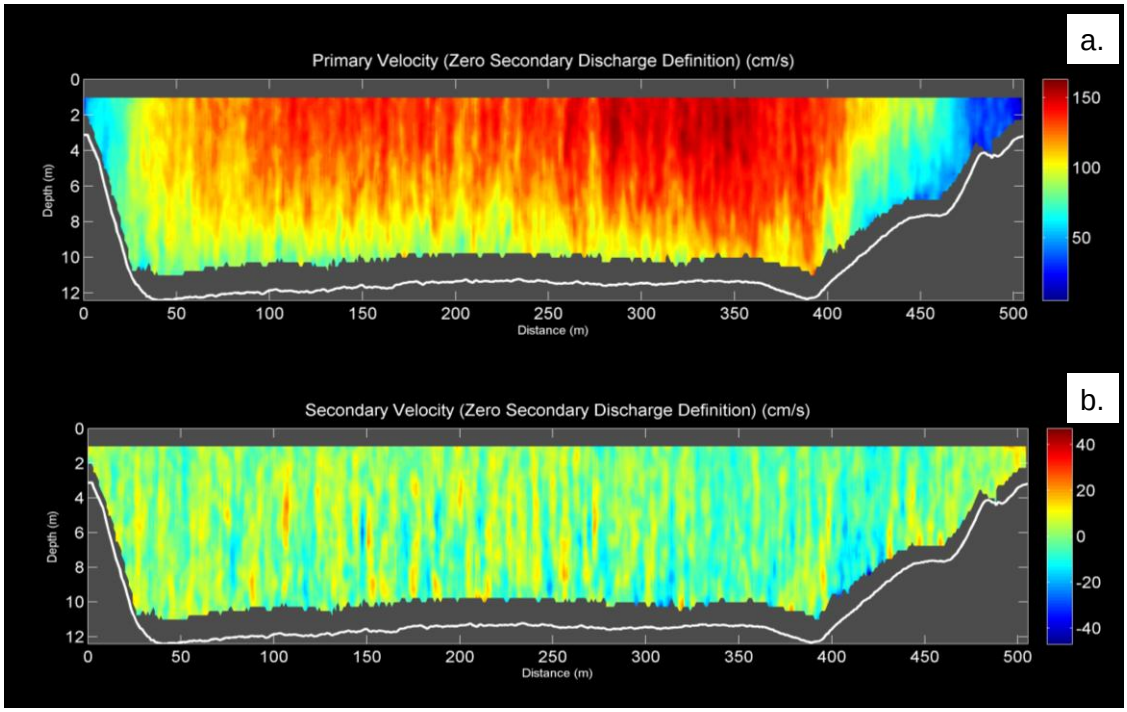

Figure A-10: June 8, 2010 velocity cross-sections from downward-looking aDcp transects a. primary and b. secondary velocity

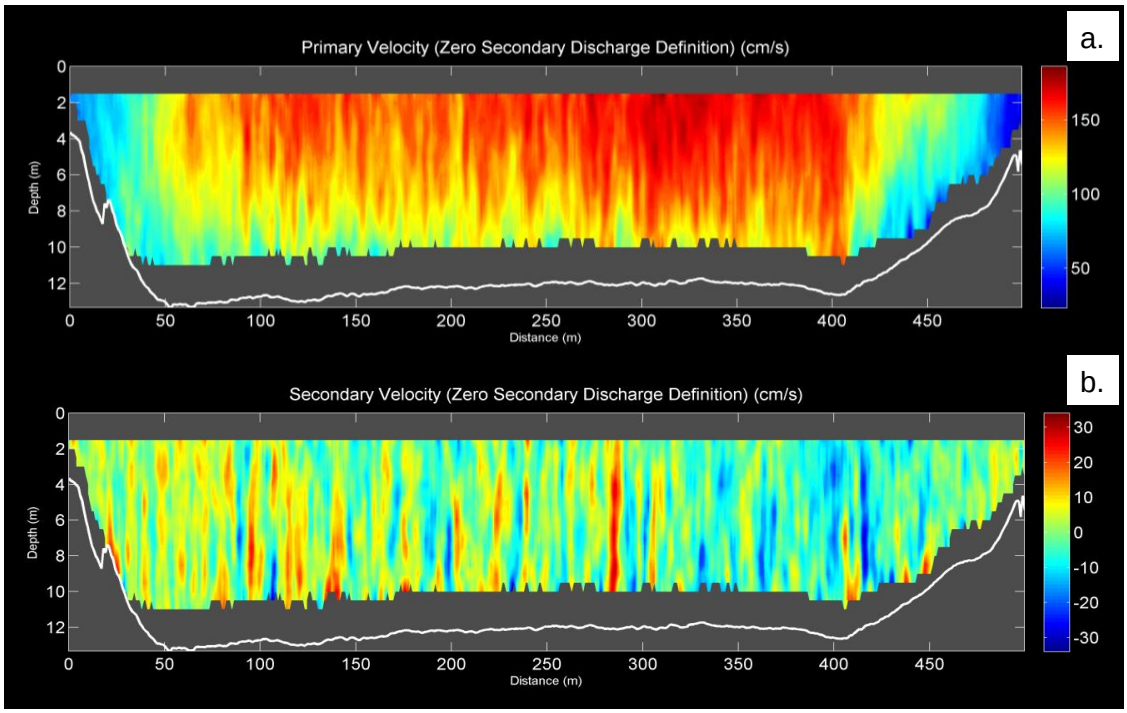

Figure A-11: June 28, 2010 velocity cross-sections from downward-looking aDcp transects a. primary and b. secondary velocity.

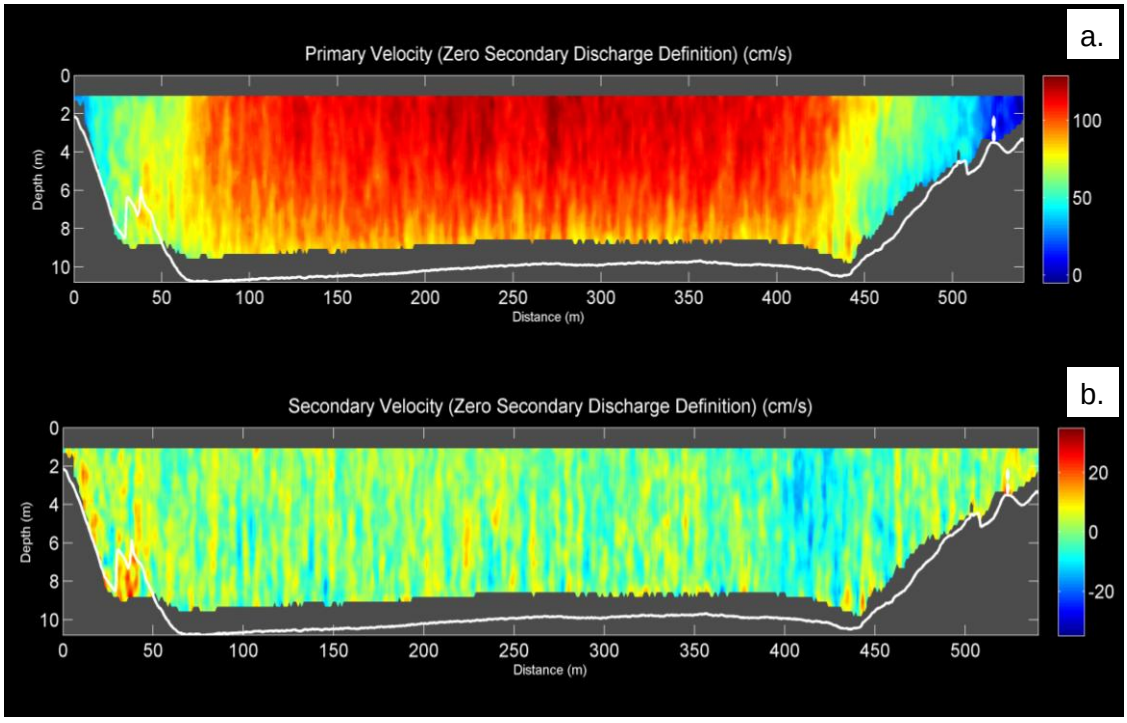

Figure A-12: August 4, 2010 velocity cross-sections from downward-looking aDcp transects a. primary and b. secondary velocity.

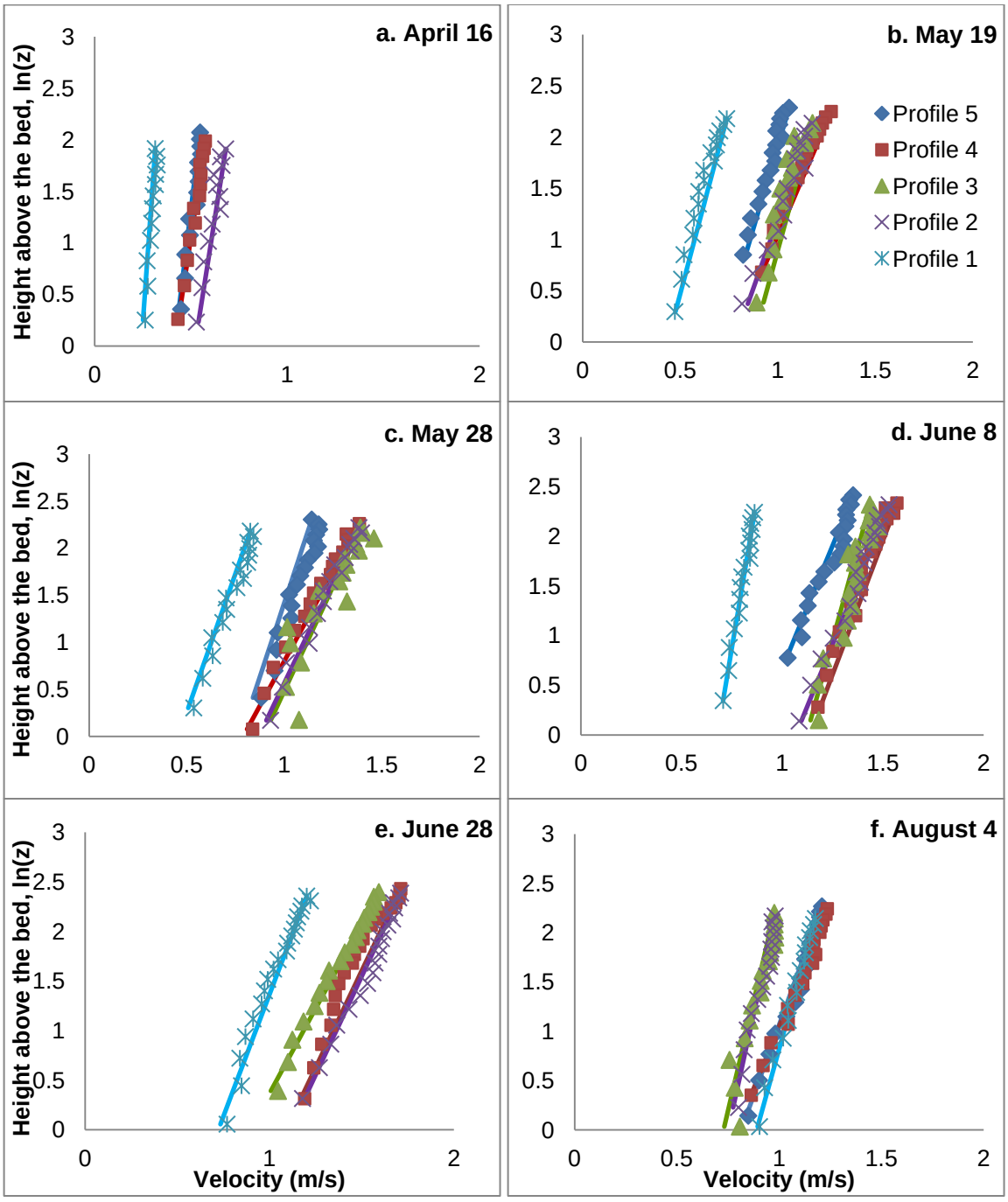

Figure A-13: Velocity profiles for all measured profile locations across the channel. a. April 16 2010, b. May 19 2010, c. May 28, 2010, d. June 8, 2010, e. June 28 2010, f. August 4, 2010. The data points are measured velocities and the solid lines are calculated from theory.

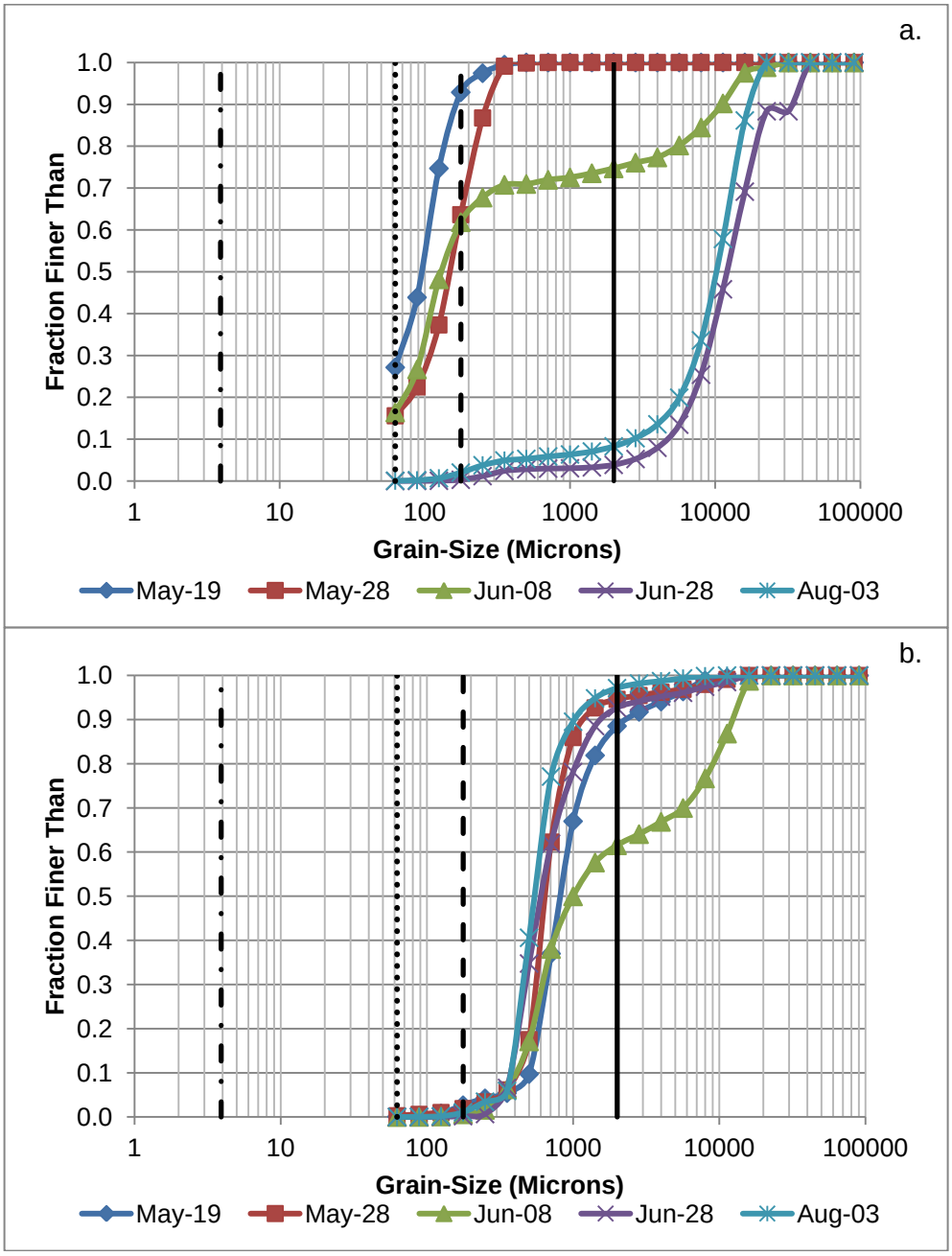

Figure A-14: Bed-material grain-size distribution for five sampling campaigns over the 2010 freshet a. Profile 1, b. Profile 2, c. Profile 4, d. Profile 5. Solid line: gravel-sand division, dashed line: bed-wash material load division, dotted line: sand-silt division, dotted-dashed line: silt-clay division.

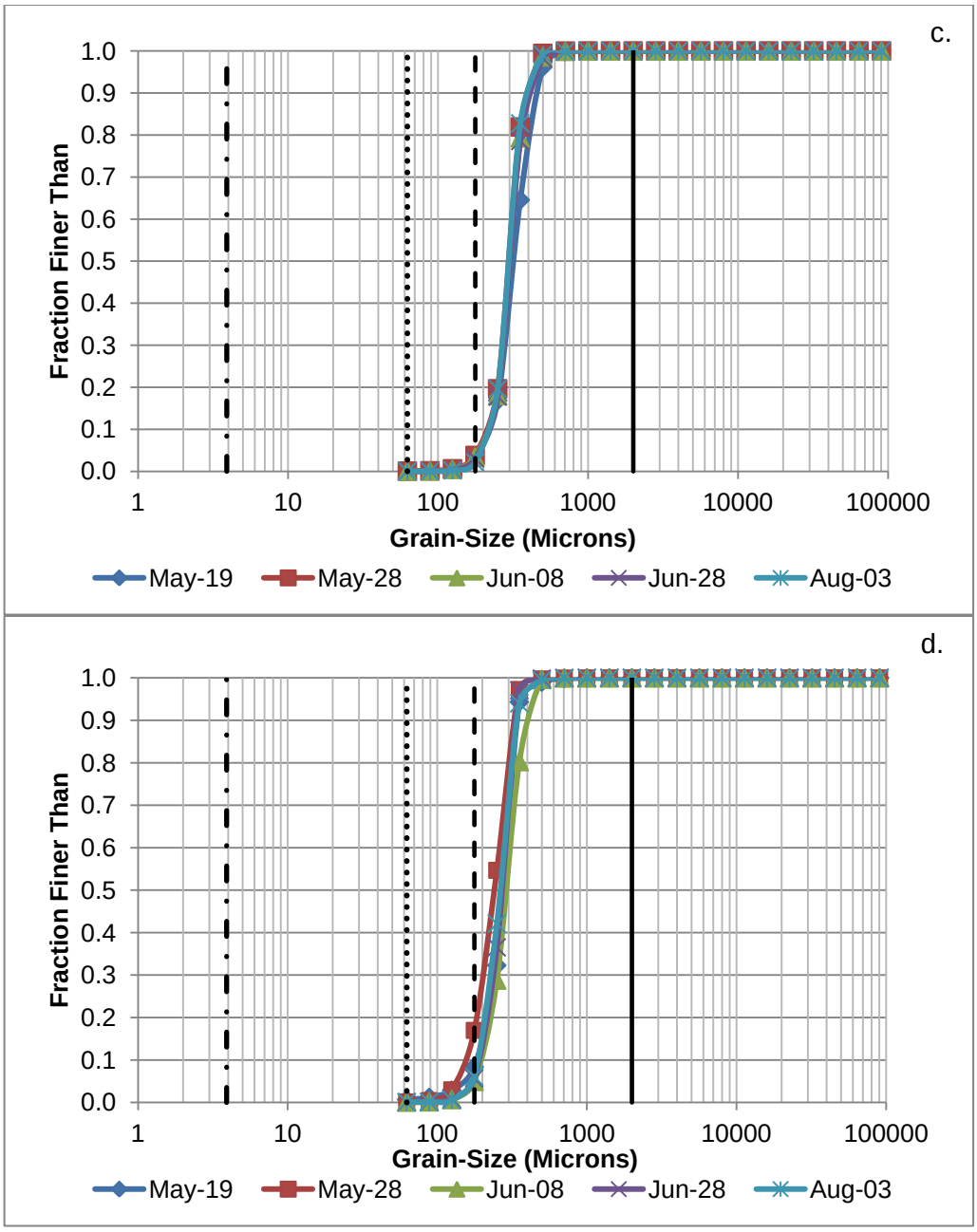

Figure A-14 continued.

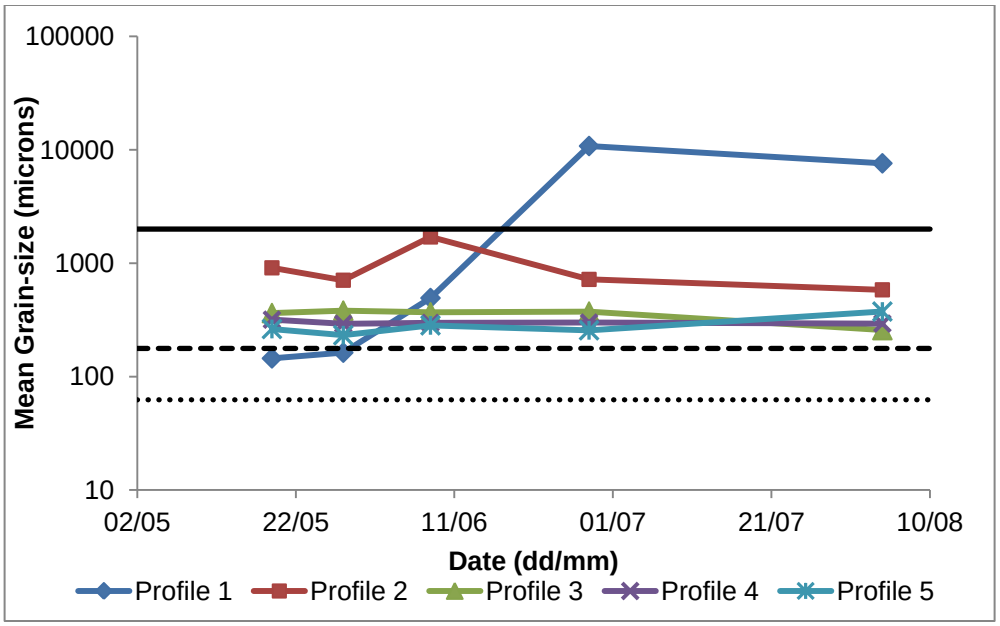

Figure A-15: Mean bed-material grain-size distribution for five sampling campaigns and 5 profile locations across the channel over the 2010 freshet. Solid line: gravel-sand division, dashed line: bed-wash material load division, dotted line: sand-silt division, dotted-dashed line: silt-clay division.

Appendix B.

Supplementary Hydroacoustics Results

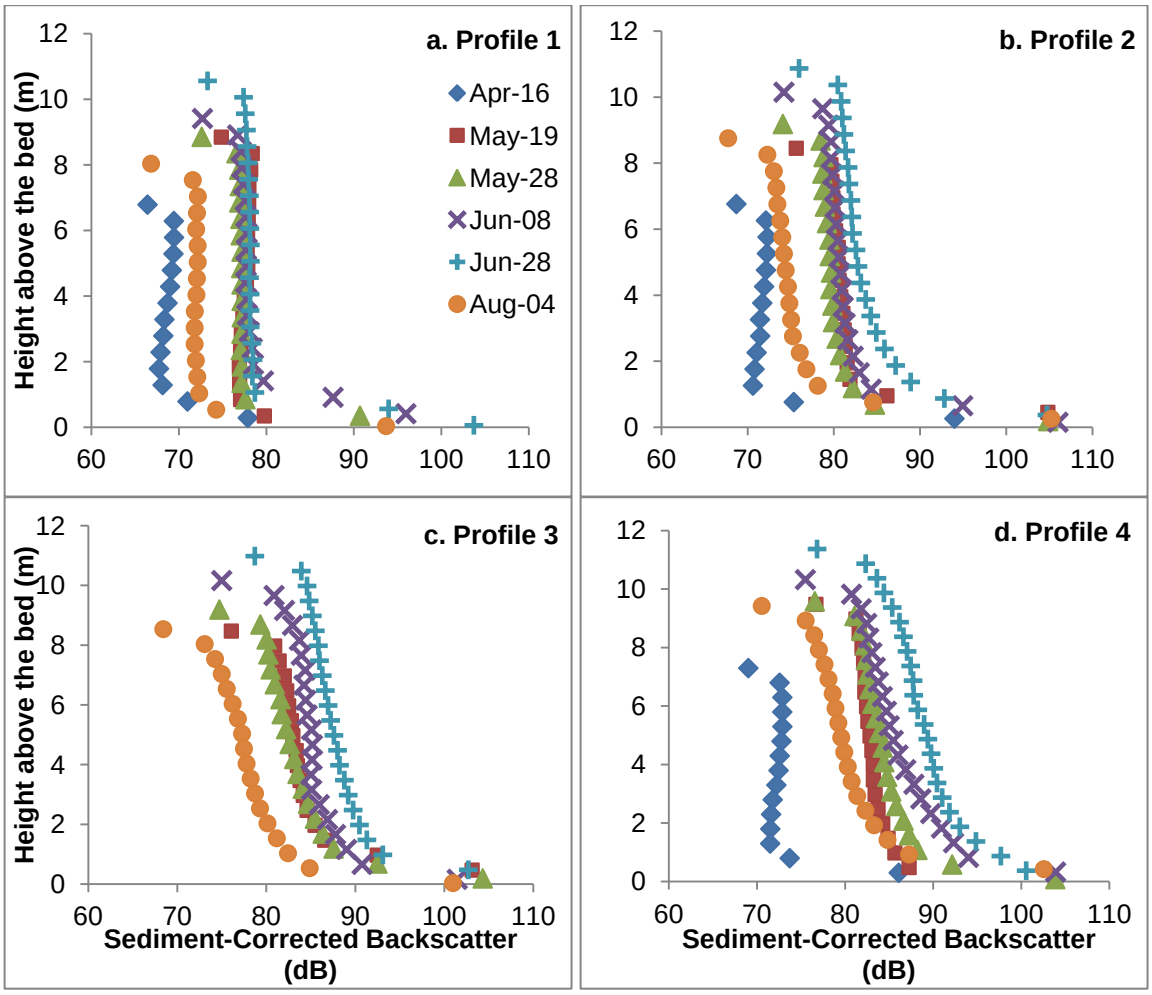

Figure B-1: Sediment-corrected backscatter profiles over the 2010 freshet for a. profile 1, b. profile 2, c. profile 3, d. profile 4, and e. profile 5.

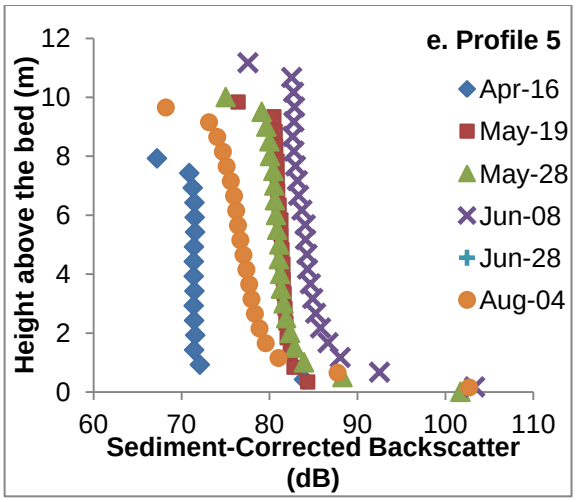

Figure B-1 continued.